Evaluating the influence of lifter face angle on the trajectory of particles in a tumbling mill using PEPT.

Prepared by:

Motena Takalimane

A thesis submitted to the Faculty of Engineering and the Built Environment, University of Cape Town in fulfilment of the requirements for the degree of Master of Science in Chemical Engineering

December 2014

ABSTRACT

The work performed in this thesis was aimed at evaluating the influence of lifter face angle on the charge kinematics for a laboratory scale mill. The study involved tracking a single particle representing the ensemble using the Positron Emission Particle Tracking (PEPT) to obtain the location of the particle with time. The particle was radiated with a radionuclide; ^{68}Ga, which has a half-life of 68 minutes.

The objectives of the study involved tests with different lifter face angles at different mill speeds and volumetric mill filling. After performing the tests the data was analysed to obtain probability density distributions for each test conditions from key charge descriptors. Charge descriptors such as the Centre of Circulation (CoC), shoulder angle, toe angle, the free surface and also kinematic information such as the velocity profile along a carefully chosen radial line from the centre of the mill that passes through the CoC were obtained. The time averaged velocity data was used when assessing the influence of the lifter face angle on the velocity profile.

The results showed notable effects of lifter face angle on charge characteristics. No real definitive trend was observed for the CoC as the lifter face angle was altered at all mill speed and filling conditions. However, the CoC showed an outward shift toward the mill shell with an increase in mill speed but an inward shift toward the mill centre with increase in charge filling degrees. Mill speed is expected to cause a load expansion as the charge approaches centrifugation.

The shoulder angle showed a general increase as the lifter angles became steeper for both an increase in mill speed and charge filling degrees. The impact toe angle displayed maxima with increasingly steeper lifter face angle depending on the condition altered. At the higher mill speeds (70 and 85 % of critical speed), the impact toe did not show as much variation with lifter face angle. However, a noticeable difference was observed at the lowest mill speed tested; which was 55 % critical speed. At 20 % charge filling degree, the impact toe increases from 45 to 90 ° lifter. At the higher filling degrees, a maximum was reached from 45 to 75 ° lifter and from 75 to 90 ° a decrease was seen. It is expected that the steeper lifter angles will cause the charge to impact the mill shell as the lifting forces are altered.

The velocity profile demonstrated changes with face angle as distances along a radial line in the mill were investigated. As the speed was increased from 55 to 85 % of critical

speed, the velocity profile showed minimal changes for the higher mill speed at distances closest to the mill shell, and more perceivable changes in the profiles at 55 % of critical speed for all radial distances investigated.

PLAIGIARISM DECLARATION

1. I know that plagiarism is wrong. Plagiarism is to use another's work and pretend that it is one's own.

2. I have used the Harvard convention for citation and referencing. Each contribution to, and quotation in, this thesis from the work(s) of other people has been attributed, and has been cited and referenced.

3. This thesis is my own work.

4. I have not allowed, and will not allow, anyone to copy my work with the intention of passing it off as his or her own work.

Signed by candidate

Signature Removed

Signature _____

Date _____3/12/2014_____

TABLE OF CONTENTS

LIST OF FIGURES

LIST OF TABLES

ACKNOWLEDGEMENTS

Firstly, I would like to extend my gratitude to my pillars of strength- my parents 'Maliehe and 'Mampeo Takalimane for their unwavering love, support and patience throughout my MSc programme. To my first best friend and super hero, my brother Lethiba Takalimane, I salute him for being my biggest cheerleader and encouraging me to always aim higher. To my grandparents, Ntate Stanley and 'Me 'Mamputi for all their prayers and always believing I could do more than I imagined I was capable of.

To all my families; the Takalimane family for their unfailing love and extraordinary support. For always celebrating and sharing in my achievements. Immense gratitude also goes to the Mpitso and Nxumalo families who have constantly been a source of support. To the Thomas family for the endless laughter during stressful times- I highly appreciated it. To my GRC family; with special mention to Mr. Dieudonne Kayemba for his fatherly advice and prayers. Special mention also goes to a friend, mentor, and sister; Yeukai Chideya for always being ready with words of encouragement and prayers.

Immense gratitude goes to the motherly figures in my life for their constant encouragement and for pouring so much of their lives into mine during this time. Ms. Moselantja Pape, the late Ms. Pulane Ramoabi who was always ready with a pep talk, prayer and words of encouragement when I needed them the most. Lastly, to Ms. Ann Marie Parrillo for the endless advice, unconditional love, life lessons and laughter that helped keep me grounded.

To my main supervisor; A/Prof. Aubrey Mainza for interrupting my daily routine and affording me this opportunity. I thank him for his invaluable advice, patience, always pushing me to think beyond the obvious and more importantly, for continuously imparting pearls of wisdom beyond the scope of the thesis. To my co-supervisor Dr. Indresan Govender for his invaluable assistance with the MATLAB and PEPT experiments.

Appreciation also goes to the CMR staff that assisted in different capacities with this work. Dr. Lawrence Bbosa who assisted with MATLAB and PEPT experiments, Nosibusiso Sunduswayo, Pathmathas Thirunavukkarasu, Amos Baloyi and Olumide Oluwaseun who all helped with the smooth running of the PEPT work. For always being ready to help when things fell apart or stopped working, I would like to thank Mr. Kenneth Masuku (Uncle Kenny) and Mr. Moegsien Southgate. From the Mechanical

Engineering Department at UCT, Mr. Glen Newins for machining the lifters at short notice, Dawi de Klerk for assisting with coding and lastly, to the iThemba staff; Michael Van Heerden and Liu Cong who worked tirelessly to ensure that I received my tracers on time daily and for assisting with running the PEPT experiments.

To the family I chose for myself, my friends. I thank them all for their support, they are all *Rock stars*!

Last but not least, I thank God for indeed in Him I found my being and strength to complete the race He set before me.

"***I have fought the good fight, I have finished the race, I have kept the faith***." 2 Timothy 4:7

GLOSSARY AND ABBREVIATIONS

Autogenous (AG) mill: A type of tumbling mill where self-grinding of the particles occurs as opposed to the use of conventional grinding media (steel balls or rods).

Caesium-137 (^{137}Cs): This is a radioactive isotope of Caesium.

Centre of circulation CoC: The point at which the charge appears to be circulating about.

Charge: The grinding media and particles within a mill.

Comminution: The process of reducing large solid material to a smaller size.

Critical speed: The rotational speed of the mill when the gravitational and centrifugal forces acting on a particle are equal.

Half-life ($t_{1/2}$): This is the time required for half of an unstable isotope to undergo radioactive decay.

Lifter bar: A small bar attached to the mill shell to aid with lifting the charge in the mill.

Liner: A protective layer attached to the mill shell against grinding mechanisms in the mill.

Megabecquerel (MBq): Becquerel (Bq) is the SI unit for radioactivity. One Bq refers to the activity of a quantity of radioactive material when one nucleus decays per second.

PEPT: Positron Emission Particle Tracking.

Semi-autogenous (SAG) mill: These are similar to AG mills but they utilise minimal grinding media to create particle breakage (approximately 15 % of steel balls).

CHAPTER 1

1. INTRODUCTION

1.1 Background

The purpose of this thesis is to use Positron Emission Particle Tracking (PEPT) to determine the influence of lifter face angle on the trajectory of charge within a lab scale tumbling mill. The mill was operated at three different mill speeds and charge fillings at each of the four lifter face angles.

In the mineral processing industry, it is necessary to liberate valuable minerals from the unwanted gangue material. Large ore particles should undergo breakage to expose the minerals of interest, which is achieved by undergoing a process referred to as *comminution.* Tumbling mills have been used extensively for coarse particle reduction from 5 to 250 mm down to sizes in the range of 40 and 300 μm (Wills and Napier-Munn, 2006). Their popularity is founded on the fact that they are able to process large quantities of ore whilst still achieving the desired particle reduction. An example of the large capacities was the 40' SAG mill installed by FLSmidth in Chile in 2010 shown in Figure 1. Tumbling mills consist of a supported horizontal cylinder shell, allowed to rotate on its axis and consequently the charge within the mill also rotates. Tumbling mills are classified as rod mills, balls mills, autogenous or semi-autogenous mills (King, 2000), depending on the grinding media used.

Figure 1: Picture of mill in Chile (www.flsmidth.com, 2011)

In tumbling mills particle breakage can occur by three different mechanisms; attrition, abrasion, impact or compression. It takes into account that most minerals are arranged in a crystalline shape. It is suggested that a combination of compressive or tensile stresses can break the crystalline structure (Wills and Napier-Munn, 2006).

Particle breakage is extremely energy intensive, and the use of tumbling mills for this purpose has shown to be rather inefficient (Wills and Napier-Munn, 2006). Reduction of these particles generally only uses about 1-5 % of the energy supplied, with the bulk of energy being transferred to heat and noise (Cleary, 1998). Thus, developing ways of minimising this energy consumption in these mills, whilst still being able to achieve the desired particle size is of significant importance.

Efforts to reduce the costs associated with running tumbling mills are being made, with particular focus on the liners and lifters within the mill shell (Rezaeizadeh *et al.,* 2010). These liners are placed on the inside of the mill and act as a protective layer for the shell. Their material of construction is of importance as it determines how often they will need to be removed and replaced, which essentially affects the economics of the entire process (Powell *et al.,* 2006). Further, they are fitted to enhance the grinding efficiency by producing a cataracting effect to induce high energy impact and creating a cascading region where abrasion and attrition breakage can occur (Hlungwani *et al.,* 2003).

As much as improving the design of liners is important for optimal mill operation, recent advances have been made in the selection of grinding balls. Grinding balls with larger diameters are being used in an attempt to increase the grinding efficiency. Traditionally, the top size was about 104 mm, but now 125 mm balls are being used with some operations using 140 and 152 mm balls (Maleki-Moghaddam *et al*., 2012). Using these larger ball sizes affects the grinding efficiency as well as the charge trajectory, highlighting the need for reviewing the design of liners. It is worth noting that the author does not recommend the use of larger balls as a strategy to improve grinding efficiency, but is merely pointing out that others have taken this path.

According to Powell (1993), this motion is thought to primarily be affected by the speed and size of the mill, type of media, slurry viscosity and the design of the mill liners.

1.2 Scope of work and limitations

This current work deals with the lifter face angle in a project aimed at studying the influence of lifters on the velocity field and key charge descriptors such as the centre of circulation (CoC), shoulder and toe angles. Earlier work conducted by Brodner (2013) investigated the impact of the lifter height on the velocity field. Extending this work to lifter face angle will assist in gaining a better understanding of two of the three main factors affecting charge kinematics from the lifter design aspect. The third design variable which can also be altered is lifter spacing, but this will be considered at a later stage as it goes beyond the scope of the current work. This work does not consider particle breakage, however, any discussion on particle breakage is merely inferred from the information gained from charge motion.

1.3 Hypotheses

The hypotheses that will be tested in this study are:

1) The charge expands with increase in lifter face angle because the larger face angles tend to lift the charge higher before releasing it into the cascading and cataracting regions.
2) Increasing lifter face angle results in an increase in the velocities for particles near the shell because these particles are locked in and move at speeds closer to that of the shell.

1.4 Key Questions

1) What effect does lifter face angle have on the charge shape for different mill speeds and volumetric charge filling degrees?
2) Will the lifter face angle have an influence on charge descriptors such as CoC, shoulder and toe angles for different mill speeds and volumetric charge filling degrees?
3) How will the velocity profile change from aggressive to gentle lifting of the charge for different mill speeds and volumetric charge filling degrees?

1.5 Objectives

The main objectives formulated to test the hypotheses for this thesis are:

1) To perform particle tracking experiments using a lab scale tumbling mill with 4 lifter face angles at 3 mill speeds and volumetric filling degrees respectively.

2) To extract velocity field data from the PEPT experiments for each lifter face angle at different operating conditions.
3) To extract the relevant charge kinematic descriptors that can be influenced by lifter face angle and determine the extent of the effect.

CHAPTER 2

2. LITERATURE REVIEW

Conducting a literature review helped form a basis for the underlying theories behind charge motion within tumbling mills and highlighted the important parameters that should be taken into account when studying the influence of lifters on this motion. The literature survey in this thesis focused on the effect of lifter face angle and liners, mill speed and the % volumetric filling of the charge.

2.1 Tumbling mills

In the minerals processing industry, comminution takes place in a series of crushing and grinding processes. Crushing would precede the grinding such that the feed material is reduced to a size that will allow the liberation of valuable minerals and unwanted gangue is achieved (Wills and Napier-Munn, 2006).

For grinding efficiency, comminution can be separated into three types of grinding; impact, attrition and abrasion. Each one of these has an influence on the wear of liners or lifters thus it is important to know which type of material to use in each case.

a) **Impact grinding**: When impact grinding is desired, the lifter bars have to be high enough to raise the charge such that when it falls, it does so with high energy impact (Wills and Napier-Munn, 2006) as seen in Figure 2 where larger material (steel balls or larger pieces of ore) would be used to break the smaller particles. The material of construction used for the lining of the mill needs to be taken into consideration here, especially if the impact poses a threat of cutting through it (Clermont and de Haas, 2010).

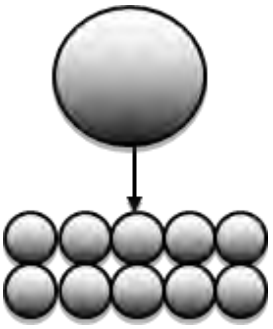

Figure 2: A schematic of impact grinding.

b) **Attrition grinding:** Figure 3 shows a schematic of how attrition occurs; with the smaller material experiencing breakage as the grinding media move past it. For cases where a fine grind is not desired, the lifter height and profile should be appropriate for a firm grip and good lift of the charge. With this type of grinding, steel linings are usually used- with the disadvantage of causing increased slip when they wear (Powell *et al*., 2006).

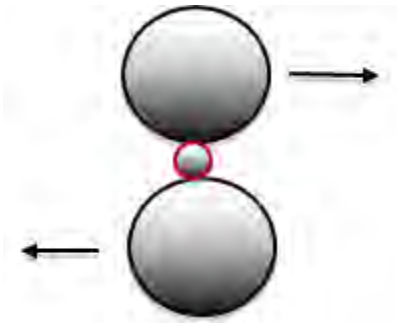

Figure 3: A schematic of how attrition occurs.

c) **Abrasion grinding**: In abrasion grinding, the ore rubs against each other, which results in ore size reduction. The notable difference between abrasion and attrition lies in the fact that two particles move past each other in abrasion as seen in Figure 4. In abrasion, the amount of packing in the mill would be very important. The particles have to be close enough to be able to move past one another to achieve this type of grinding, thus spacing between lifters is an important variable to consider (Powell *et al*., 2006).

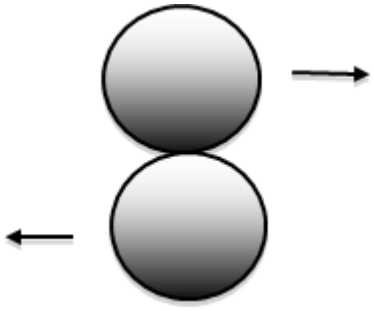

Figure 4: A schematic of how abrasion occurs

The rate at which the particles move past each other in both attrition and abrasion is referred to as the shear rate. Recent research has shown that shear rate by abrasion and attrition is the main mode of breakage (Brodner, 2013). Thus, this work is aimed at assessing the influence of lifter face angle on charge motion which leads to the various modes of breakage in tumbling mills.

Tumbling mills use different grinding media and methods of grinding to achieve the particle breakage required. The common types of tumbling mills include:

a) **Ball mills:** These mills use steel balls (ball charge of up to 40 %), to produce the required product size from a given feed. This particle breakage occurs due to the impact of the grinding media with the particles as well as by attrition. They are either used in primary or secondary grinding operations following AG or SAG mills. When operating in primary grinding, the charge level is usually as low as 20 % (Morrell, 1993).
b) **Autogenous mills (AG)**: These mills do not utilise any steel grinding media for breakage. Large ore particles break into smaller particles or act as grinding media as the mill rotates. They are generally used for coarse feed from primary crushers or even uncrushed ore directly from the pit. The mill load has been said to be dependent on the ore characteristics such as ore hardness, feed size and distribution (Morrell, 1993)

c) **Semi-autogenous mills (SAG):** These mills are almost the same as autogenous mills except steel balls are used for breakage to supplement large rocks as grind media. SAG mills use steel balls in the order of 4 – 15 % volumetric filling and the rest of the charge is comprised of rock load and slurry. The feed size is generally higher in comparison to AG mill, and they can be used to treat material from secondary crushers (Morrell, 1993). An advantage SAG mills have over AG mills is their flexibility in accommodating hardness fluctuations in ore (Maleki-Moghaddam *et al.,* 2012).

2.2 Methods used for studying charge motion

A number of authors have studied the motion of the charge using various methods. Powell (1993) studied charge motion in tumbling mills using X-ray to track the motion of charge in a lab scale tumbling mill. Using discrete element modelling, Cleary (2001) and Pérez-Alonso and Delgadillo (2012) validated 2D DEM results using digital image analysis of charge descriptors such as velocity profiles, shoulder and toe angles. Later, Cleary *et al*., (2003) also used DEM accompanied with experimental work on a lab scale tumbling mill to predict the accuracy of DEM models.

In tumbling mills, the charge rotates due to the motion of the mill (Wills and Napier-Munn). Dong and Moys (2003) noted that if particles are lifted high enough they will reach the shoulder region and be thrown against the mill shell on the opposite side (cataracted). This type of motion which causes high energy impacts on the mill shell resulting in increased wear on the mill lining is observed mostly in SAG and AG mills where large rocks (in the order of 0.5 m in diameter) undergo breakage (Dong & Moys, 2003).

Being able to trace the trajectory of particles within a mill has been of great interest over the years. The Discrete element modelling (DEM) was introduced into milling simulation and optimization by Mishra and Rajamani (1990). This modelling has gained a great deal of popularity and evolved from being used in 2D to 3D. Hlungwani *et al*. (2003) and Cleary (1998) also used DEM to predict the interaction and trajectory of particles within the mill with various lifters and liner configurations.

2.2.1 Charge characteristics

The breakage that occurs in tumbling mills is strongly associated with the charge motion (Clermont and de Haas, 2010). Throughout the life of a liner, its shape evolves, which has a direct influence not only on the grinding efficiency but ultimately on the charge motion (Powell *et al*., 2011). Therefore, it is important to analyse the influence of lifter angle on charge characteristics.

The key charge characteristics that are considered in this work include the CoC, shoulder and toe positions, and the free surface, which have been defined by Powell and McBride (2004) and are discussed in more detail below.

Equilibrium surface

The equilibrium surface is used to differentiate between charge that is ascending and descending (indicated by the black line in Figure 5). As a result of the rotational motion of the mill, the velocities of the charge in each of these regions will differ. Due to the fact that the equilibrium surface separates the velocities viewed in these two regions, it suggests that the surface must represent a region where the velocity is zero.

Centre of circulation (CoC)

Another important feature of the charge is the location of the centre of circulation (CoC), which is described as the point where the entire charge appears to rotate or circulate about (Powell and Nurick, 1996). The CoC is shown in Figure 5, but it varies with the changes in mill speed at the same charge filling (Powell and McBride, 2004). The CoC has been said to be identified by the intersection of equilibrium surfaces; the vertical and horizontal surfaces vertical surface has been defined as the surface generated when the mill is sectioned with control surfaces, which have their normals in the vertical direction (Powell and McBride, 2004). For the horizontal surface, it is the group of control surfaces possessing normals in the horizontal direction. As a result of the principle of conservation of flow, it is shown that the flow along the control surfaces passing through the CoC results in a maximum. Showing that the point of maximum flow along any of the control surfaces represents the CoC on any of the equilibrium surfaces and the final CoC position is determined by averaging the CoC positions across the different control surfaces.

Departure shoulder

At higher speeds, the charge is thrown into flight and will either land on the mill shell or on the bulk charge. The uppermost point where the charge departs from the mill shell and goes into free flight is referred to as the departure shoulder.

Bulk toe

The region at the bottom of the mill where the cascading charge is in contact with the mill shell is referred to as the bulk toe. This is differentiated from the impact toe, which is the region where the cataracting charge will impact the shell or the bulk charge. The impact toe is characterised by where the ball would potentially fall if the mill were running at a higher speed settings.

Free surface

The free surface is the boundary separating the rising en masse region from the charge that is in free flight (cataracting).

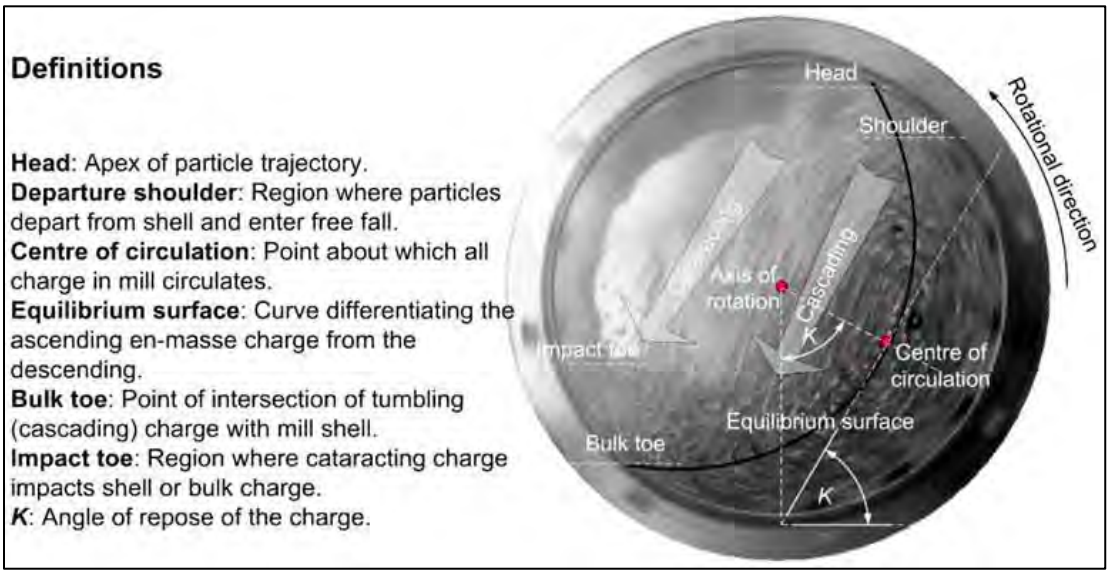

Figure 5: A cross sectional view of the inside of a tumbling mill of one layer (After Powell and McBride, 2004)

It is worth noting that the trajectories of this outer layer should be different to the inner layers simply because the outer layer will experience the effect of the lifters. The inner layers however will be lifted by the adjacent layers therefore making their flow patterns different (Dong and Moys, 2003). Moreover, Dong and Moys (2003) also suggested that as a result of the effect of the lifters, the outer layers will also be lifted higher indicating that the outer layer height is strongly influenced by the mill speed. Conversely, the lifting height of the inner layers is a strong function of the mill speed, coefficient of friction and dynamic pressure of the mill (Dong and Moys, 2003).

Impact toe and shoulder positions

As charge enters into free fall, it will impact the bulk charge or the liner- where the latter is undesirable. Should the free falling charge impact on the bulk charge, this will lead to the breakage of any large particles present in the charge, which typically constitutes charge of 3 to 300 mm in size (Powell, 1993). Morrell *et al*., (20001) hypothesised that

the impact breakage is a function of the drop height and that this type of breakage will likely take place at the toe of the charge.

Figure 6 displays the effect of lifter angle and how it influences where the charge is expected to impact. The angle here was measured from the vertical and so a 7 ° angle corresponds to an 83 ° face angle (according to the way the angles were defined in the current work). Maleki-Moghaddam *et al*., (2012) have shown in Figure 6 that the least aggressive angle measured from the vertical (30 °) predicted that the charge would impact the mill shell closest to the bulk charge. It is worth noting that the definition of the lifter angle by the authors is different to the way it has been defined for this work. Thus for a lifter that is less aggressive in this work (45 °) for example, could have resulted in the charge impacting the bulk charge instead.

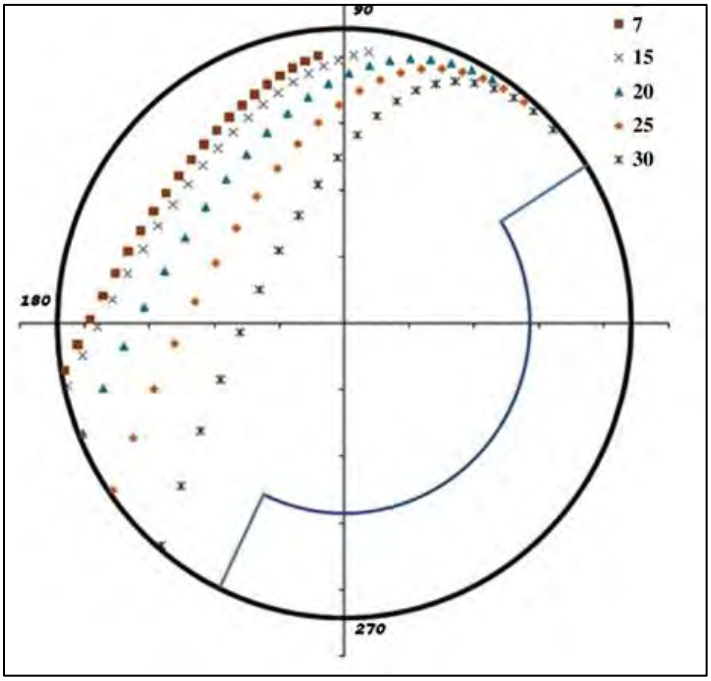

Figure 6: Simulation of ball trajectories at different lifter face angles, at 24 % filling. The authors did not indicate the direction of rotation. (After Maleki-Moghaddam et al., 2012)

The direction of measurement is based on the direction of the mill rotation as demonstrated by Maleki-Moghaddam *et al*., (2012) and the same can be seen in the work done by Morrell *et al.,* (2001).

2.2.2 Profiles of the en masse region

Due to the complex nature of rotating drums (tumbling mils); the free surface will be different at varying operating conditions. It is more likely to be flat at lower mill speeds and the slightest curvature is observed as the mill speed is increased.

Typically the free surface shape of the en masse region is referred to as the S-shape (Taberlet *et al.,* 2008). The observation of the curvature has been attributed to the centrifugal forces acting on the granular flow quantified by the Froude number described by Equation 1 (Taberlet *et al.*, 2008). The shape can only be observed for low values of the Froude number, indicating that there needs to be a more plausible explanation for the S-shape, which also takes into consideration the end effects of the drum.

$$\boldsymbol{Fr} = \frac{\boldsymbol{R\Omega^2}}{\boldsymbol{g}} \qquad \text{Equation 1}$$

Where:

R is the radius,

Ω is the angular rotation speed

g is the gravitational acceleration

Taberlet *et al.,* (2008) have postulated an expression to describe the S-shape for charge in a rotating drum. Drawing from previous work by Khakhar *et al*., (2001), a law linking the free surface (ϕ), flow thickness (*h*), the channel length (*L*), coefficient of internal friction between charge layers (μ_i) and wall friction coefficient (μ_ω) was used as the starting point (shown in Equation 2).

$$tan\varphi = \mu_i + \mu_\omega \frac{h}{L} \qquad \text{Equation 2}$$

With further development and expressing h as a function of x, the equation to describe the S-shape was found to be the expression seen in Equation 3, which uses the x and y coordinates.

$$\frac{\partial y_{surf}}{\partial x} = \boldsymbol{\mu_i} + \boldsymbol{\mu_\omega}\left(\frac{\partial \omega^2}{g}\right)^{\frac{1}{4}} \frac{1}{L}\sqrt{\boldsymbol{R^2 - x^2 - y_{surf}^2}} \qquad \text{Equation 3}$$

The resultant application of the model is illustrated in Figure 7, which demonstrates that the varying of the wall friction coefficient will affect the resultant shape. When μ_ω=0, the expression falls to: $\mu_i x$, which would be expected to be a straight line. This is represented in Figure 7 with the black line. Further increasing the effect of the end plates leads to the different S-shaped curves observed.

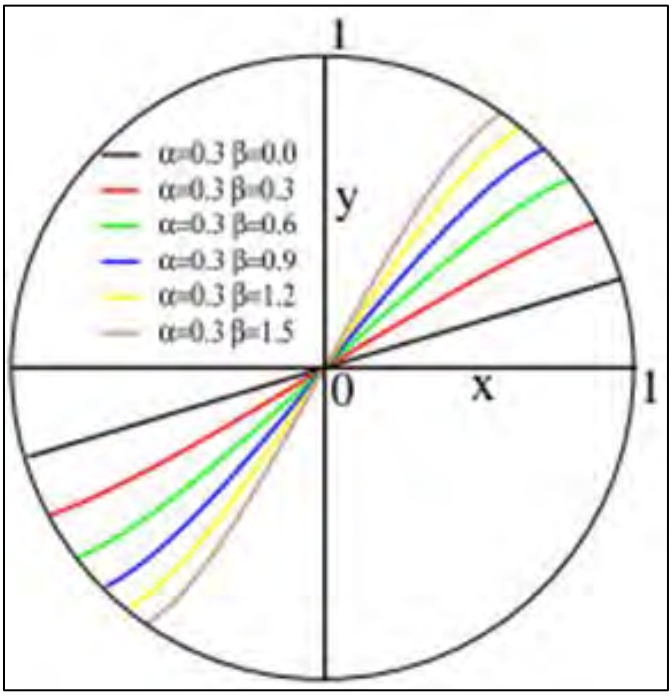

Figure 7: Numerical solutions for the S- shape model (After Taberlet et al., 2008).Rotational direction is anti-clockwise.

However, Equation 2 was derived for uniform flow, which does not hold in the case of tumbling mills since the flow patterns will vary axially through the drum. Further, the model works in cases where length of the drum is increased and the friction caused by the end plates is taken into consideration. Unless a mill of a different length can be used to investigate this, then it is impossible to test this theory. Thus, Equation 3 would require further development, to determine the end effects of the mill and the axial component of the charge, which are not considered. With that said, the development of this model by Taberlet *et al.*, (2008) provides a sufficient understanding of what contributes to the formation of the observed S- shape.

Another way of defining the shape of the free surface was described by Dong and Moys (2003) in their work, where they showed that the profiles can be categorised into 4 types

demonstrated in Figure 8. The direction of rotation for this work was not explicitly indicated by the authors, but the mill is rotating in the anti-clockwise direction. The different profiles are:

- **Linear**: This profile is usually observed at lower speeds and high filling
- **Bilinear**: More probable to be observed in low filling and high speed
- **Trilinear- chair**: Usually seen when both filling levels and mill speed are low
- **Trilinear-saddle**: When filling levels are low but mill speed is high

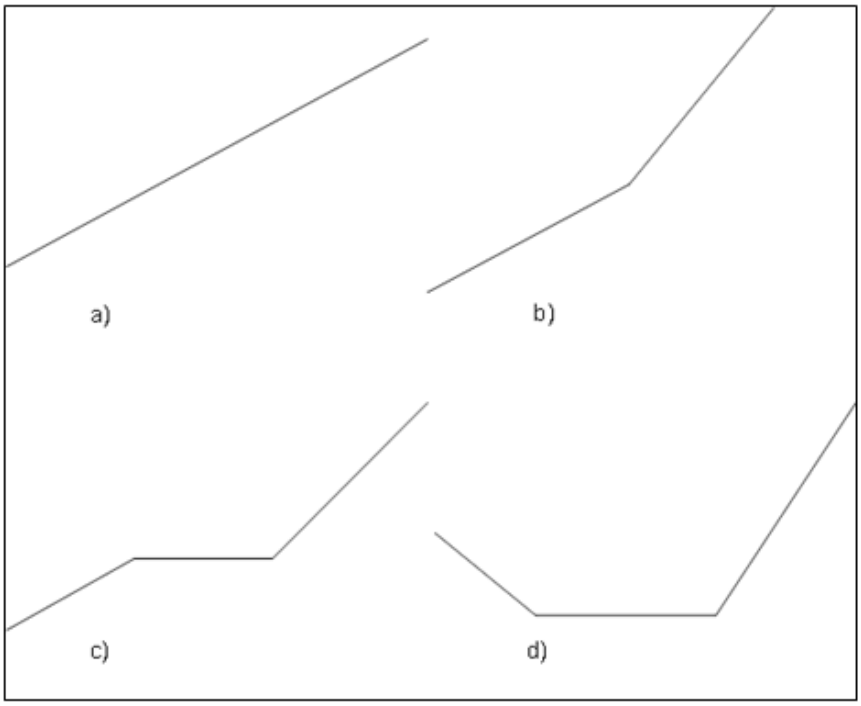

Figure 8: Free surfaces of charge in the en masse region with a) linear, b) bilinear, c) trilinear-chair and d) trilinear-saddle. The mill is rotating in the anti-clockwise direction (After Dong and Moys, 2003).

2.3 Parameters affecting the charge motion and power draw in the mill

As a result of the inefficiencies of milling, mill power plays a major role in the economics of the process (Cleary, 2001). Varying and optimising the parameters that affect this power draw could lead to drastic reductions in costs. Further investigation can allow for a deeper understanding of how lifters can be used to influence the trajectories of the charge with considerations made for energy consumption.

2.3.1 Lifter and liner design

Liner condition and maximising the lifter life have been two factors that most mill operators focused on because they affect mill availability directly (Powell *et al.,* 2006). Rezaeizadeh *et al*, (2010) allude to the different approaches that have been investigated in trying to increase the longevity of lifters. These factors include increasing the lifter height, changing the lifter release angle, decreasing the number of lifters, increasing the charge level, decreasing the mill speed and using high-low lifter configuration.

Mill liners are fitted to the mill shell to protect the shell from hard impact and any contact the charge may have with the shell (Powell *et al*., 2006). Although, this is the main aim of fitting them, they have also been known to influence the performance of the mill, which was believed to peak after the mid-point in the liner life and then decrease as the liners are worn (Rogers *et al*., 1982). Rogers *et al*., (1982) performed work using a mill with a diameter of 0.91 and a length of 1.52m using different liner designs (displayed in Figure 9). The following were highlighted from the study by Rogers et al., (1982):

1) The design that favoured more cascading within the mill led to better energy efficiency as a result of the mill being used to break down a feed that was already relatively fine.
2) If the mill had been operated to break a coarser feed, the more energy efficient liner design would have been one that favoured cataracting.
3) The need to design the liners and lifters with a good knowledge of the grinding media is important.
4) Knowing whether the feed material is going to be coarse and to which degree the particles are to be ground to is an important factor to consider when deciding on the type of liner design and material of construction.

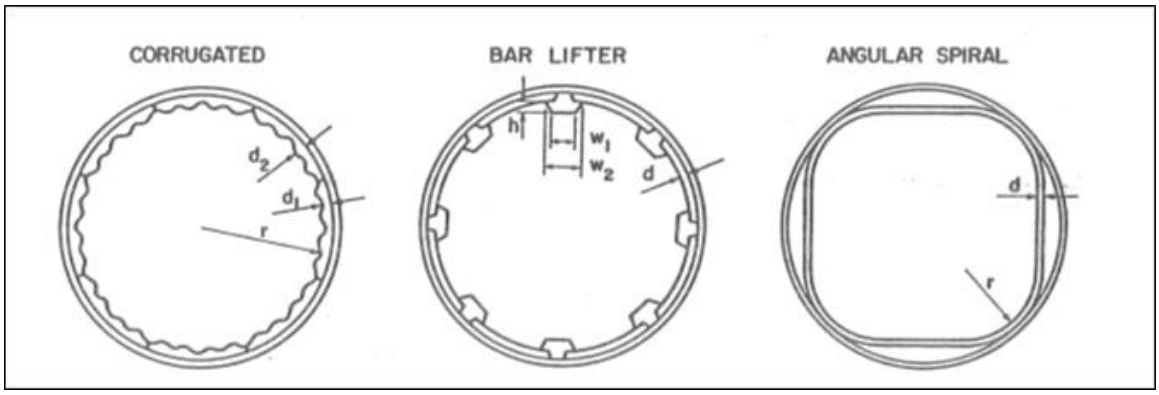

Figure 9: Cross sectional view of the corrugated, bar and angular spiral lifters used in the study (After Rogers et al., 1982)

In their experimental work, Rezaeizadeh *et al*., (2010) used a 3D mill, lined with equally spaced lifters of differing number of rows (15, 30, and 60), load levels (10, 15 and 26 %) and a lifter face angle of 14.5 ˚. The speed was varied up to 200% of the critical speed and pictures of the mill load were taken at 60 and 1200 frames per second (fps) to monitor the motion of the load. The results obtained from this study showed that for the lower lifter heights, mill power increased to a stable value with an increase in the number of lifters.

Liners are also fitted to the mill shell to transfer the rotating motion of the mill to the charge and grinding media (Powell *et al.,* 2006). Liners are made using different materials of construction depending on factors such as; the type of ore used (is it abrasive), size of balls and the mill and the mill speed. Material construction varies from High Carbon Chrome Moly Steel (325 to 380BHN) which is usually used for SAG mill liners, with varying carbon and chrome contents to Chrome Moly White Irons (600 to 700BHN) WI which is used mostly in some of the largest ball mills in the world (Powell *et al.,* 2006).

Rubber liners (or more formerly referred to as “elastomer”) have also been used, and in the past, they have been used in secondary and regrind milling applications (Powell *et al.*, 2006). With recent advances in modelling and computer aided design programs, rubber liners are now finding use in primary grinding applications (Powell *et al.,* 2006). It is said that a good rubber liner should be able to stretch from 5 to 6 times its length

without considerable damage. To ensure that the rubber liners are used most efficiently, they are designed to have a 90 ° degree impact (Powell *et al.,* 2006).

Powell *et al.,* (2006) have also shown that composites of rubber and steel liners have also been used as shown in Figure 10. The composite can be made of metal lifters and rubber plates; where over the years improvements have been made where metal capped rubber lifter bars are being designed. The advantage of using these composites lies in the fact that they each have different wear characteristics and therefore, for the life of the liner it will maintain its profile.

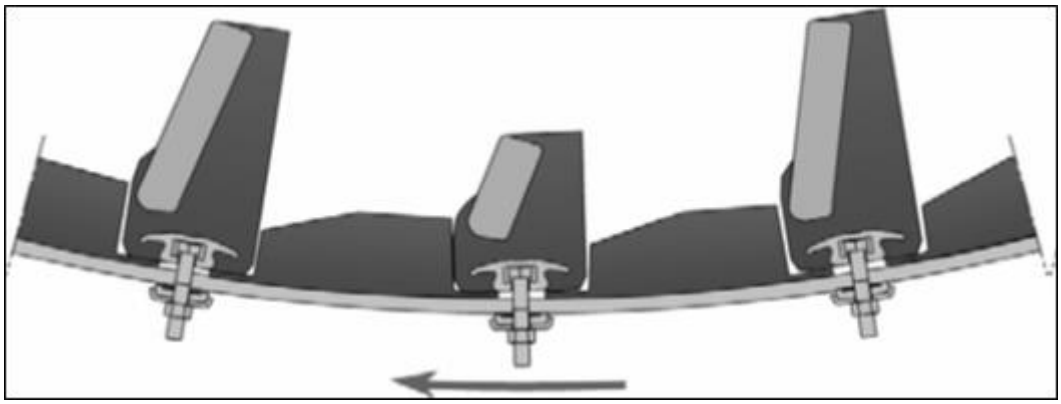

Figure 10: A figure showing the metal capped rubber liners (After Powell et. al., 2006)

Furthermore, Powell *et al.,* (2006) have shown that magnetic liners have also been used, where the lining system consists of permanent magnets embedded in a rubber moulding. It is the magnets that help keep the lining in place without the use of bolts. Unfortunately, the magnets are quite brittle and are affected by the impact of the grinding media.

Liner wear

Lifters have been known to assist with extending the liner life by acting as a cushion from the hard impacts of grinding media and ore (Rezaeizadeh *et al*., 2010). With prolonged exposure and contact to the grinding media, the lifters will become worn and the face angle alters. Thus, wear can be described as the loss of material due to this contact and frictional interactions (Rezaeizadeh *et al*., 2010), where a 10 to 20 % loss in mass deems the liner unusable and ready to be changed (Makokha *et al*., 2007).

Makokha *et al.,* (2007) have suggested the use of detachable lifters should aid decreasing the costs associated with the cycle of the liner life. The authors suggest that these detachable lifters would be more exposed to the load; therefore leading to an increased wear rate. Although this could lead to a decrease of life of the liner, these detachable lifters would be cheaper. Figure 11 illustrates the relationship between the liner life and performance with the optimal extension of the life when using the detachable retrofits.

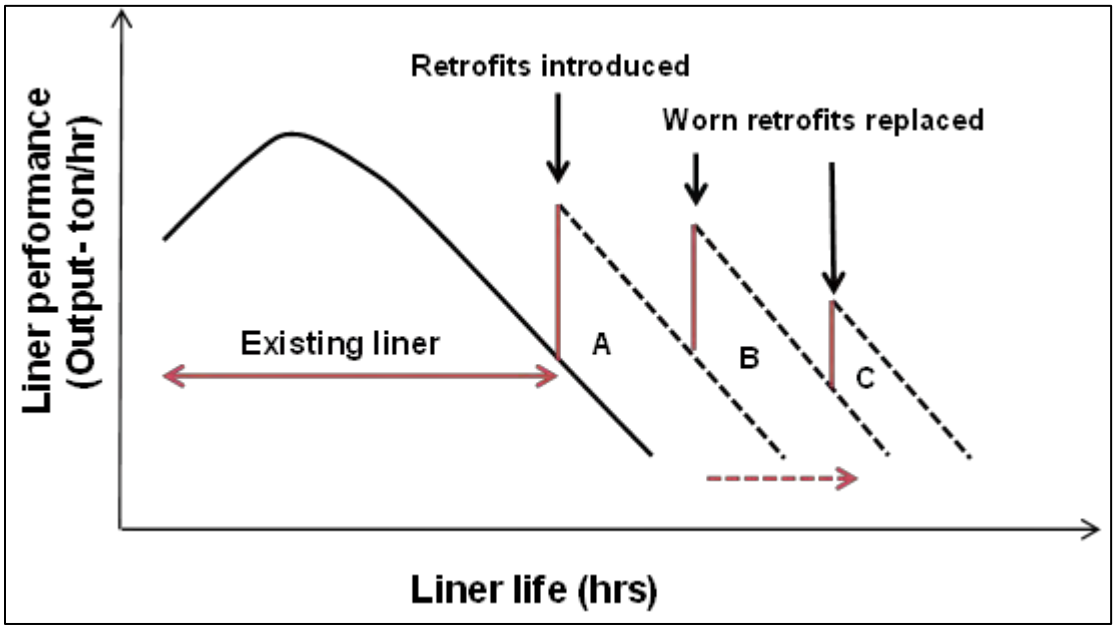

Figure 11: A schematic showing the relationship between liner life and liner performance as well as the liner life path when using detachable lifters (retrofits). (After Makokha et al., 2007)

This work performed by Makokha *et al.,* (2007) used DEM to predict the charge motion in an attempt to evaluate the interaction between the lifters/liners with the charge. Using DEM creates room for liner designers to improve on the existing liner/ lifters configurations.

This concept of prolonging the life of the liner is echoed in the work conducted by Kalala *et al*., (2008). Figure 12 demonstrates how the liner life can be extended by merely tilting the liners by 50 mm. Initially the unworn liners had a height of 110 mm, whereas the worn liners had a height of 80 mm. With the addition of 50 mm bars to raise this height, the liners are essentially sitting on top of each other. Observations made after doing this

showed that the throughput was restored; however this led to an increase in the ball wear rate. This observation was attributed to the fact that as the liners wear, the charge was sliding more and this resulted in a decrease in the tangential velocity of the balls. Thus, the tilting of the liners helped to increase this velocity as the sliding effect was reduced.

Further, Kalala *et al*., (2008) indicated that liners have a direct influence on high energy impacts of the charge and grinding media on the mill shell. They defined the cumulative energy as shown in Equation 4.

$$\boldsymbol{E_i} = \sum_{i=1}^{n} \boldsymbol{f_i}\, \boldsymbol{I_i} \qquad \text{Equation 4}$$

Where f_i is the frequency of collisions and I_i is the impact energy. From Equation 5 they concluded that the total cumulative energy dissipated in collisions between the balls and the liners decreased, suggesting that there is less total energy available in the mill as liners begin to wear. This would make sense in cases where impact breakage was a major contributor of the overall energy, since worn liners would not result in lifting the charge as high as new lifters would.

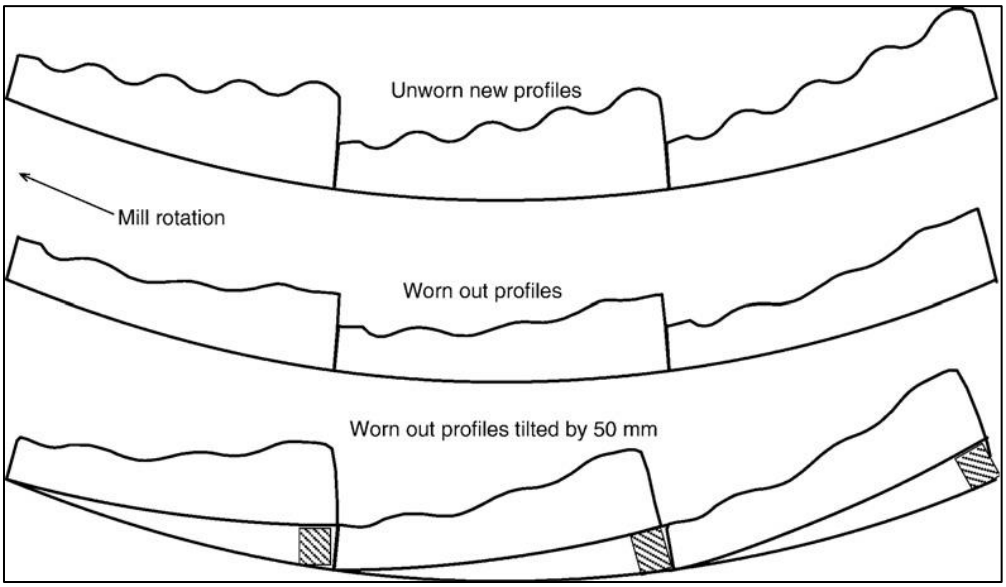

Figure 12: An illustration of liners in a mill after being tilted to increase the liner life (After Kalala et al., 2008).

A study was conducted by Toor *et al*. (2013), in order to quantify the advantages of using liners with shorter life cycles in order to improve performance. Data from the 32

foot SAG mill at Cadia Valley Operations was used and the results showed that the liners with the shorter life cycle exhibited better performance, throughput and product size than the liners designed to have a longer life. With the wearing of the liner, the throughput increased from 650 tph to 730 tph (equating to a 12 % increase).

New lifters tend to lift the charge higher resulting in more high energy impact breakage (cataracting) of the coarse material. This is the converse for the worn liners which are believed to favour cascading of the charge, which encourages abrasion and attrition, leading to a finer product size. Figure 13 compares the breakage rates of the new and fully worn (with interpolated intermediates) liners.

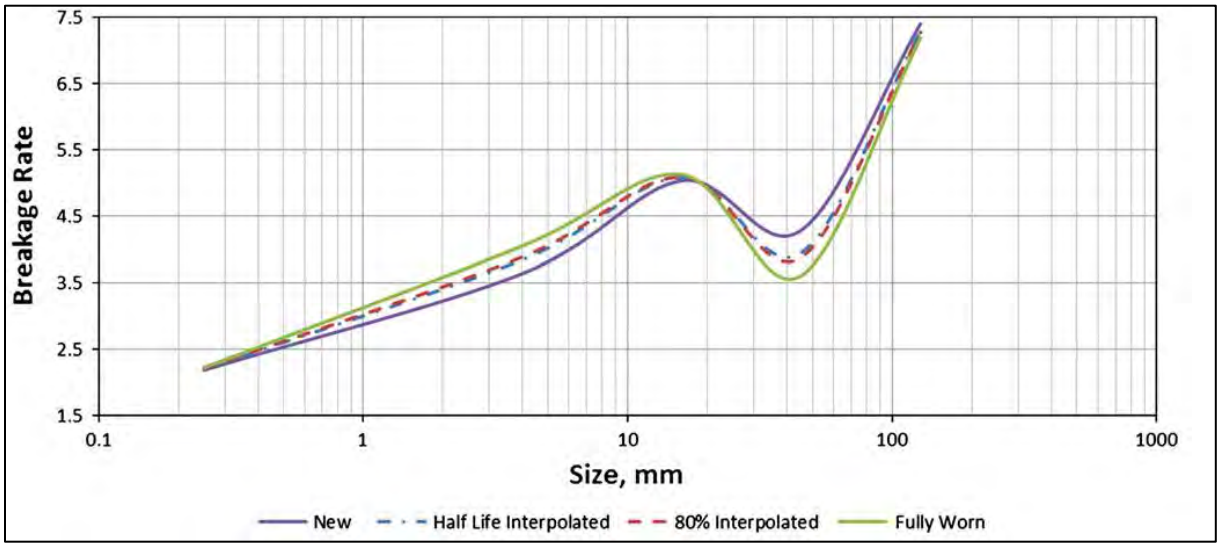

Figure 13: The SAG breakage rates over the liner life (with intermediates interpolated) (After Toor et al, 2013)

The results show that at the smaller particle sizes, the breakage rates are higher for the fully worn liners, but the converse is evident at the larger particle sizes. It can be concluded that in this case, the throughput was directly linked to the condition of the liner.

It is worth noting that it cannot be inferred from these results that high energy impact leads to a lower throughput in all operations since variables such as the grate discharge, residence time and feed size need to be taken into consideration. In this work, the aim was to show that installing liners which are less cumbersome and with shallower angles,

led to increased throughput. But, ultimately this needs to be weighed up against the economics of having to shut down in order to incorporate frequent relining schedules.

Lifter Face angle

Another important parameter when considering the lifter and liner influence on charge behaviour is the lifter face angle. The lifter configuration can have an effect on the operation of the mill by influencing the motion of the charge and ultimately the transport and breakage mechanisms in the mill (Makokha *et al*., 2007).

Hlungwani *et al*., (2003) investigated the effect of changing the face angle on power draw. A 0.55 m diameter mill with length 0.0235 m was used, which was constructed from glass on the front end where charge motion and load behaviour observations and photographs were taken. They used twelve of each of the two types of lifters; square lifters with a cross-section of 22 × 22 and trapezoidal lifters with dimensions of 24 (bottom) × 8 (top) × 22 (height). The square lifters were used to represent unworn or new lifters whereas the trapezoidal lifters represented worn lifters. Figure 14 demonstrates the dimensions of the lifters used in the study. Load levels of 25, 35, and 45 % were used with varying speeds up to 200 % of the critical speed.

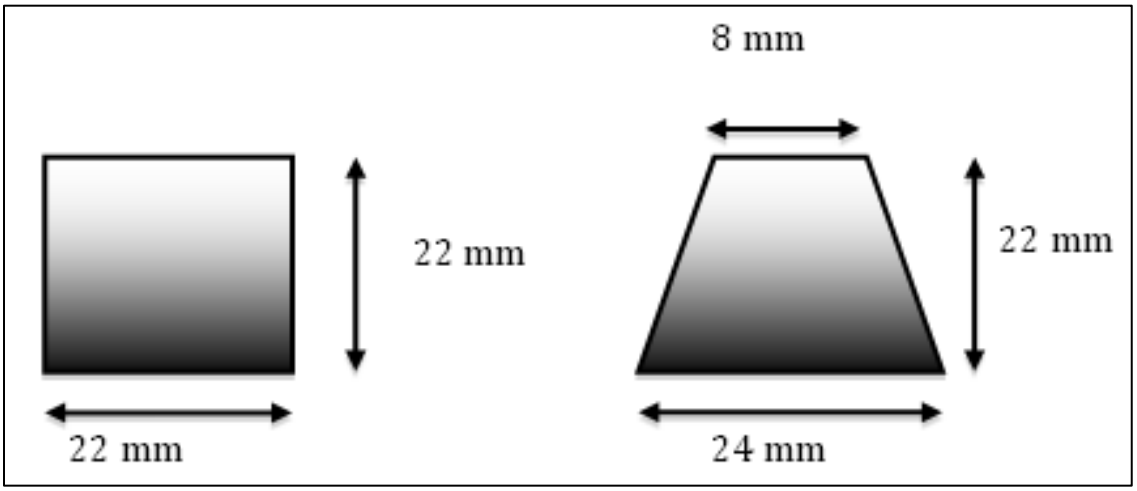

Figure 14: Cross sectional view of the lifters used. (After Hlungwani et al., 2003)

The effect of the different lifter profiles showed that for speeds below critical speed, the trapezoidal lifters drew more power than the square lifters suggesting that the best operating conditions for new lifters (square lifters), does not take place at normal speed (80 % of critical). A plausible explanation for this could be the fact that the square lifters

would project the charge further into the cataracting region, once again highlighting the importance of designing lifters with an understanding of the milling requirements.

At Gol-E-Gohar iron ore concentration plant, three 9 m × 2.05 m dry operating AG mills are used in parallel, but for the purpose of the experimental work, a 100 cm x 3.6 cm mill was constructed and operated using a 2.5 kW motor with a variable speed drive. The lifters, shown in Figure 15 were designed to emulate those in the actual mills and the specifications of the liners are shown in Table 1.

Figure 15: Liners fitted into the lab scale mill for the Gol-E-Gohar concentration plant (After Maleki-Moghaddam et al., 2012).

The aim of this research was to convert the existing AG mills to SAG mills in order to improve the grinding, efficiency and decrease the sulphur content of the concentrate. This was going to be achieved by increasing the degree of liberation of the sulphur bearing minerals.

Increasing the lifter face angle (keeping the lifter height at a constant 22.5 mm), the throughput increased by 27 % whereas the product size decreased from 515 to 501 micron.

Table 1: Specifications of the liners used at the Gol-E-Gohar concentration plant (*After Maleki-Moghaddam et al., 2012*)

Plate thickness (mm)	Lifter			Lifters in row	Number of rows
	Face angle (°)	Height (mm)	Width (mm)		
75	7 – 30 °	22.5	125	3	36

The study also showed that before increasing the face angle, the charge was not hitting the toe region, leading to very little breakage occurring in this region. Under these conditions, the difference between the point of impact of the balls and the position of the toe was determined to be 55 °.

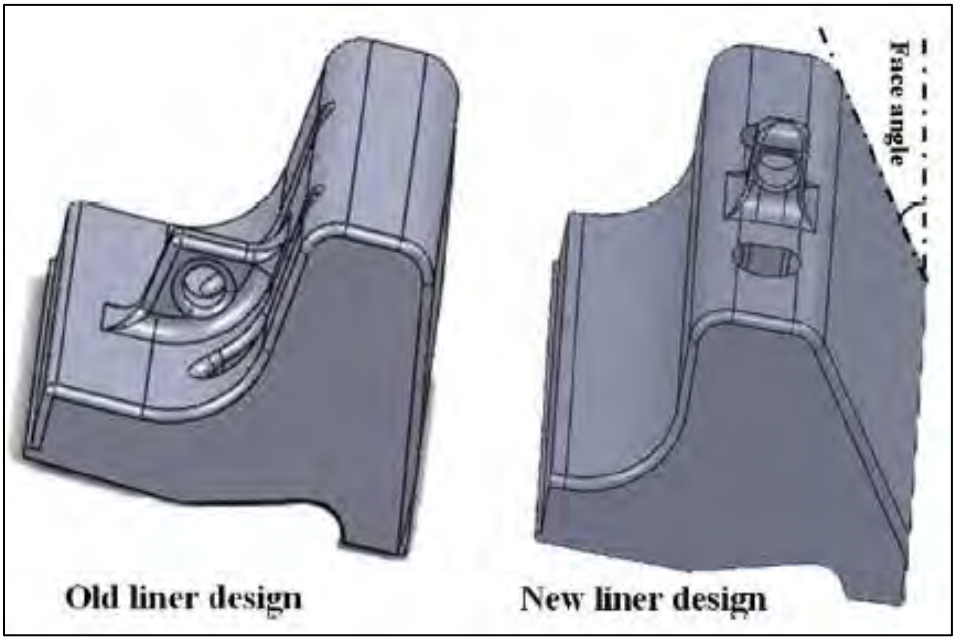

Figure 16: A comparison of the old and the new liner design used at the Gol-E-Gohar plants. (After Maleki-Moghaddam et al., 2012)

With the increase in face angle from 7 to 30°, the distance between the impact point and the toe position, decreased from 55 to 14° and 63 to 22° at charge filling of 24 % and 18 % respectively. Figure 16 shows the two types of liner designs with the face angle being measured from the vertical. This once again reinforces what was found by Hlungwani *et al.,* (2003). Indeed it seems that there is some advantage gained from "worn liners" or liners whose face angle is not steep especially in increased liner life and mill performance as well as decreased ball breakage.

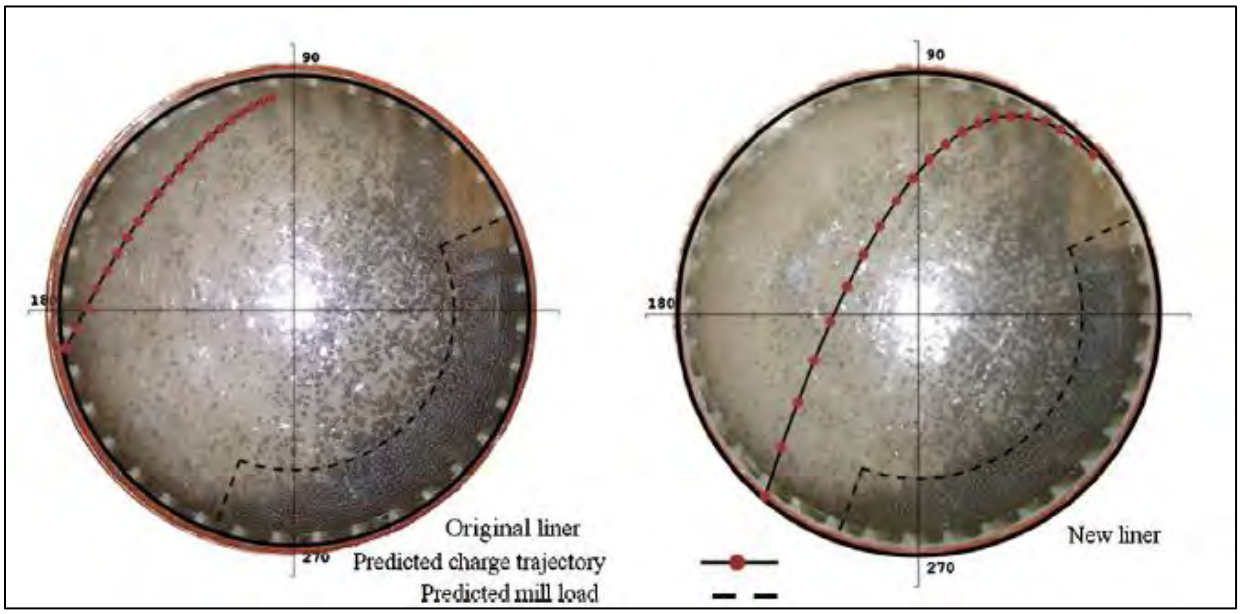

Figure 17: The shape and trajectory of the charge with the original (left) and the new (right) liner at 20 % filling. (After from Maleki-Moghaddam et al., 2012)

Lifter height and spacing

The spacing to height (S/H) ratio of lifter bars is an important design criterion, which is heavily dependent on mill speed. Since packing of charge between the lifters is undesirable, adequate spacing has to be made in order to reduce this effect especially in SAG / AG and primary ball mills. The A/B ratio which is a ratio of the shell plate (A) and lifter height (B) developed by Skega as an empirical formula for this ratio is now widely used. The S/H ratio varies as the liner wears; therefore goes from a low value to a high one with the replacement of the liner. The relationship between the liner spacing to mill throughput and power draw is illustrated in Figure 18.

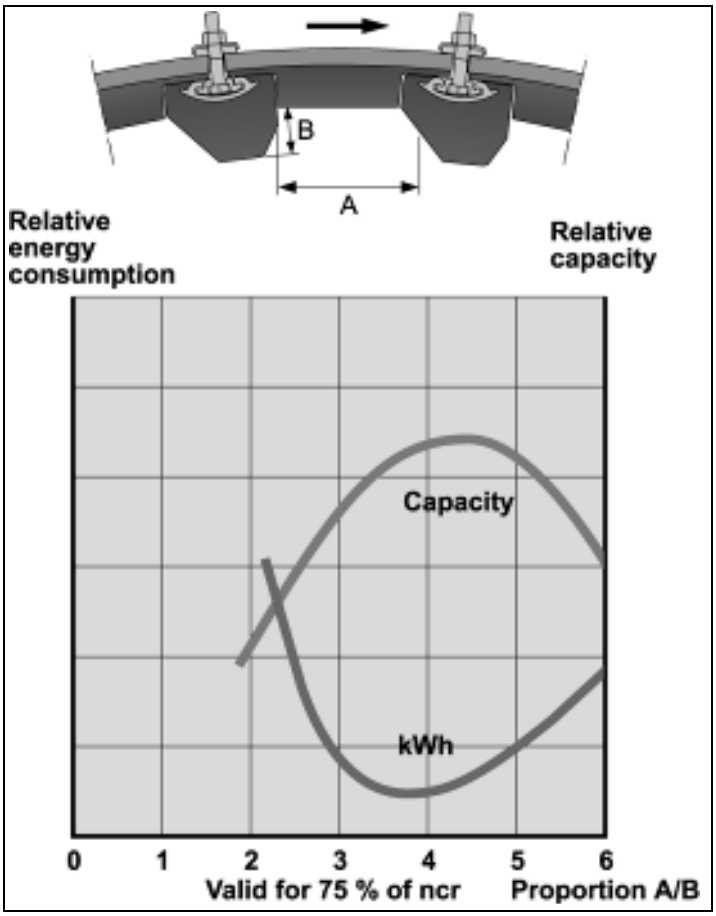

Figure 18: The Skega A/B ratio as related to mill capacity and throughput. (Powell et al., 2006)

The effect of lifter bars in a tumbling mill was investigated by Hong and Kim (2002). In their experimental work, they used a stainless steel container of 150 mm inner diameter, 50 vol % charge, and 16 mm diameter steel balls. The number of steel bars was varied from 1, 2, 4 and 8 at different speeds. Results of the study showed that an increase in the number of lifters lead to a decrease in the sliding action of the charge, but an increase in the centrifugal motion.

It would be expected that extended centrifugation would lead to increased wear on the liners as the charge media would be in contact with the liners for a long period. Using different arrangements for spacing alters the packing between the lifters. The “Hi-Lo” lifter configuration has been used (where a high and low lifter alternate around the mill) and the packing between the lifters was noted to increase to the level of the lower lifter bar. The packing decreased since the low and high lifter heights decreased at almost the

same rate resulting in the impact point of the charge being predominantly found in the toe region.

From their PhD work, Powell (1993) showed that there exists a critical lifter height, which is dependent on the speed and the face angle. It was noted that above this critical height, balls will generally follow the same trajectory independent of the lifter height. This was attributed to the fact that the balls were projected off the face of the lifter before reaching the tip in the case of lifters whose angle is close or equal to 90 °.

2.3.2 Mill speed

The mill critical speed has been defined by McIvor (1983) as "… that rotational speed at which an infinitely small particle will centrifuge, assuming no slippage between the particle and the shell."

When traveling inside a mill, any given particle will follow a distinct path. When it is closest to the mill (from toe region to shoulder region) and the mill is rotating in an anti-clockwise direction, the particle will initially follow a circular path as shown in Figure 19. When it falls from the shoulder back to the toe region it follows a parabolic path.

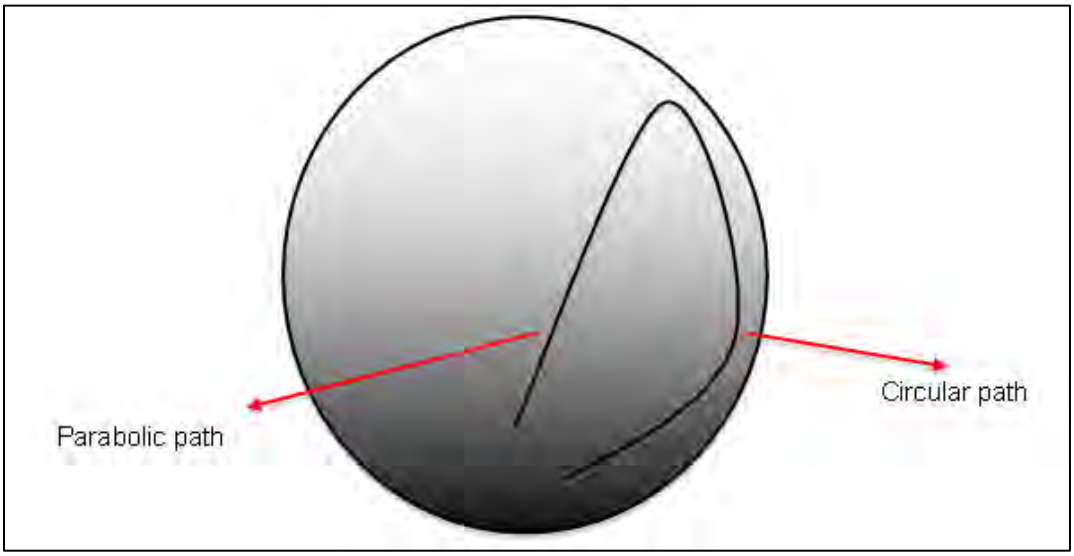

Figure 19: Trajectory of a particle in tumbling mill (After Wills and Napier-Munn, 2006).

Research conducted by Cleary (2001) using a 5 m diameter mill and filling of 40 % showed that an increase in mill speed led to a change in the charge behaviour. The study demonstrated that at a fraction of the critical speed; N = 60 % the charge moved with the rotation of the mill to the shoulder region. An increase in the speed to 70 %

resulted in the rise in the shoulder region, which moved the toe region lower. Further increase to 80 % of the critical speed led to an increase in the cataracting region, with a further decrease in the toe region. The results showed that an increase in mill speed causes the particles to be trapped between the lifters and thus centrifuge (barely leave the mill wall), leading to increased wear of the liners.

Cleary (2001) also demonstrated the effect of coupling mill speed and different lifter configurations on power draw; namely “hi - lo”, “hi - hi” and “hi - blank”, where the “hi - blank” refers to omitting every second lifter. This led to an increase in spacing between the lifters. Removal of this second lifter resulted in less cataracting and an increase in the toe region as well as more energy input for higher speeds.

It is evident that mill speed has great bearing on the wear of the liners. According to Nillson (1979), the wear of liners has been approximated to be proportional to the square of the mill speed. This is confirmed by the fact that smooth lining requires higher speeds to achieve the same grinding observed when lifters are fitted.

In an attempt to demonstrate which operating conditions would lead to cascading or cataracting, Figure 20 shows that when mill filling is a function of the mill speed, the relationship is non- linear, but rather increases exponentially. Fortsch (2006) has shown that although it is beneficial to operate in the cascading region as this will lead to higher grinding efficiency, there could be a disadvantage to having solely cascading motion as the charge could become stagnant. Similarly, operating solely in the cataracting region would have adverse effects on the mill shell and decrease the probability of beneficial collisions of the charge. This further emphasises the need to design and operate mills with a better understanding of the expected motion of the charge.

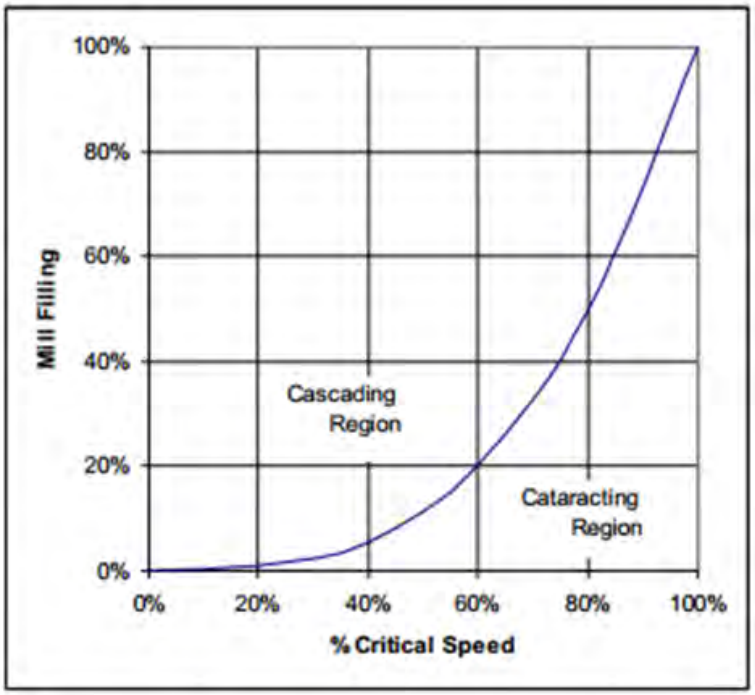

Figure 20: Cascading and cataracting regions with respect to the mill filling and speed (After Fortsch, 2006)

The work done by Hlungwani *et al*., (2003) investigated speeds beyond 85 % of the critical and it is at these higher speed settings that the power began to decrease as a result of the keying of the charge as centrifuging is experienced. The square lifters are more likely to encourage keying of the charge than the trapezoidal lifters, but in both cases further increase of the mil speed led to drastic decrease in the power as shown in Figure 21. Again, this demonstrates the importance of mill speed as a variable that affects the power consumption in tumbling mills.

In their work Govender and Powell (2006) developed a power model using 3D tracking in the form of an X-ray system. They used a 142 x 142 mm Perspex mill filled up to 40 % with 6.1 plastic beads. The basis of their model was to extend the torque-arm principle by relating the position of the Centre of Circulation (CoC) to the radial and angular positions of the centre of mass (COM). They related the power drawn by the charge using Equation 5.

$$Power = MgR_{COM}\cos(\theta_{COM})\,\omega \qquad \text{Equation 5}$$

Where *M* is the mass of all the charge in the mill (includes the cataracting and cascading charge)

g is acceleration due to gravity

R_{COM} is the radial position of the centre of mass of the charge

θ_{COM} is the angular position of the centre of mass of the charge

ω is the rotational speed of the mill

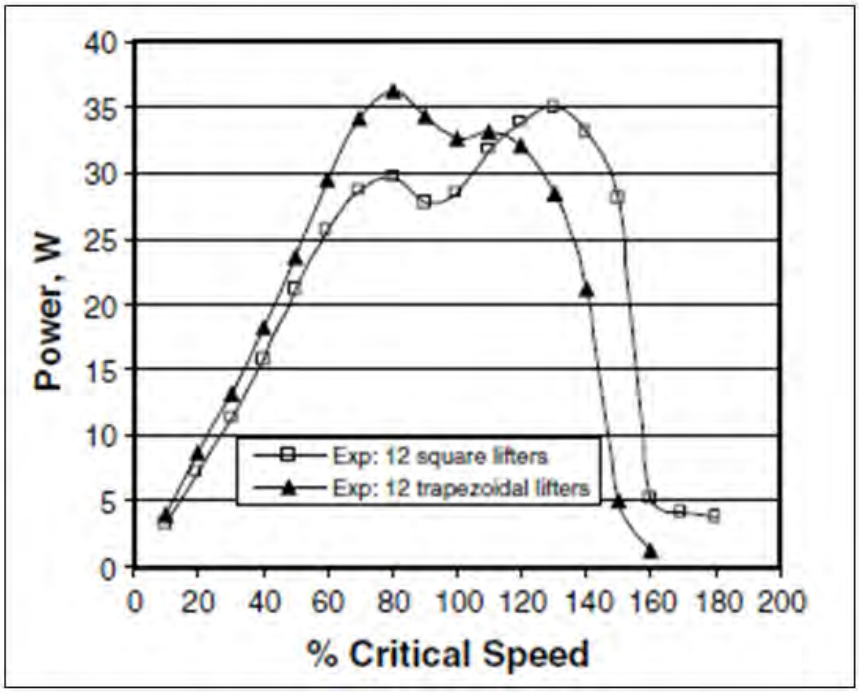

Figure 21: Experimentally measured power draw for square and trapezoidal lifter bars at 35 % filling (After Hlungwani et al., 2003)

2.3.3 Charge filling

The observed trend when considering the effect of charge filling is that a decrease in the filling will lead to a decrease in the cascading region within the mill. Cleary (2001) noted that a decrease of load at relatively constant velocity, leads to more shear action within the charge, thus better grinding is achieved. For even lower charge depth, more particles were projected into the cataracting region leading to increased wear on the mill liners.

This finding is of importance for this work since it gives an indication of the relationship between the charge filling levels and the possible resultant trajectories of the charge. It also provides insight (given a certain charge filling degree) as to what design of lifter face angle would lead to attrition, abrasion or impact breakage.

These results can be directly compared to the results obtained by Cleary (2001), where he used DEM to show the effect of lifter profiles, fill level, particle size, shape distribution and mill speeds ranging from 50 to 130 % on power draw (as seen in Figure 22).

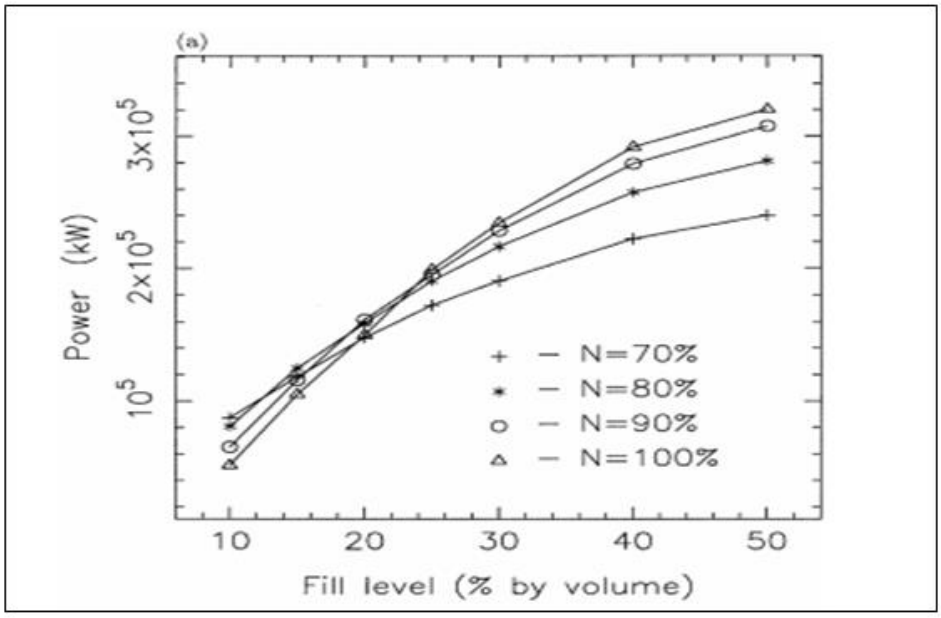

Figure 22: Effect on power with charge filling with charge filling for square lifters at different mill speeds (After Cleary, 2001)

2.4 Positron Emission Particle Tracking (PEPT)

Positron Emission Particle Tracking (PEPT) is a technique, which has been developed to track a single particle, which has been labelled with a radionuclide. PEPT was adapted from Positron Emission Tomography (PET) which has been used in medicine to determine body metabolism and drug design development (Fan *et al*., 2006). One of the main differences between PET and PEPT is that the former uses fluid tracers (Bridgewater *et al*., 2004). PEPT has proven to be a useful method in studying the behaviour of engineering related systems such as granular material in mixers and fluidised beds (Parker *et al*., 1997). The limitations that existed with regards to investigating opaque systems and observing flow phenomena in three dimensions are

overcome with the use of PEPT (Barigou, 2004). About 50 % of the energy emitted from the labelled particle is able to penetrate through 11 mm of steel or 30 mm of aluminium, showing that PEPT can be used to investigate motion within vessels which have previously been deemed to have thick walls (Bridgewater *et al.,* 2004).

2.4.1 Particle labelling

A single particle labelled with a radionuclide (^{18}F, ^{64}Cu, or ^{68}Ga) is placed into a system before tracking is begun. This particle is called the "*tracer*", and is chosen such that it has the same properties as the bulk particles (Fan *et al*., 2006). Information gained from tracking and observing the behaviour of this single particle, can be used to infer the behaviour of the bulk particles (Barigou, 2004).

Before particle tracking can take place, a positron (β^+) is emitted and once it comes into contact with an electron cloud, annihilation takes place. Upon annihilation, two back-to-back gamma (ɣ) - rays are released each travelling at 180 ˚ with energy of 511 keV (Barigou, 2004). Figure 23 shows a schematic of the PEPT process as two back-to-back ɣ - rays are detected. When the gamma rays are detected in coincidence, the two detection points form a line of response (LOR). This LOR is an indication that the event took place along the line. As more and more of the LOR's are mapped, tracking of a single particle is made easier since the LOR's are recorded in chronological order (Cole *et al*., 2012).

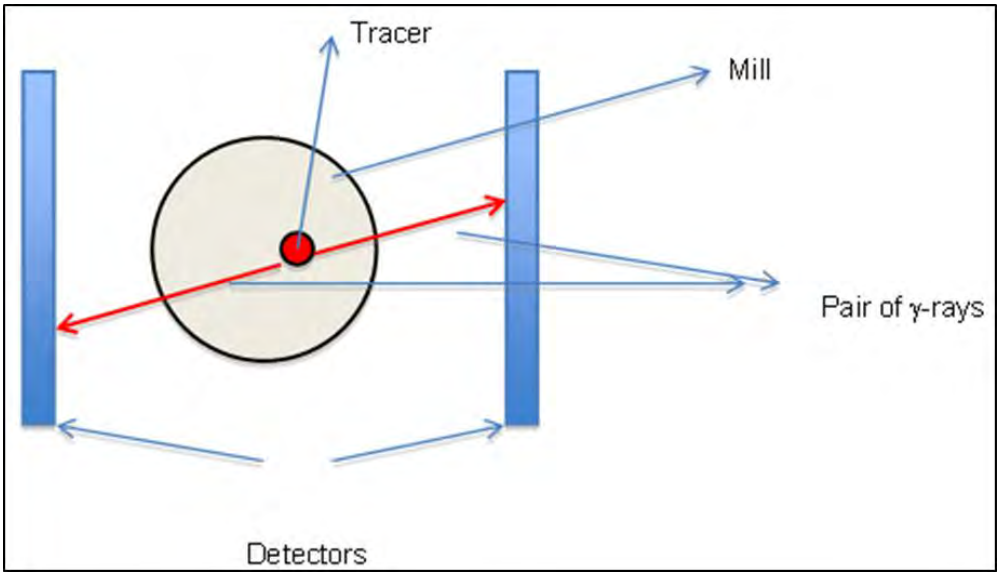

Figure 23: Schematic of the PEPT method used to detect the particle position (After Sichalwe et al., 2011).

2.4.2 Triangulation

Due to the fact that several events can be detected by the camera, a certain number of detected events (*N*) can be chosen for the purpose of analysis. Further, a certain percentage of the events (*f*) can be chosen in order to work out the triangulation of particles. An iterative algorithm is used to calculate the *centroid* and discards any lines that pass too far from the centroid. This *centroid* is defined as the point that minimises the sum of the perpendicular distances to all the lines (Bridgewater *et al.,* 2004). Thus, if the outliers are discarded correctly, then the precision of locating a stationary tracer is given by the expression $\omega/\sqrt{fN}$ (Bridgewater *et al*., 2004), where *ω* represents the spatial resolution of the camera. In the case of a moving tracer however, *N* is set to be large enough to provide adequate precision, but it is not too large that the tracer moves too far during tracking measurements.

This phenomenon can occur several times per second, allowing for many lines to be detected as seen in Figure 24. However, as shown not all the lines produced are used in the analysis, since it is expected that there will be some outliers and only a fraction of these lines are used for further analysis. Figure 24 a) shows the lines of response before the outliers have been removed, whereas Figure 24 b) demonstrates the triangulation after discarding of these lines.

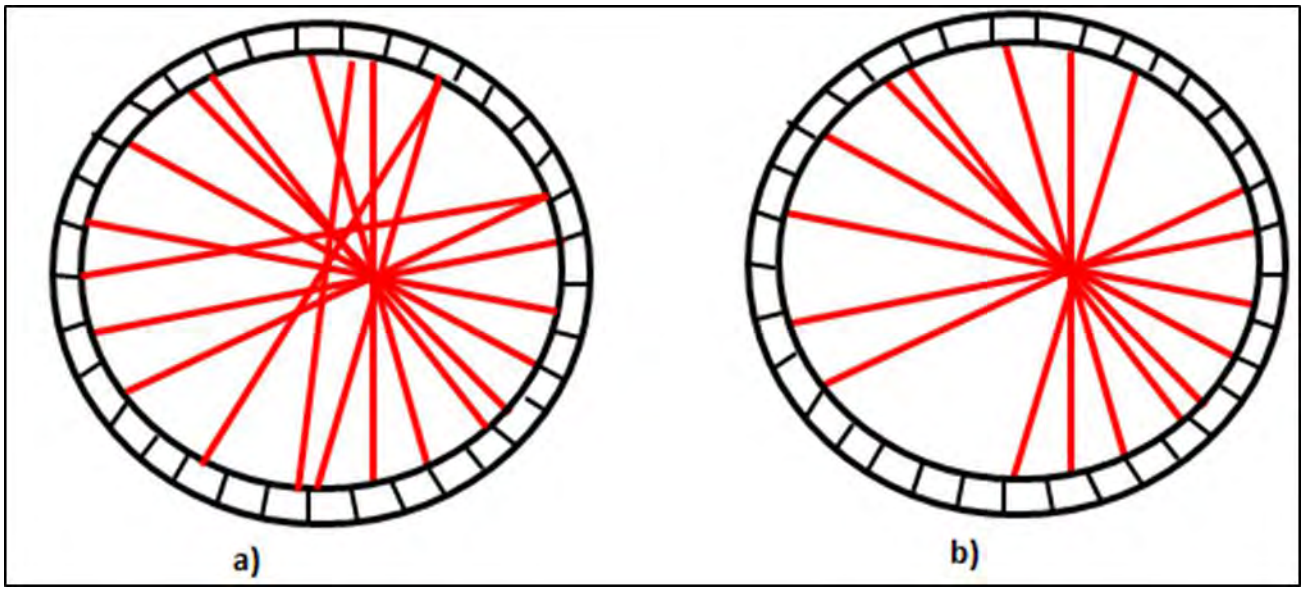

Figure 24: Schematic of triangulation of the particle using several lines as seen in rotating drum.

2.4.3 Correcting noise/ scatter

The cause of scattering in PET was seen to come from the interactions of the gamma rays with the medium, which caused the rays to change direction and energy (Shao and Karp, 1991). Thus, it made it increasingly important to have a uniform medium around the point source, which would force the scatter to occur isotropically (having the same value when measured in different directions). Shao and Karp (1991) showed that a point source scattering profile with an ideal detector system would be as illustrated in Figure 25, where the scattering profile is similar in all planes.

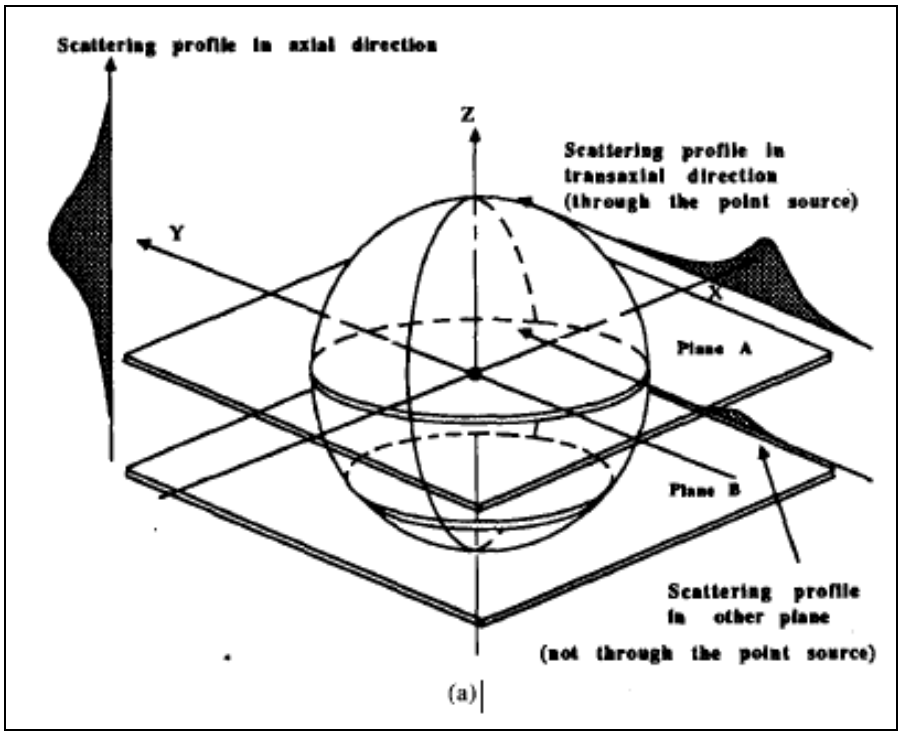

Figure 25: Scattering profile of an ideal detector system (After Shao and Karp, 1991).

In an attempt to reduce scatter and noise, Koral et al., (1986) investigated the asymmetric windows about the photo peak, Bergström *et al.,* (1983) conducted work to test the use of a measured line source response function to deconvolute the scatter events. However, the work done by Bergström *et al.,* (1983) only considered the average cross-plane scattering, making this method only plausible when all the planes of the PET data possess the same distribution. Further work was also done using the Monte-Carlo simulation by Logan and Bernstein, (1983) and convolution subtraction by Axelsson *et al*., (1984).

Shao and Karp (1991) realised that most of the solutions to scattering had been focused on the assumption that the events for a single transaxial plane would be independent of any axial variations. They then went on to show that this was inaccurate as it leads to the omission of the cross- plane scattering. Shao and Karp (1991) proposed a new point source scattering deconvolution method (2D), where scattering is dependent on both axial (*z*) and transaxial (*r*) directions. This was done by using both computer simulations and experimental studies (where the data was recorded at low count rates to reduce the random coincidences), and the scatter fraction was defined as the ratio of the scatter events to the true events. The limitation of this method was that it did not use an iterative technique for the 2D deconvolution. Further, the decay constants and scale factors used for the analysis were not varied with position (rather averaged values were used), which led to inaccuracies.

Bailey and Meikle (1994) also attempted to resolve the issue of scatter in PET cameras as it has been the focus for a number of years. Their approach was steered away from 2D methods and towards 3D acquisition and reconstruction in PET. An illustration of scattered events in PET is shown in Figure 26, where it can be seen that scatter events can be recorded beyond the object due to the dual-photon nature of PET.

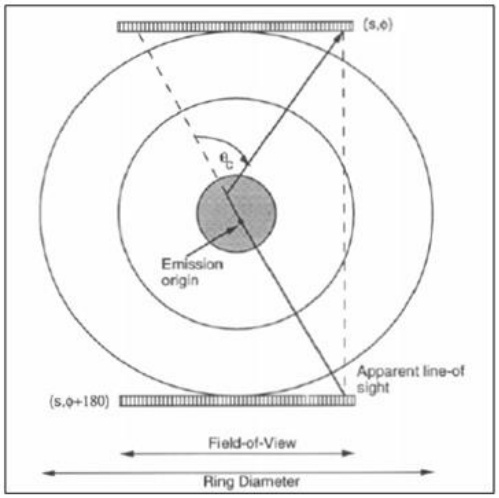

Figure 26: Geometry of scattered coincidences. The angle θ_c represents the Compton scattering angle (After Bailey and Meikle, 1994)

Bailey and Meikle (1994) proposed a scatter correction method, where an estimate of the scattered photon distribution is subtracted from the data before reconstruction for PET 3D data. The measurements were conducted using a whole-body tomograph (CTI-

Siemens 951R), which is comprised of 16 rings of detectors. The ring diameter was 102 cm and the measurement of the scatter correction was based on the 2D projections obtained from reformatting the 2D sinograms to 2D projections.

Although, the method managed to confirm what was found by Shao and Karp, (1991), which is that the scatter function and fraction both vary with position in a constant attenuating medium. However, the spatial variation of scatter was only investigated by placing a line source at various radial distances in a uniform cylinder.

2.4.4 3D PET camera

The 3D PET camera was developed out of a growing need to maximise the signal-to-noise ratio in imaging and yet still have high spatial resolution for a given unit of radiation exposure (Spinks *et al*., 2000). The ECAT EXACT3D (model 966, CTI) has been designed with the sole intention of improving data quality, and obtaining high spatial and temporal resolution PET data. As a result, the camera has been designed with a larger field of view (FOV) in comparison to other commercial cameras. The increased FOV is advantageous as it allows for higher overall efficiency and sensitivity.

The data acquisition system has the ability to store data in both list and frame modes, where the former was not a standard manufacturing option but has proven to be an important feature of the tomograph (Spinks *et al*., 2000). Some of the benefits of capturing the data in list mode include:

1. Efficient data storage
2. High temporal sampling
3. Flexible frame rebinning lengths
4. Increased flexibility for iterative image reconstruction routines.

The camera uses a single photon point source and the source consists of 150 MBq of 137 Cs ($t_{1/2}$= 30.2 years), and is the only moving part of the tomograph, making it increasingly more accessible for servicing in comparison to other cameras. Moreover, another advantage of using the EXACT3D is that the detector is much smaller in comparison to earlier designs, such as the ECAT 95 series and ECAT EXACT (CTI, Knoxville, TN).

A limitation of the EXACT3D camera is that it is designed to have a wider FOV in comparison to other models. To demonstrate this, the EXACT HR+ device has an axial FOV of 15.5 cm, which means that the points on the axis have a direct line of sight to the detectors of 33 cm from the edge of the FOV (Spinks *et al*., 2000). For the EXACT3D this distance is increased to 60 cm. Laforest *et al*., (1999), have shown that this can be reduced by additional side-shielding.

2.4.5 Uses of PEPT

PEPT can be used in different processes to provide both qualitative and quantitative information on velocity distributions and flow patterns in opaque systems. The food and chemical industry has found beneficial use of PEPT especially when dealing with opaque fluids as they tend to have intricate rheological properties, which tend to be time dependent. Bakalis *et al*., (2006) have shown that being able to experimentally and numerically determine the flow and thermal field of fluids is very important for better manufacturing practices. Complex units used for food manufacturing such as scraped surface heat exchangers (SSHE) and extruders, which can be used for the production of pasta, pet food and breakfast cereals make it difficult to accurately observe and determine the desired velocity profiles (Bakalis *et al*., 2006). Techniques such as discrete methods; finite difference by Chiruvella *et al.,* (1996), and magnetic resonance imaging (MRI) by Agemura *et al*., (1995) have been used. The shortfall of using MRI lies with the fact that the experimental equipment is unable to contain metal, highlighting that PEPT is a suitable method. Bakalis *et al*., (2006) showed that the velocity distributions in a specifically designed single screw extruder could be determined with the use of PEPT and numerical simulations. When compared to the 3D simulated results, the PEPT results were within statistical agreement, emphasising the power of using PEPT to describe complex flows.

PEPT has been used in the precipitation of aluminium hydroxide, which forms a complex precipitate of aluminium hydroxides and oxyhydroxides. This product exhibits non-Newtonian rheology, making it difficult to fully understand the effect of mixing parameters during this process. Edwards *et al.,* (2009) combined Electrical Resistance Tomography (ERT) and PEPT to investigate the effects of mixing parameters on the precipitation of aluminium hydroxide (AlOOH). In conjunction, these two methods can shed light on how the feed reactants become dispersed into the bulk reactant during semi batch

precipitation. On its own ERT is only able to provide information on the quality of mixing but not on the localised velocities, which can lead to an understanding of the flow field during precipitation. Gaining insight into the flow field is useful as it changes throughout the batch process function as it is a function of the filling level (Edwards *et al*., 2009). Once again, this is where PEPT is a useful tool as it provides this complementary information to ERT. The results of the study using an ^{18}F tracer, which was tracked for 45 minutes (with 5 minute incremental volume increase) to study the effect of volume change on the flow field showed that PEPT was able to adequately characterise the flow fields. This highlights that the uses of PEPT are expansive and adaptable to different industries.

2.5 What is missing in this body of research?

PEPT

The literature has shown that the tracking of a single particle in opaque systems has been studied extensively. There does however seem to be a gap in knowledge with regards to obtaining accurate tracking data for two or more particles without the tedious task of having to navigate and discard out-of-view scatter (Yang *et al*., 2007). The complexity of tracking more than one tracer is not only due to the difficulty of predicting their positions, but is dependent on the camera. For example the data logging rates can be significantly different when the tracer is in the centre and when it is towards the edges of the detectors. Should the weaker tracer be in the centre, while the stronger tracer is found towards the edges of the detectors, the stronger tracer will have a lower data logging rate in comparison to the weaker tracer (Parker *et al*., 1993). This shows that the tracer with the higher gamma ray density will not necessarily lead to a higher data logging rate resulting in inaccurate tracking data.

Previously, Yang *et al*., (2006) developed an algorithm that tracked the rotation of a large particle by tracking three small positron-emitting tracers, which were mounted on a surface at fixed distances. This method was valuable in determining the behaviour of granular materials in flow and mixing processes, but it was unable to track multiple freely moving particles as they were kept at a fixed distance (within 25 mm) at all times. Thus Yang *et al*., (2007) have proposed an algorithm for location calculation, gamma-ray density detection for particle identification and time reconstruction at every tracking step.

Furthermore, PEPT is limited in that test work is limited by the camera's dimensions. Although it is has proved to be a powerful tool for investigating flow patterns, it is not helpful if experiments cannot be performed to due to restrictions imposed by the camera's open area. Of particular interest in comminution, PEPT does not give direct information on collisions or breakage. Breakage mechanisms can only be inferred depending on the charge motion information obtained. This is why DEM is a good supplemental method to PEPT.

CHAPTER 3

3. RESEARCH APPROACH

The current study involved tracking the motion of a single particle within a bulk charge using the Positron Emission Particle Tracking (PEPT) system. This was followed by the data analysis, which involved post processing of the data using numerical methods program in MATLAB and interpretation of the results.

3.3.3 Experimental Apparatus

3.1.1 Mill description

For this work a mill constructed from high density polyethylene (HDPE) was used. Some of the advantages of using HDPE include its high impact and wear resistance, and more importantly good radiation stability. A picture of the mill used for the experimental work is shown in Figure 27.

Figure 27: The experimental mill made of HDPE

This 300 x 285 mm mill fits 20 lifters and had a variable speed motor, which allowed for speeds ranging from 25 to 180 % of critical speed to be tested. The mill was designed to fit within the field of view (FOV) of the PEPT camera without any obstruction to the camera's functionality. Figure 28 displays the mill as it was placed in the PEPT camera for this work. This shows the yellow trolley, which was used to support the motor and the attached torque sensor outside the FOV but the main cylinder of the mill completely within.

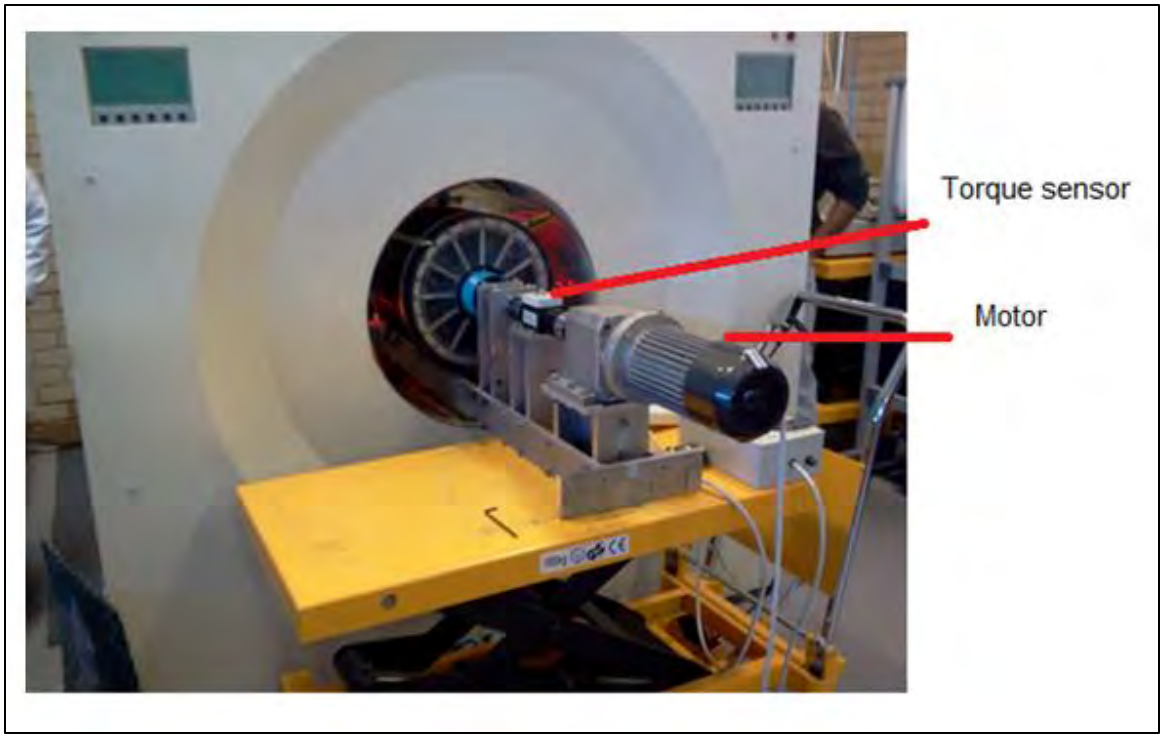

Figure 28: Mill placed in the PEPT camera

A 100 N torque transducer was attached to the drive shaft, which sent output signals to a computer in order to calculate the measured power draw of the mill as a result of the rotating mill. Further descriptions of this will be discussed in section 3.5.

3.1.2 Lifter bars

The lifters were machined in the Department of Mechanical Engineering at the University of Cape Town (UCT), with face angles of 75, 65, 55, and 45 °, a constant height and width of 10 and 12 mm respectively. The final angle investigated was 90 ° where the data was taken from Brodner (2013).

The lifters were machined out of aluminium with three 6 mm holes machined along the top of each lifter. The lifters were kept in place using stainless steel bolts, which were bolted onto the mill shell from the outside. **Error! Reference source not found.** is a schematic of the lifters with dimensions.

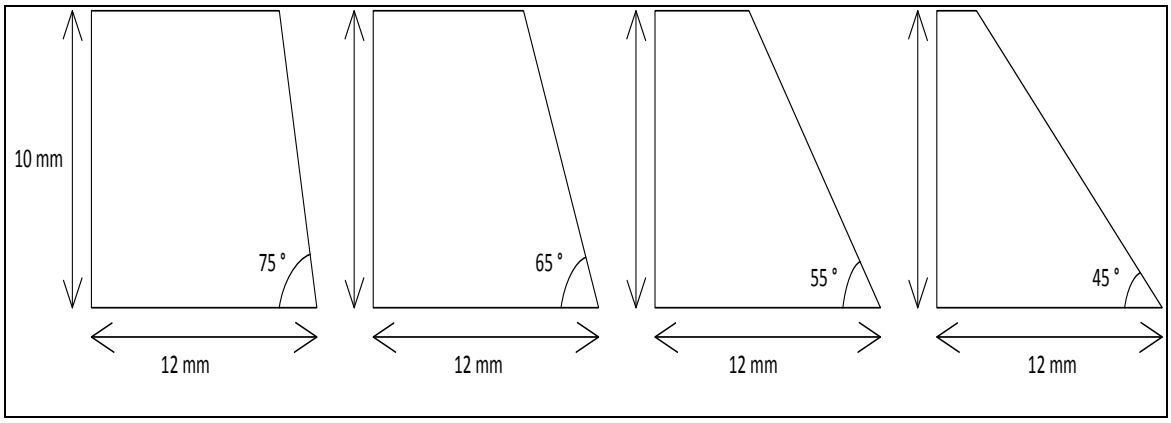

Figure 29 A cross sectional view of lifter bars in the mill.

3.1.3 PEPT experimental work

PEPT camera

For this test work, PEPT was chosen for its unique advantage of allowing the study of opaque systems. The ECAT EXACT3D (Model: CTI/ Siemens 966) camera shown in Figure 28 was used at iThemba labs. This camera was designed with the intention of enabling researchers to acquire high spatial and temporal resolution PET data (Spinks *et al*., 2000). It consists of detectors, which are sectioned into 8 x 8 elements per block, where each has dimensions of 4.39 x 4.05 x 30 mm^3 (with centre-to-centre spacing of 4.85 x 4.51 mm). There are six rings of blocks, giving an axial field of view (FOV) of 23.4 cm. This increased FOV is disadvantageous due to the increased scatter and random coincidence events, which can be reduced with the use of side shielding (Spinks *et al*., 2000). The 48 rings of detectors each have a diameter of 83 cm and comprise of 576 elements within each ring. These block detectors are arranged into “buckets”, where each contains 12 blocks.

The total lines of response (LOR) which can be obtained amount to 190 million and the computing hardware can process an acquisition rate of about 4 million coincidence events/ second (Spinks *et al*., 2000). Lead side-shielding (thickness 2.5 cm) has been added on either side of the detectors and extends 8 cm beyond the face of the detectors. This acquisition system has been designed to process data in both frame and list modes and is sent to a PC where the raw data is recorded and stored. It is important to note that without any radial or axial rebinning a single frame has the ability to occupy more than 300 MB (Spinks *et al*., 2000).

For this work, the number of events (*N*), and fraction (*f*) of these used for the analysis is shown in Table 2. The process of choosing these values required several combinations, and this was found to be the best for this work when considering resolution and the presence of outliers.

Table 2: Variables used for triangulation

Variable	Value
Number of events (N)	200
Lines used for triangulation (*f*), %	15
Maximum error, %	10

Location markers

In order to make sure that the PEPT data lies within the actual mill, location markers were done using ^{22}Na isotope, which has a half-life of 2.6 years. Location markers are done so that the PEPT data can be aligned to the centre of the coordinate system. Three washers were placed at equal distances along the shell of the mill, which acted as holding places for the ^{22}Na isotope. The ^{22}Na was placed in the first washer and the mill was run at a slow speed (this was the same for all the conditions) for 60 s and repeated for the other two positions. Once all three markers were done, the isotope was placed back into the lead holder to avoid any accidents.

3.2 Experimental conditions

The test work involved varying lifter face angle, mill speed and charge filling in order to investigate the influence of these parameters on the trajectories of the charge.

3.2.1 Lifter face angle

Lifter face angle was the main variable for the work and the range tested was from 45 to 90 °. This range was chosen because it was found to be the typical range used for tumbling mill investigations. Rezaeizadeh *et al.*, (2010) used lifters with face angles of 16 °, when measured from the vertical (corresponding to 74 °). Similarly when determining the effects of lifter design in AG mills using DEM, Djordjevic *et al.*, (2004) used rectangular shaped lifters (90 °).

The lower lifter angles were further chosen to give a broader range of understanding to determine what the effect on charge motion is when using shallower lifter face angles.

It is also worth noting that the angles that were finally tested were the most mathematically sound when considering the length and height of (12 and 10 mm respectively).

3.2.2 Mill speed

The speeds investigated were 55, 70 and 85 % of mill speed, which corresponded to 42.5, 54.1 and 65.6 rpm respectively and were measured using the Tachometer shown in Figure 30 (which was kept a constant distance for all readings for consistency). The mill speed in rpm was determined using Equation 7**.**

$$\boldsymbol{speed\ (rpm) = \frac{speed\ (\%\ of\ critical) \times 42.3}{100 \times \sqrt{D}}} \qquad \text{Equation 6}$$

Where D is the diameter of the mill in meters.

In the South African gold industry, the typical mil speed was quoted to be between 90 to 92 % of critical speed by Moys (1993). This range is extremely high and would only encourage cataracting, thus undesirable. Whereas Powell *et al*., (2006) have stated that AG/SAG and RoM mills operate at 70-80 % and 75-90 % of critical speed respectively. These ranges are still slightly higher than what has been chosen for this test work, but give a more realistic range. The 55 % of critical speed has been chosen for this work as a way of gaining a better understanding of the motion of the charge. At a lower mill speed, it is possible to investigate the motion of the mill when there is minimal cataracting.

Figure 30: Tachometer used in experimental work to measure the speed of the mill.

3.2.3 Charge filling

For this work, 5 mm glass beads were used as the charge media in the mill. The volumetric charge filing levels investigated were 20, 30 and 40 % and the mass equivalent was determined by assuming a packing fraction of 60 %. This corresponded to masses of 6.05, 9.08 and 12.1 kg respectively. Since the manufacturing process results in a wide variety of sizes (even though they are intended to be 5 mm), it is difficult to ascertain the exact size of the beads. Thus, to ensure that a consistent distribution of 5 mm beads was used, a 4 mm sieve (shown in Figure 31) was used to eliminate the 3 mm beads and a 5.6 mm sieve to separate the 5 mm beads from anything higher (6 and 8 mm).

Figure 31: Picture showing the sieving of the glass beads using the 4 mm sieve.

At the beginning of the test work for a particular lifter angle, the charge filling was increased from 20 % to 40 %. Logistically it was easier to start the lower filling and adding the particles to increase filling degree than to begin at the higher filling and removing beads to reach a lower filling level.

The charge was added to the mill by tilting the mill such that one of the trolleys was lower than the other. The beads were added using a scoop and a funnel from the feed side while the mill was running at a low speed. Once the mill was filled to the desired amount, the mill was levelled and checked using the spirit level and the laser lines were aligned with the marks made on the mill.

3.3 Tracer preparation and labelling

Tracer particle integrity and labelling of the particle is among the most important considerations in conducting PEPT experiments. If the particle is not conditioned properly, it can lead to the glass bead breaking in the tumbling mill as it is jolted around the mill, which would compromise the tracking because the algorithm is set up to track a single particle. The other challenge that needs to be overcome is the fact that the radioactivity can leak out of the mill. If an isotope with a high half-life was used and the bead broke inside the mill (such as ^{22}Na, where $t_{1/2}$ is 2.6 years), the radioactivity would contaminate the system and would result in isolation until the activity had reached acceptable levels.

Measures have been put in place at iThemba labs and screening is done when leaving the lab where the mill and PEPT camera are located before entering into other offices. Latex gloves were worn throughout the duration of the experimental work, and if contamination was detected on any person within the lab they were escorted to the wash room with further scanning to ensure that the activity was indeed within acceptable levels.

Each experimental condition was run for one hour in 20 min segments, requiring a radioisotope that would cover this time. It would have been ideal to use ^{18}F, not only because it has a half-life of 109 min but it also only emits the 511 keV gamma rays, which would result in high accuracy of detection locations (Fan *et al*., 2006).

For this work, the tracer was made by labelling the NRW100 resin with ^{68}Ga (half-life of 68 min) radioisotope using the ion exchange technique. The ^{68}Ga was washed out from the ^{68}Ge / ^{68}Ga generator in the presence of Hydrochloric acid (HC*l)*. Then in dilute HC*l* and mechanical shaking, good circulation of the ^{68}Ga around the resin bead was achieved. The tracer was then placed into a 0.6 mm wide and 2.5 mm deep hole, which was drilled into the 5 mm glass bead and sealed with a cyanoacrylate (fast acting adhesive). Work done on the effect of drilling a hole of this size to assess if it represents the entire ensemble, concluded that there is no significant change in the physical properties of the bead (Fan *et al*., 2006). Thus, a hole of this size will not alter the physical properties of the glass bead significantly. Figure 32 is a schematic of the glass bead with the resin particle inserted inside it.

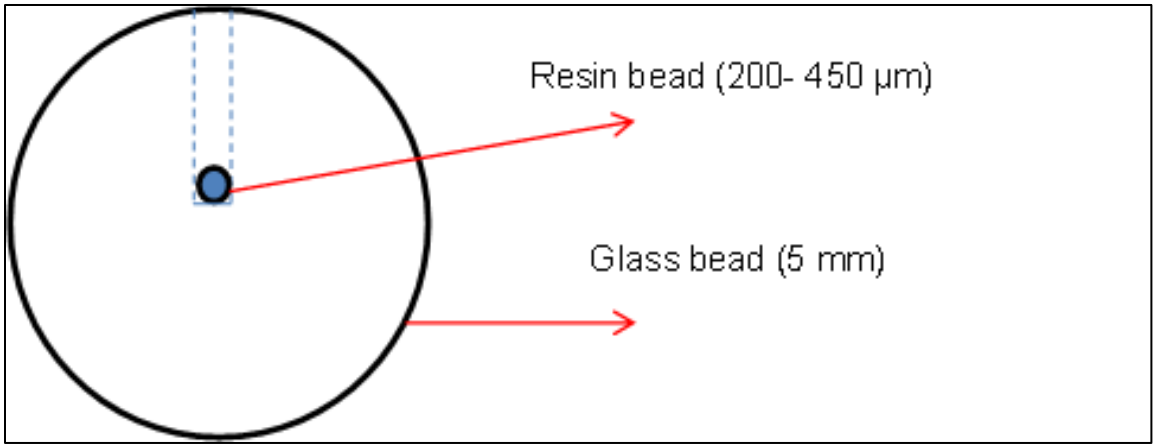

Figure 32: Schematic of the tracer - glass bead with the inserted resin bead.

This procedure was repeated twice a day. The first tracer was made ready to be used between 10:30 am and 11:00 am and the second tracer was made in the afternoon between 2:30 pm and 3:00 pm. The tracer was then brought to the lab in a case shown in Figure 33 (Type A packaging) that was in line with the regulations for transporting radioactive materials.

Figure 33: The Type A case used to transport the radioactive tracer to the lab.

3.4 Procedure

1) Once all the lifters were fitted into the mill and the mill was filled with the glass beads, the mill was placed into the camera and was secured by two trolleys (with the brakes on), on either side of the camera. To ensure that the mill was horizontal, spirit levels were placed on the mill at various positions and the levers on the trolleys were adjusted accordingly. Figure 34 illustrates one of the spirit levels with the bubble in the centre to demonstrate that the mill was level. To further ensure that the mill was in the same position for all the test work, location markers were placed on the outside of the mill shell and these were aligned with the camera lasers.
2) To commence particle tracking, the tracer was placed in the mill through the feed and pushed in further with a brush to ensure that it was not lingering in the chute. Due to the nature of the work and the use of radioactive sources, the radioactive decay, which is also referred to as the activity occurs. The activity is determined by the count rate, which was displayed on the camera. Thus, the count rate is a measurement of the emitted gamma particles, expressed in counts per second (cps). A good indicator of whether the tracer was in the mill or not was when the initial count rate was anywhere between 150 000 - 200 000 cps.

Figure 34: Picture of one of the spirit levels placed on the mill to ensure that the mill is horizontal

3) The mill speed was adjusted using the dial on the motor until the desired speed was reached (in rpm). This was monitored every 10 minutes using the

tachometer throughout the test work. Once the desired speed had been reached, the timer on the stop watch was started and simultaneously the computer began tracking the tracer.

4) The count rate was recorded every 20 minutes, which marked the end of one tracking segment and the beginning of another. The count rate decreased as the test work continued. If the count rate remained constant, it could have indicated that the glass bead was broken and needed to be replaced. Thus an unchanging count rate warranted the test work to be stopped since it was an indication of the integrity of the glass bead.
5) A new file was opened for tracking the next 20 min run. Steps 4 and 5 were repeated for the remainder of the hour.
6) At the end of the first hour, the file was saved; the mill speed was decreased to 0 and the power was then switched off.
7) Steps 3 to 6 were repeated for the new set of conditions. At the end of the second hour, the mill was switched off and taken out of the field of view of the camera (as shown in Figure 35) to remove the tracer since it was still considered radioactive and would create background noise for the next set of experiments.
8) After completing three speeds at the 20 % filling, the pre measured charge was added to increase the filling to the next level and the procedure repeated.

Figure 35: Picture showing the mill when it is taken out of the field of view of the camera to take out the tracer before the next set of experiments.

For each lifter face angle tests were performed at the three filling degrees and speeds. Therefore a total of 36 experiments were conducted. It was not necessary to take the second tracer of the day because the radioactivity would deteriorate overnight ($t_{1/2}$ = ^{68}Ga is 68 min) to negligible levels, thus step 7 was repeated for the morning tracer only.

The experiments were not repeated because it was assumed that they are run for long enough for the system to reach steady state. Once the tracer bead was located amongst the other glass beads, it was placed against the Geiger counter (shown in Figure 36) and if it read “OVERLOAD”, it was an indication that this was indeed the tracer particle.

The experimental conditions are shown in Table 3, which demonstrates that a total of 36 experiments were conducted. Results for the 90 ° were obtained from the work performed by Brodner (2013).

Figure 36: Geiger counter used to determine the count rate of the radioactive tracer.

Table 3: The experimental conditions used for the PEPT work.

Angle (°)	**Charge filling (%)**	**Mill speed (% of critical)**		
75	20	85	70	55

	30	85	70	55
	40	85	70	55
65	20	85	70	55
	30	85	70	55
	40	85	70	55
55	20	85	70	55
	30	85	70	55
	40	85	70	55
45	20	85	70	55
	30	85	70	55
	40	85	70	55

3.5 Torque measurements

Torque measurements were made to calculate the power being transferred to rotate the system. The T2OWN torque sensor (HBM, 2012) was used and calibrated using a known mass of 0.492 kg in conjunction with the shaft and a piece of string. The clamp and shaft are shown in Figure 37.

Figure 37: A picture of the shaft and clamp used for torque measurements (After Bbosa, 2013) .

The mass was tied to the lever arms at known distances to determine the torque. The signal output of the voltage was recorded using the Lab View software (National Instruments, 2010), which is shown in Figure 38. The screen shot displays the fluctuations in voltage with time as the mill was rotating. The difference in the averaged voltage (when the output seemed to displaying the least fluctuations, as circled in red), was used for further calculations.

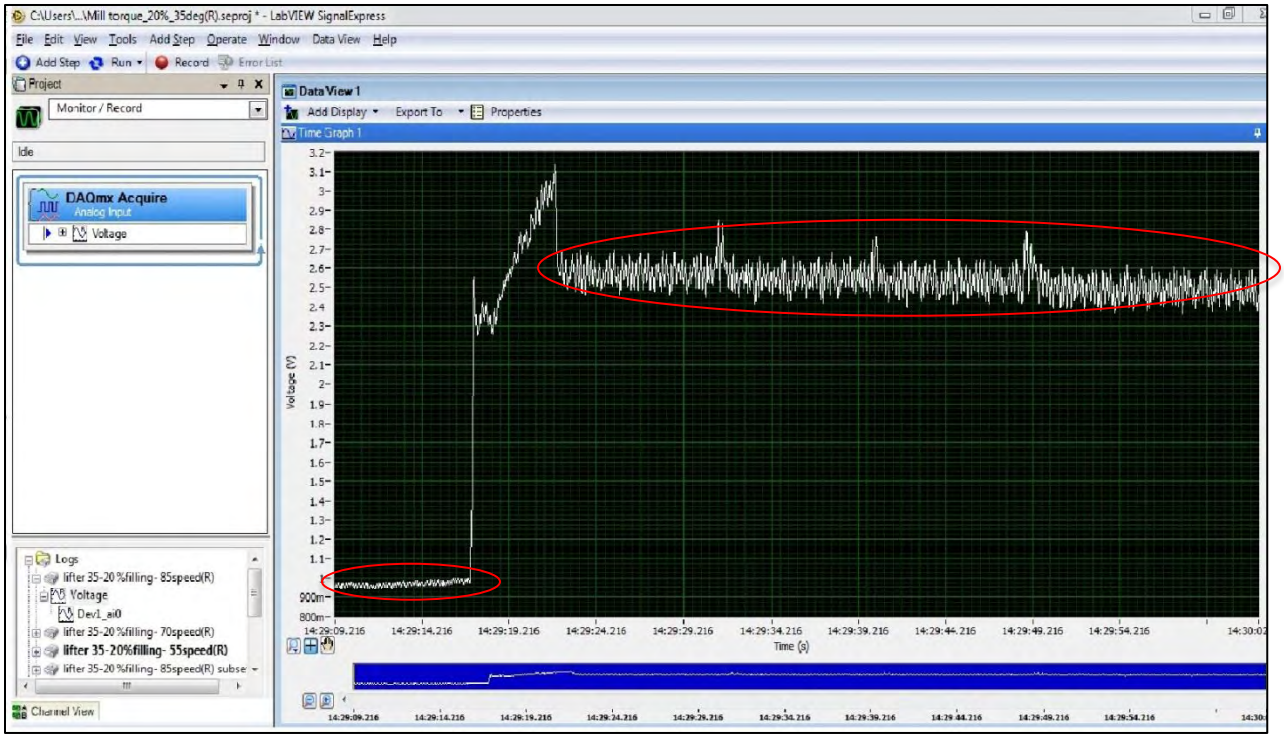

Figure 38: Screen shot of the LabView software output.

Having determined the difference in voltage at each distance, the torque was calculated and the results can be seen in Table 4.

Table 4: Results for the torque sensor calibration

	Groove	Distance (m)	Mass (kg)	Voltage (V)	Torque (Nm)
Left	1	0.001	0.492	0.177	0.386
	2	0.002	0.492	0.299	0.627
	3	0.003	0.492	0.417	0.869
	4	0.004	0.492	0.514	1.11
Right	1	0.001	0.492	0.179	0.386
	2	0.002	0.492	0.297	0.627
	3	0.003	0.492	0.414	0.869
	4	0.004	0.492	0.530	1.11

Plotting the torque against the voltage gave the calibration curve (seen in Figure 39) for the torque sensor; where the gradient is the calibration factor constant K. In this case the calibration constant was 2.10 and all torque and subsequently measured power calculations were normalised using this calibration constant.

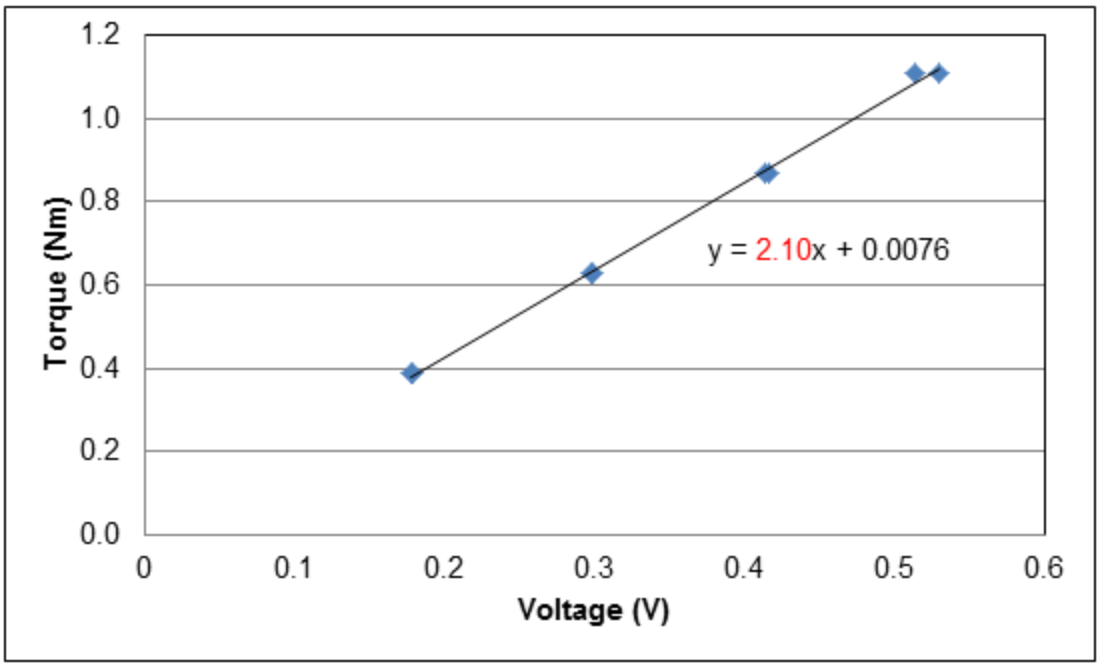

Figure 39: Calibration curve for the torque sensor

CHAPTER 4

4. RESULTS AND DISCUSSION

This chapter focuses on the key results obtained from the experimental work. The analysis of results is segmented into three main areas, which are:

- The influence of lifter face angle on charge kinematic descriptors such as equilibrium surface, Centre of Circulation (CoC), shoulder and toe angles, and the free surface.
- The effect of lifter face angle on power draw for the different filling levels and mill speed.
- The comparison of the lifter particle trajectories from PEPT experiment to those obtained from the commercial software MillTraj, which is commonly used for liner design.

The results from PEPT are given in terms of x, y and z position at a time interval of micro seconds. The advantage of using PEPT is that it provides measurements of the average velocity of the particle as it is tracked within the system. The PEPT data and algorithms are used to extract time-averaged tangential velocities instead of instantaneous data. For each experiment key data such as velocity vectors, porosity, shear rate and probability distribution can be extracted. From these the motion of charge from the tracked particles can be analysed.

The probability distribution for the tracer particle's position is generated using an iterative binning algorithm. The cross section of the mill is divided equally into a Cartesian grid of 100 x 100 cells, and each of these cells represents a bin. This algorithm makes is possible for any measured variables (velocity and probability) to be expressed as a function of position inside the mill. The end effects as a result of the interaction between the charge and the front and back of the mill are ignored in this work.

All the experimental data is analysed using a MATLAB code developed at the University of Cape Town (UCT), through several PEPT projects. The code was modified for the current work and Dr. Govender helped with the key modifications to generate the analysis specific for this work. The algorithm provides statistical information of charge motion and key measured features such as velocity, acceleration and probability

distribution of a tracked particle within the mill. The direction of rotation for the mill in all the results is clockwise.

4.1 Charge characteristics

This sections is aimed at assessing the influence of lifter face angle on key charge motion features, which include Centre of Circulation (CoC), velocity profile along a radial line going through the CoC, the shape of the charge free surface, the shoulder and impact toe angles. These features were chosen because mill performance has been associated to these descriptors in work done by Powell (1993); Powell and Nurick (1996); Morrell (1993); Powell and McBride (2004). The influence of lifters on the motion of charge should give an indication of which mode of breakage will be most favoured in mills. Square lifters are associated with more aggressive impacts and are expected to lead to more cataracting with the charge landing mostly on the mill shell than a less aggressive and shallower angle (Maleki-Moghaddam *et al*., 2012). The definitions of the charge features are given in the sub sections that follow prior to discussing how these are affected by lifter face angle.

4.1.1 Centre of circulation (CoC)

The Centre of Circulation (CoC) is said to be the point about where the charge seems to be circulating (Powell & Nurick, 1996). If a line is drawn along the CoC it makes it easier to understand the velocity profile exhibited by the charge. This phenomena is best illustrated in Figure 40, where it can be seen that at approximately (-0.0624, -0.0589) the direction of the charge changes from an upward direction, goes to zero and continues in a downward direction. Powell and McBride (2004) showed that the CoC is identified by the intersection of equilibrium surfaces; the vertical and horizontal surfaces. In Figure 40 it can be seen that to the left of the proposed CoC position, the charge is in the bulk bed region and is expected to have lower velocity magnitudes. The colour bar represents the tangential velocities along the radial line going through the CoC. To the right, the charge is a combination of cascading charge as well as charge undergoing free fall, which has higher velocity magnitudes (indicated with the blue and red colours respectively). The colour bar indicates the tangential velocity magnitudes along the radial line.

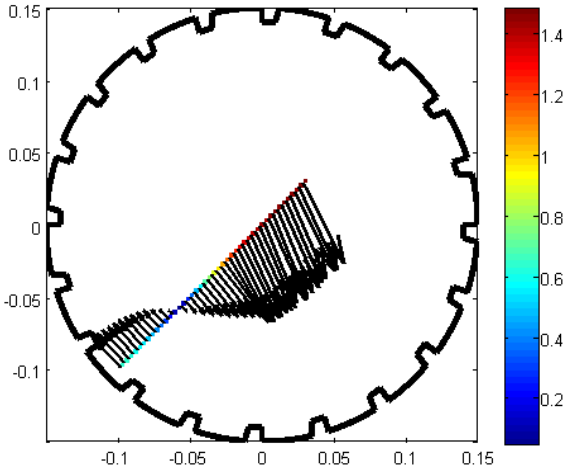

Figure 40: Demonstration of the Centre of Circulation (CoC) taken at 55 % critical speed and 30 % charge filling.

4.1.2 Velocity profile

In this work, the velocity profile was analysed for the region between the mill shell and the CoC (bulk bed region). In the work performed by Brodner (2013), the velocity profile analysis was also performed for the same region. This section focuses on showing the influence of the lifter face angle on the velocity. Figure 41 shows the velocity profile of all the lifter face angles at 30 % filling level and mill speed of 55 % of critical speed. This result is consistent with what was concluded by Brodner (2013) when he investigated the influence of lifter height on the velocity profile. The inclination would be to trust the data for the current work since the experiments were run for 1 hour in total in comparison to Brodner's (2013) which were run for 45 minutes.

Despite the similarity in the type of curve for all the lifter face angles, there are still distinctions to be seen in terms of the magnitude in velocity as lifter face angle is altered. Therefore, vertical lines (chosen along the radial distance) were chosen and the velocities plotted against the lifter face angles. For the conditions shown in **Error! Reference source not found.**, it can be seen that the lifter face angle that results in the highest velocity is the 75 °. This seems counter-intuitive as the 90 ° angle would be expected to be the one that causes the charge to have the highest velocity as it would catapult the charge higher and further due to the steep angle. A plausible explanation for this discrepancy could be attributed to the fact the 90 ° lifter data was taken from the work conducted by Brodner (2013), thus could be the result of differences in data recording.

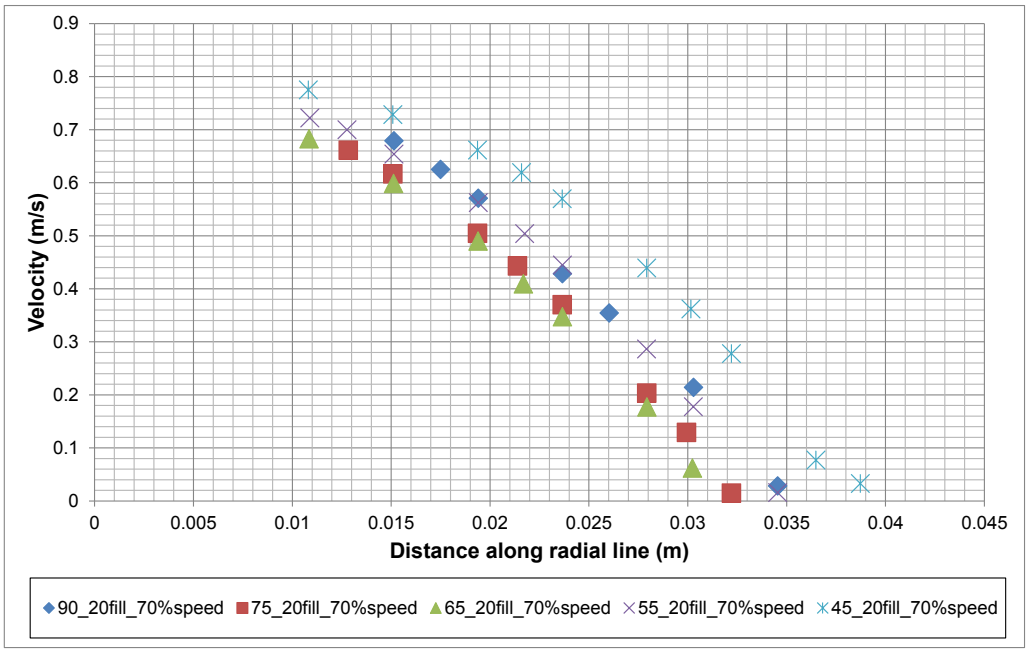

Figure 41: Velocity profiles for the different lifter face angles at 30 % filling level and mill speed of 55 % of critical speed

4.1.3 Free surface

The free surface defines the boundary between the cascading and the cataracting charge (Dong and Moys, 2003). This surface is shown in Figure 42 by the red line. Different definitions have been used to describe this surface by Khakhar *et al*., (2001), Dong and Moys (2003) and Taberlet *et al*., (2008).

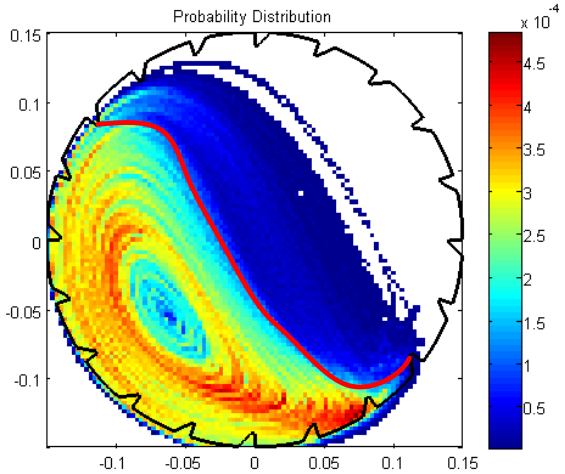

Figure 42: The free surface of charge at 20 % charge filling and 70 % critical speed for a 65 ° lifter angle.

4.1.4 Toe and shoulder positions

The bulk charge was not used as a basis for this analysis since it was difficult to accurately define the boundaries of the en masse charge from the cataracting charge. Using the outermost charge was done because the PEPT results were compared to MillTraj outputs, which only consider the outer layer. Thus, the path followed by the outer layer was chosen as a proxy for determining the effect of face angle on the trajectory of the charge as far as the impact toe and shoulder angles are concerned. The direction of measurement for the toe and shoulder angles for this study are summarised in Figure 43. Thus the impact toe angle was measured from the horizontal and in the direction of the mill rotation, which is the technique employed by Morrell *et al.,* (2001).

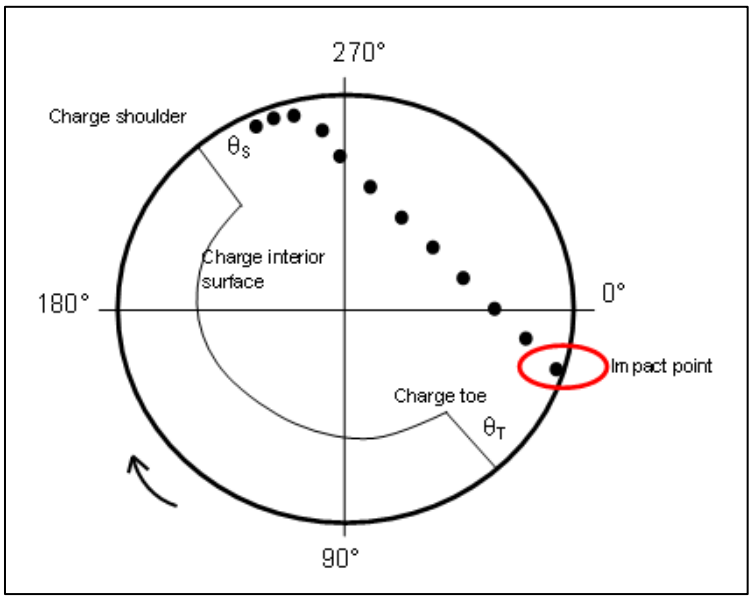

Figure 43: Schematic showing how the shoulder and impact toe angles were measured.

4.2 Effect of lifter face angle on charge characteristics at different mill speeds

This section will focus on the effect of lifter face angle on the charge as the mill speed was varied. The results of the probability density distribution of the charge are shown in

Figure *44*, where a direct comparison of the different features of the charge can be made. The data shown is from tests that were performed at 30 % charge filling.

Across all the angles, it can be seen that majority of the charge is most likely to be found in the densely packed region close to the CoC, with only a small percentage being found in the cataracting region. This is depicted in the colour bars, which show the densely and sparsely packed regions in the mill. At the least aggressive angle of 45 ° and the lowest mill speed setting of 55 % of the critical speed, most of the charge lies in the densely packed region. In contrast, the 75 ° lifter at all mill speed conditions tested showed the charge being thrown into the cataracting region.

At 85 % of critical speed, the highest mill speed condition tested, the distinction between the surfaces (cascading and cataracting) is not easily identifiable as they seem to merge into one another. This can be attributed to the fact that the mill is approaching centrifuging at this condition, leaving less charge to undergo cascading motion. In their work, Clermont and de Haas (2010) measured the media angle and its evolution of a 4.8 m diameter grate discharge mill. They measured the static and dynamic load angles when the mill had been crash stopped and with Sensomag ® respectively. The ratio of the dynamic to static media load angle gave an indication of the expansion of the charge. This method would be ideal where definitive information cannot be obtained as it can give valuable insight for liner design.

The results of the varying speed on the motion of the charge showed that more cataracting motion is achieved at higher speed. Most of the charge appears to be impacting on the charge. While this is good for the liner life, it will not be desirable for throughput if the mill is operated at lower speed settings.

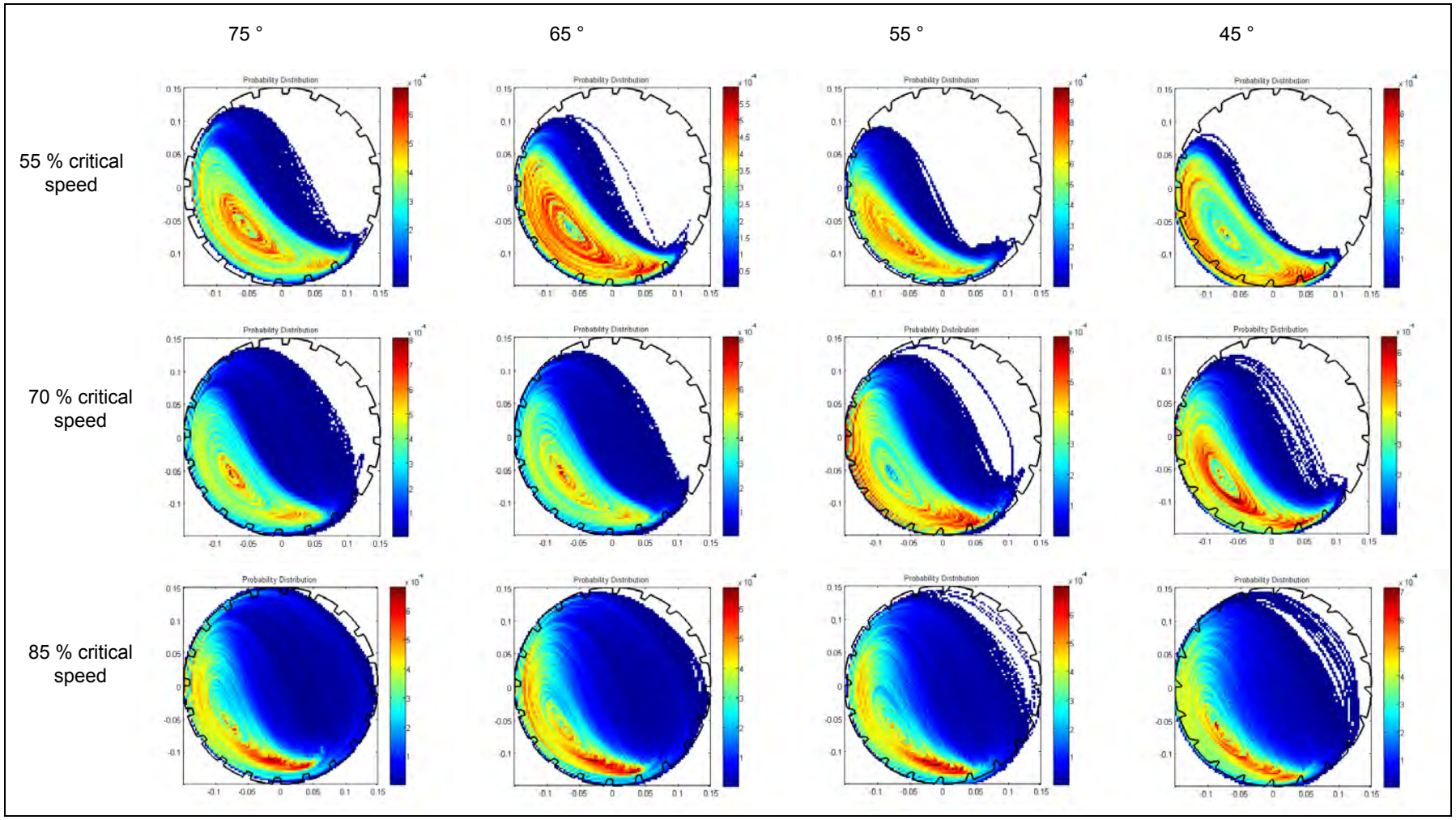

Figure 44: Probability distribution at varying mill speeds at 30% charge filling for all lifter face angles investigated.

Centre of Circulation (CoC)

The Centre of Circulation has been determined from the velocity field plots obtained from PEPT results. The coordinates of the CoC for the four lifter angles evaluated at three different speeds are shown in Table 5. The data shown was obtained at the 30 % volumetric filling level. It can be seen that the CoC shifts as the lifter face angle changes.

Table 5: Coordinates for the CoC at varying mil speeds and constant volumetric filling level of 30 %

Mill speed (% of critical speed)	**CoC at different lifter face angles**			
	75 °	**65 °**	**55 °**	**45°**
55	(-0.0593, -0.0582)	(-0.0643, -0.0660)	(-0.0684, -0.0588)	(-0.0725, -0.0769)
70	(-0.0738, -0.0619)	(-0.0776, -0.0555)	(-0.0774, -0.0617)	(-0.0772, -0.0654)
85	(-0.0799, -0.0548)	(-0.0773, -0.0611)	(-0.0772, -0.0635)	(-0.0833, -0.0629)

The location of the CoC for the various lifter face angles at three different mill speeds was plotted and shown in Figure 45. There is no definite trend relating the CoC location with face angle. This can be attributed to the data logging in PEPT, which could have resulted in the data lying outside the confines of the mill shell and ultimately misplacing the CoC position. It was observed that the CoC positions for each speed banded together in the same region. At the lowest mill speed, the CoC was closer to the centre of the mill and shifted towards the mill shell with increase in mill speed, though not by a large margin. Powell and Nurick (1996) showed that the radial position of the CoC will alter with changes in mill speed for a fixed charge filling level. Further, their work showed that the position of the CoC moved toward the mill shell due to the increased presence of grinding media that was cascading and cataracting towards the mill centre. However, as the mill speed was increased beyond the highest critical speed the position of the CoC was expected to move towards the centre of the mill and eventually coincide with the mill centre. This would result in the angle of repose of the charge to approach 90 °,

which is its upper limit. The shift of the CoC position away from the mill shell toward the mill centre is not observed in this work since the highest mill speed investigated is 85 %.

It is not advisable to operate mills at much higher speed than 85% of critical speed because the charge may start centrifuging as shown by Hlungwani *et al*., (2003). At the lower speeds, charge slipping will be more pronounced at the extreme end of the spectrum for the lifter angle (45 °). This can result in more charge being found in the cascading region and hence the CoC position would be expected to be closer to the mill centre. At high speeds, the charge is lifted higher and hence the CoC is expected to move away from the mill centre (Powell and Nurick, 1996).

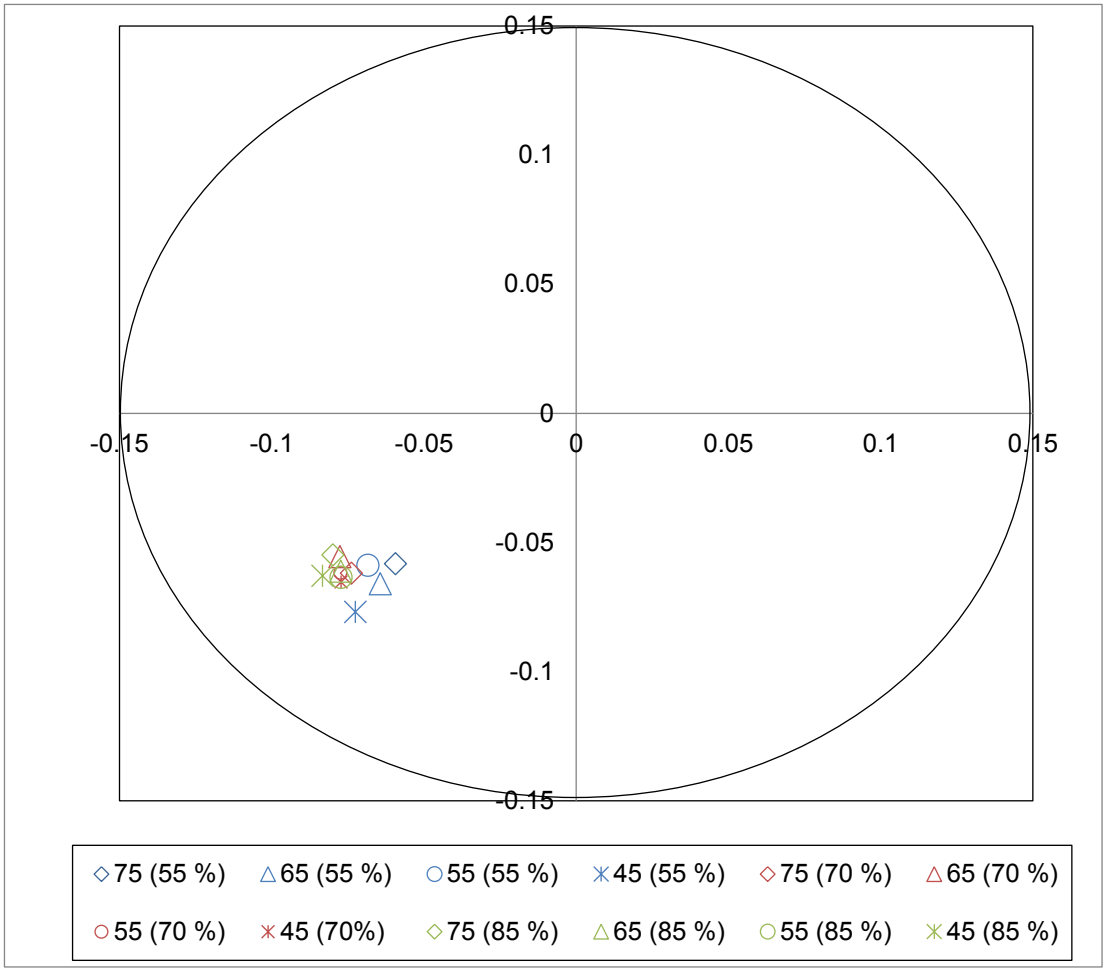

Figure 45: Relative positions of the CoC in the mill at each lifter angle and varying mill speeds.

Impact toe angle

The impact toe is an important charge descriptor in mills, as it is used to determine where the charge will impact in the mill. The liner may be damaged from aggressive impacts of the charge on the shell. Figure 46 shows the variation of the impact toe with lifter face angle for the three different mill speeds at the 30 % volumetric filling. The impact toe angle increases with lifter face angle up to the 75 ° lifter and then drops off between 75° and 90 °.

The trends were similar for all the mill speeds tested. The differences observed between the 55 and 70 % critical speed was that the toe angles were shallower for the 55% speed compared to those from the 70%. Further, it is observed at 70 % critical speed, there are minimal changes in the impact angle with lifter face angle. At 85 % of critical speed, there is an outlier at approximately 75 ° lifter, which could be due to the recording of the PEPT data. The 75 ° lifter is consistently higher at all the mill speeds, which suggests an error could have occurred with the experimental technique. This outlier exaggerates the distance between the 70 and 85 % critical speed data and makes it seem as though there is a drastic increase and then decrease in impact angle for the shallower and steeper angles respectively. Had this data point been lower, the data would show that at the higher mill speeds, there isn't much difference in the impact toe angle in comparison to the lowest mill speed setting with changes in lifter angle. Maleki-Moghaddam *et al*., (2012), showed that the shallower angles would not be expected to cause the charge to impact on the mill liner and rather on the bulk charge unless the volumetric filling is very low.

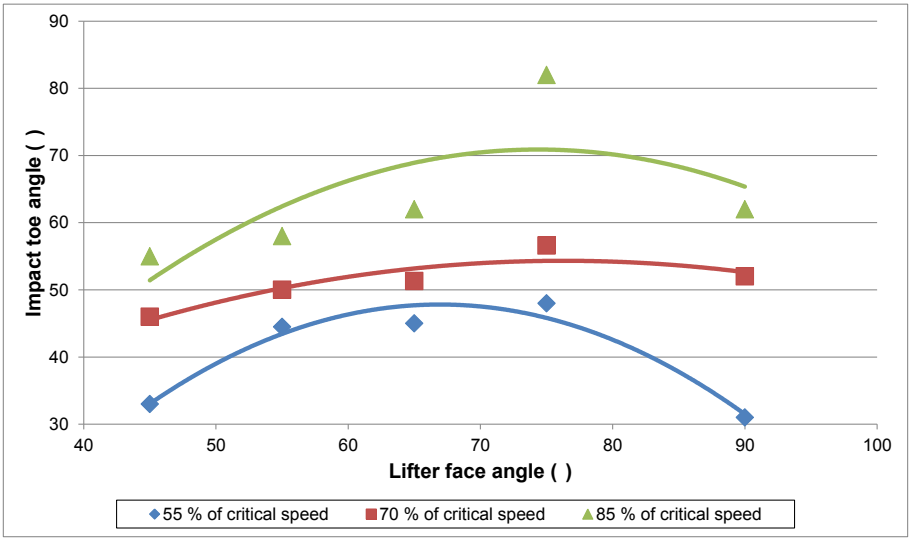

Figure 46: Effect of lifter face angle on the impact toe (at 30 % charge filling level)

Shoulder angle

The shoulder angle is one of the measurements used to describe charge motion in tumbling mills. It is also one of the inputs in power models developed as shown by Morrell (1993). The shoulder angle has many definitions but is usually measured just before the charge begins to undergo free fall. Figure 47 shows the departure shoulder angle associated with the various lifter angles, measured for the mill rotating at 55, 70 and 85 % of critical speed at a constant charge filling degree of 30 %. The general trend shows that the shoulder angle increases with lifter face angle for the range of lifters tested. This shows that as the lifter angle becomes steeper, the charge experiences more lifting action and thus possesses a higher departure shoulder angle. This is in agreement with the observations made by Maleki-Moghaddam *et al.,* (2012) who performed experiments using Grinding Media Trajectory (GMT), a software that was used to determine the trajectory of charge in a mill with liner specifications shown earlier in Table 1.

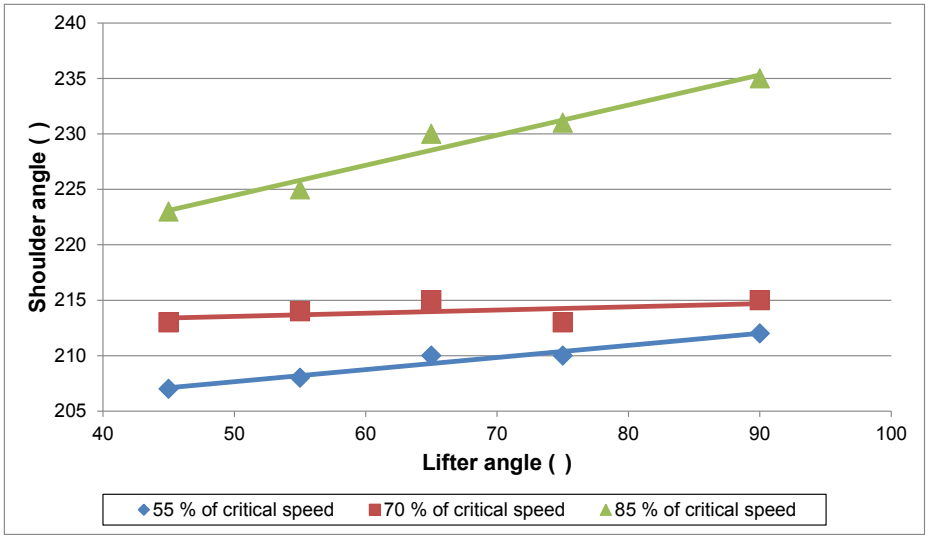

Figure 47: Variation of shoulder angle with the lifter face angle (at 30 % charge filling level)

Velocity profile at various radial distances

The results of the velocity data for the different lifter angles at varying mill speeds are shown in Figure 49 to Figure 51. The data given here was extracted from different distances along a radial line shown in Figure 40. The profile at 70 % of critical speed (Figure 50) shows that there are minimal differences in the magnitude of velocity across the lifter angles for a particular line. Figure 49 shows that the velocities at all the radial lines increases from 45 to 70 ° and then drops off from approximately 70 to 90 °. Closer to the mill shell, the gaps between the profiles become smaller, whilst closer to the CoC the velocities are lower. This can be attributed to the fact that the charge closest to the mill shell will travel at the speed of the mill, whilst the velocity of the charge closer to the CoC will approach zero. This can be observed in Figure 48 where the velocities closer to the mill shell are high and decrease to zero along the equilibrium surface. Figure 48 is used as an example to show how the tangential velocities are distributed in the mill for all the lifters.

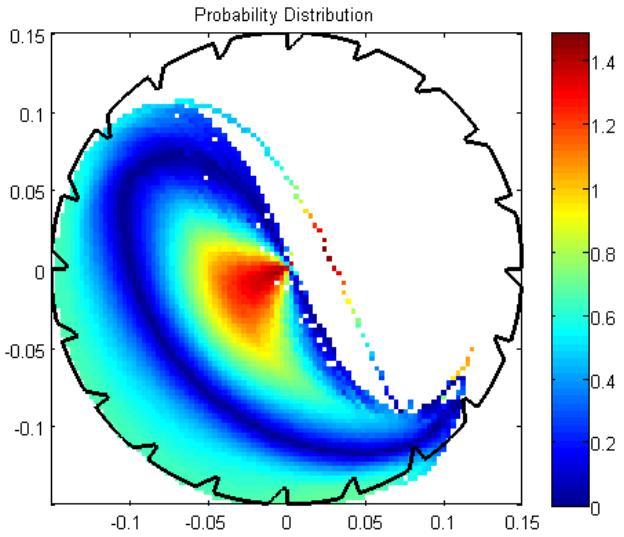

Figure 48: Plot showing the tangential velocity map for a 45 ° angle at 30 % charge filling and 55 % critical speed.

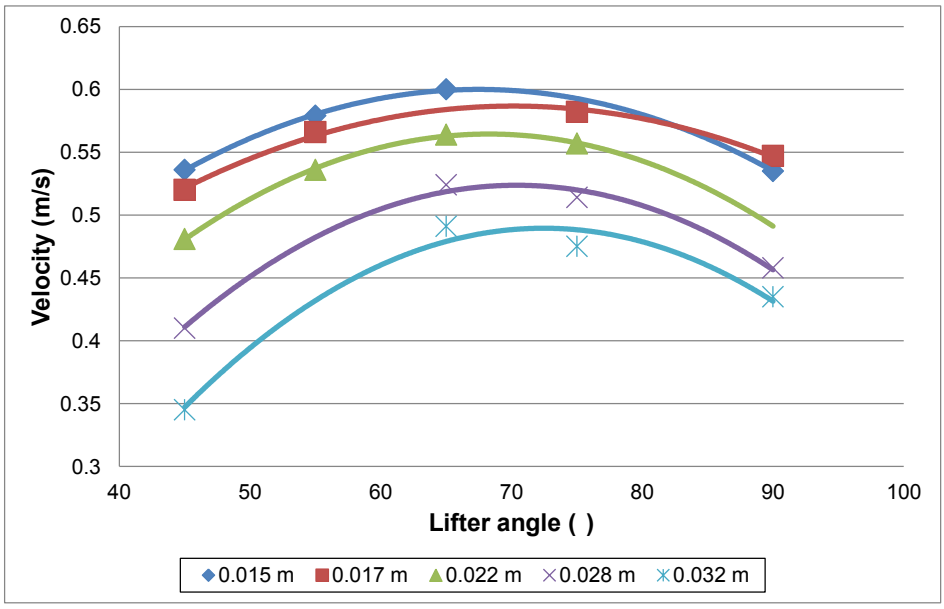

Figure 49: Effect of lifter face angle on the velocity profile at 55 % of critical speed at various radial positions in the mill for the filling degree of 30 %.

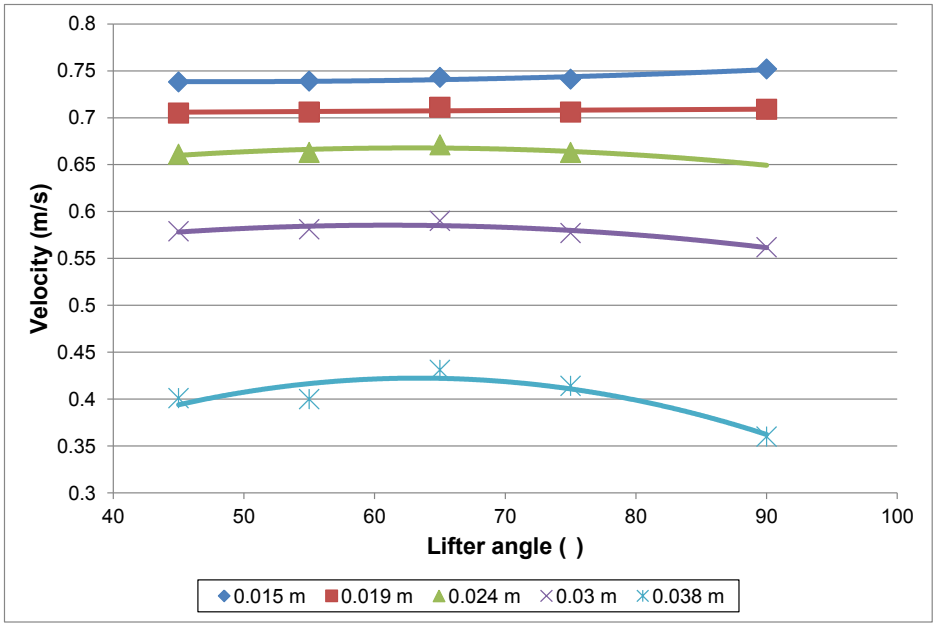

Figure 50: Effect of lifter face angle on the velocity profile at 70 % of critical speed at various radial positions in the mill for the filling degree of 30 %.

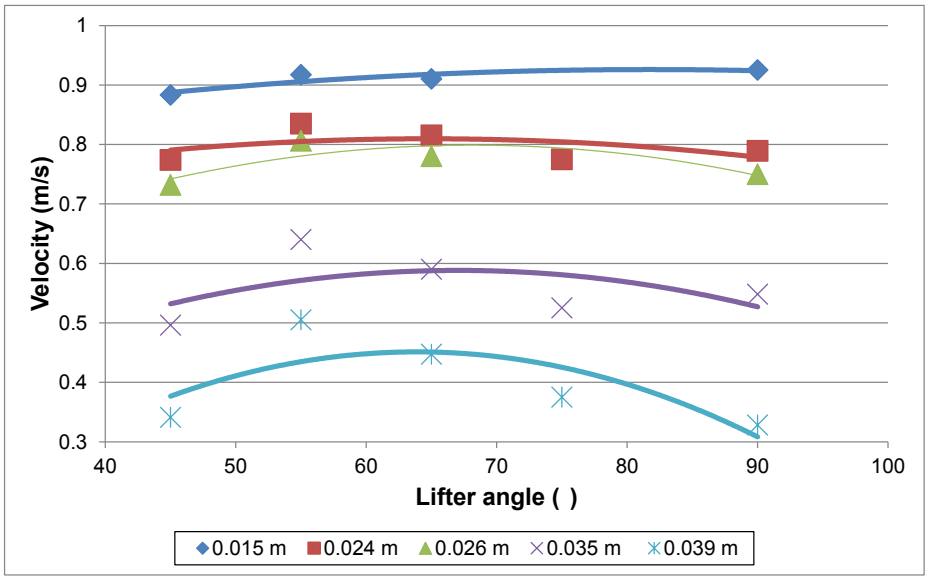

Figure 51: Effect of lifter face angle on the velocity profile at 85 % of critical speed at various radial positions in the mill for the filling degree of 30 %.

4.3 Effect of lifter face angle on charge characteristics at different filling degrees

An increase in the charge filling would be expected to change the shape and the position of the different characteristics of charge and ultimately affect the modes of breakage. The work done in this thesis does not consider breakage but assesses the charge motion data that contributes to it.

Figure 52 shows the probability density distribution as lifter face angle and charge filling degrees were varied at a constant speed of 70 % of critical speed. This speed was chosen because most of the mills in industry are operated close to that speed (Powell *et al.,* 2006).

The probability density distributions for the lifter face angles at different filling levels are shown in Figure 52. Focusing on the 30 % filling level, it can be seen once again that it is most probable that the charge will be located in the densely packed region closest to the CoC. The steeper angles show the lowest probabilities in the cataracting region, which reiterates what was concluded by Brodner (2013). The probability of charge in the cataracitng region is lower than in the rising, densely packed region.

When considering the lowest filling level of 20 %, it can be seen that there is more of the blue (suggesting that more charge is cataracted). This would be expected as the charge would experience more lifting action as there wasn't a lot of charge being keyed in between the lifters. The consequence of this is the likelihood of charge impacting on the mill shell instead of the bulk toe at the bottom of the mill.

The free surface shape evolved across the lifter angles as the charge was increased; the shape of the free surface became more curved. At the 20 % filling, the shape of the free surface exhibited more of a bilinear shape, which evolved to the trilinear-saddle, which is most visible at the highest charge filling. As a comparison, the result at a filling and speed of 40 % and 70 % of the critical speed respectively are similar to those found by Dong and Moys (2003).

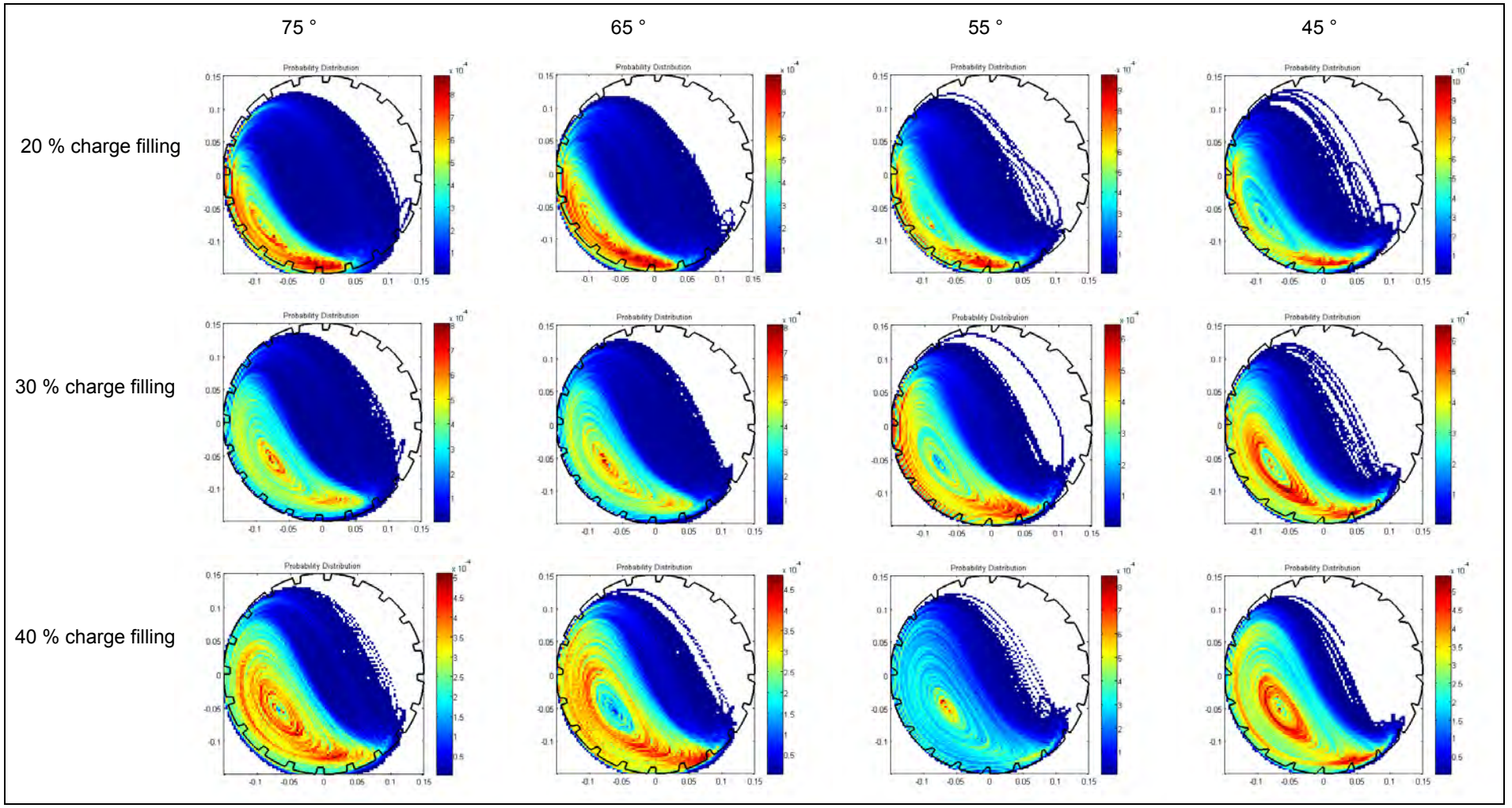

Figure 52: The probability distributions at all charge filling levels at 70 % of critical speed for all the lifter angles investigated.

The influence of changing the lifter angle on the CoC coordinates at the same speed and varying filling levels at constant speed of 70 % of critical are shown in Table 6. To gain a better appreciation of the relative positions, the data has been demonstrated in Figure 53.

Table 6: Coordinates for the CoC at different filling levels and constant speed of 70 % of critical speed.

Charge filling level (%)	**CoC at different lifter face angles**			
	75 °	**65 °**	**55 °**	**45°**
20	(-0.0857, -0.0825)	(-0.0983, -0.0684)	(-0.0895, -0.0779)	(-0.0864, -0.0745)
30	(-0.0738, -0.0619)	(-0.0748, -0.0583)	(-0.0735, -0.0645)	(-0.0766, -0.0648)
40	(-0.0645, -0.0591)	(-0.0618, -0.0589)	(-0.0622, -0.0563)	(-0.0647, -0.0559)

The diagram shows that there is banding together of the CoC positions at each filling level, but there is no clear influence of the lifter face angle on these positions. In the case of charge filling level, it seems that as the filling level is increased from 20 to 40 % there is an increase in position (moving closer to the mill centre) of the CoC. For each lifter face angle, there is consistently an increase in the CoC position and this shift appears to be more predominant in the 65 ° lifter (depicted here by the triangles).

It would be beneficial to operate at an angle and filling degree that is not too close to the mill shell the mill centre. If the CoC is closer to the mill shell, it implies that the charge is being thrown into flight more than it is undergoing cascading (encouraging attrition and abrasion). The converse could insinuate that the mill is overburdened, which could lead to the mill not operating efficiently and possibly becoming the bottleneck in an industrial scale circuit.

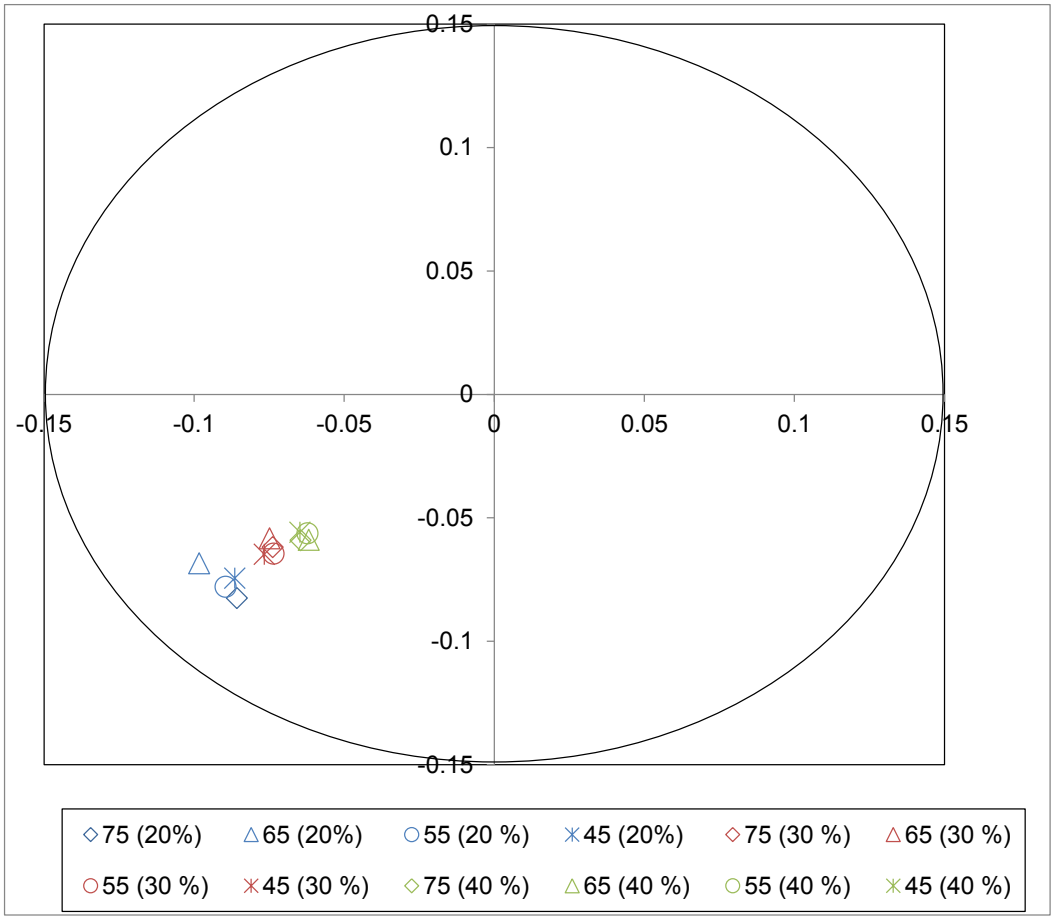

Figure 53: Relative positions of the CoC at all the lifter angles and varying charge filling levels

These results show that in order to be able to take advantage of the best grinding efficiency, the mill should be operated at a filling where there appears to be a good balance of the both cataracting and cascading motion as suggested by Fortsch (2006). It should also be noted that as volumetric charge filling is increased, in order to encourage more cataracting the mill speed would have to be increased to ensure that the charge does not slip. This will be more beneficial for shallower lifter face angles, which are not designed to lift the charge high enough for cataracting to take place.

In their work Clermont and de Haas (2010) showed that for the platinum industry an increase in solids content made the product finer. However, as the solids content was increased beyond 74 %, the product reverted to being coarse, which decreased the grinding efficiency and led to load expansion. This is a good example of how carefully thought out increases in mill filing can be a valuable input for mill grinding efficiency. Moreover, they showed that increasing the ball filling level does not equate to higher

grinding efficiencies being reached because having more grinding media in the mill does not mean all the grinding zones are saturated with pulp. Should this be the case, it means that a large percentage of the balls in the mill are merely rolling around and consequently being worn without any useful grinding taking place.

Impact toe angle

The variation of the toe position with changes in lifter face angle is shown in Figure 54. It can be seen that the toe angle increases with lifter face angle from 45 to 65 ° and decreases from 65 to 90 °. The trend is similar for all three filling degrees tested but the toe angle at each lifter increases with filling degree. At 40 % charge filing, there is more of an increase and sharper decrease in toe angle in comparison to the lower charge filling degrees. At the 30 % charge filling there is an outlier at the 75 ° lifter creating a higher maximum. This gives the illusion that there is a significant change in the impact toe angle as the lifter face angle becomes steeper. Thus, it can be said that if this point had been lower down, there wouldn't be a noticeable decrease in impact angle as the lifter face angle went from 75 to 90 °. The data shows that the impact angles are lowest for the shallowest lifter face angle, which can be a result of slipping as the lifters aren't able to lift the charge as high as the steeper lifters.

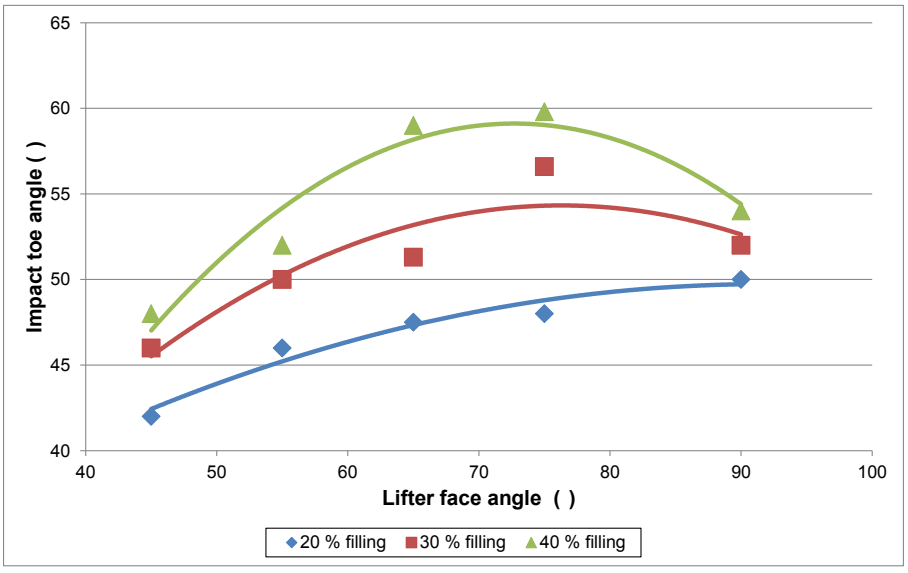

Figure 54: Influence of lifter face angle on the impact toe (at 70 % of critical speed)

Shoulder angle

The general trend on the influence of lifter face angle on the shoulder angle can be seen in Figure 55, where there is an increase in the shoulder angle as a result of the lifter face angle becoming steeper for all the filling levels investigated. This increase can be attributed to the fact that as there is more charge in the mill, the charge will display shoulder (and consequently head) positions that are higher.

The implications of this on breakage is that even if the charge is to land on the bulk bed, it will probably not cause high breakage rates as a result of the dense or bulkier bed at the bottom of the mill. Morrell *et al*., (2001) hypothesised that a dense bed will cause the impact breakage to be more dissipated throughout the bed, hence reducing the initial energy which the charge had as it was undergoing free fall before it struck the charge. This suggests that a balance needs to be made where the lifter angle is able to cause the charge to be lifted high (such that is gains potential energy), and strikes a bed that is sparesely packed, resulting in reduced impact upon contact.

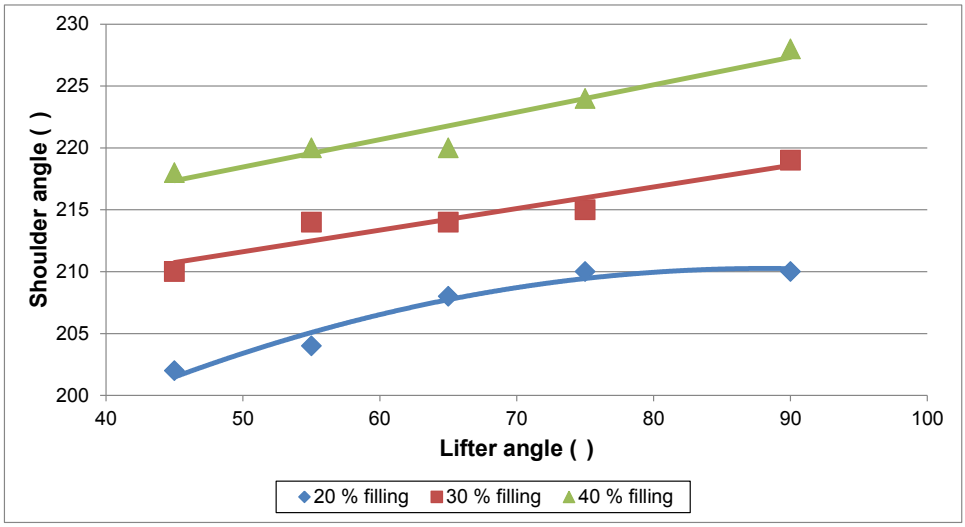

Figure 55: The variation of the shoulder angle with lifter face angle (at 70 % of critical speed)

Velocity profile at various radial distances

The results for the velocity profile at the different filling levels can be seen in Figure 56 to Figure 58. At the 30 % filling degree it appears there are no significant changes in the velocity as the lifter angle becomes steeper for distances closer to the mill shell. This is

not the case moving closer to the CoC, where it can be seen that the velocity increases from 45 to 65 ° and subsequently decreases from 65 to 90 °.

At the highest filling degree, a similar trend can be seen in the velocity profile as demonstrated for the 30 % filling level as far as no significant changes in velocity. However the velocity values seem to be decreasing for distances closer to the mill shell and displaying a different profile closer to the mill centre. The velocity experiences a decrease from 45 to 75 ° lifter then an increase from 75 to 90 °. The decrease in velocities can be attributed to the fact that the increase in charge filling means the charge is not experiencing as much lift from the lifters especially when moving away from the lifters at the mill shell. Higher filling will result in the charge that is in flight landing on the bulk bed much sooner and thus not experiencing high velocities.

At 20 % filling level, the profile displays a decrease in the velocity to a point from 45 to 70 ° and begins to increase from 70 to 90 °.

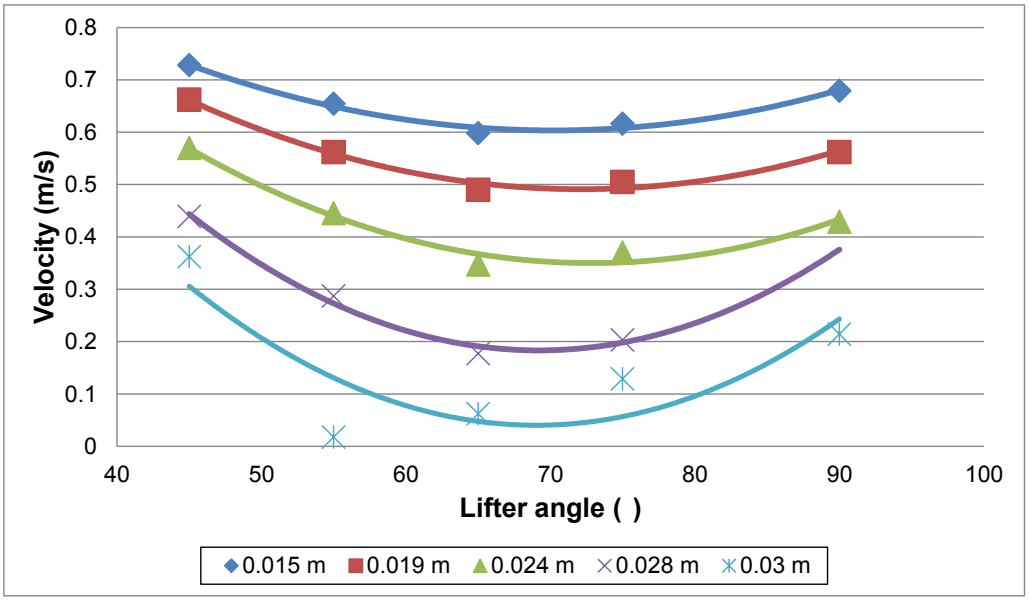

Figure 56: Effect of lifter face angle on the velocity profile at constant mill speed of 70% of critical and 20 % filling level.

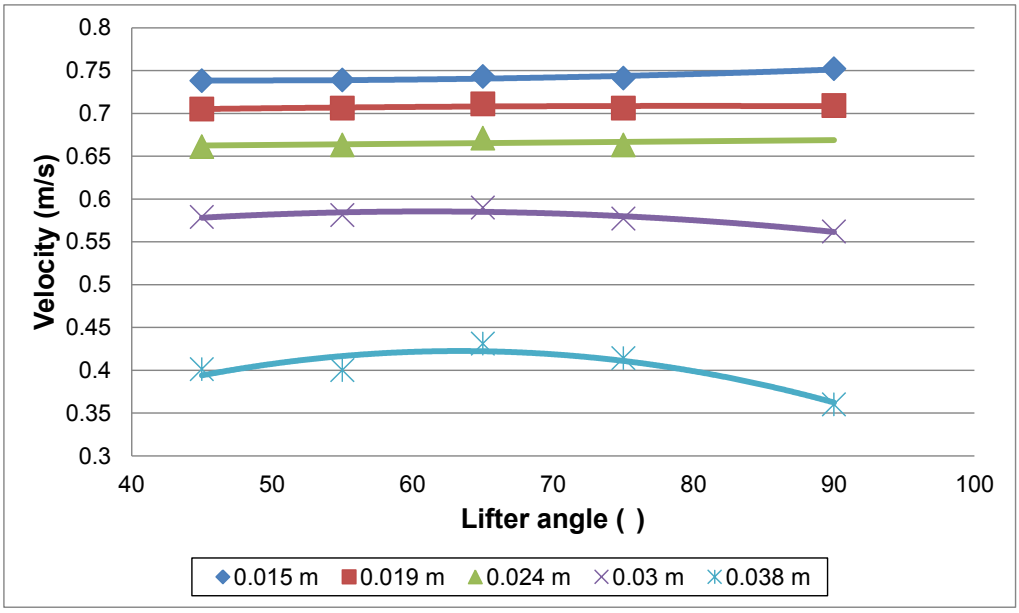

Figure 57: Effect of lifter face angle on the velocity profile at constant mill speed of 70% of critical and 30 % filling level.

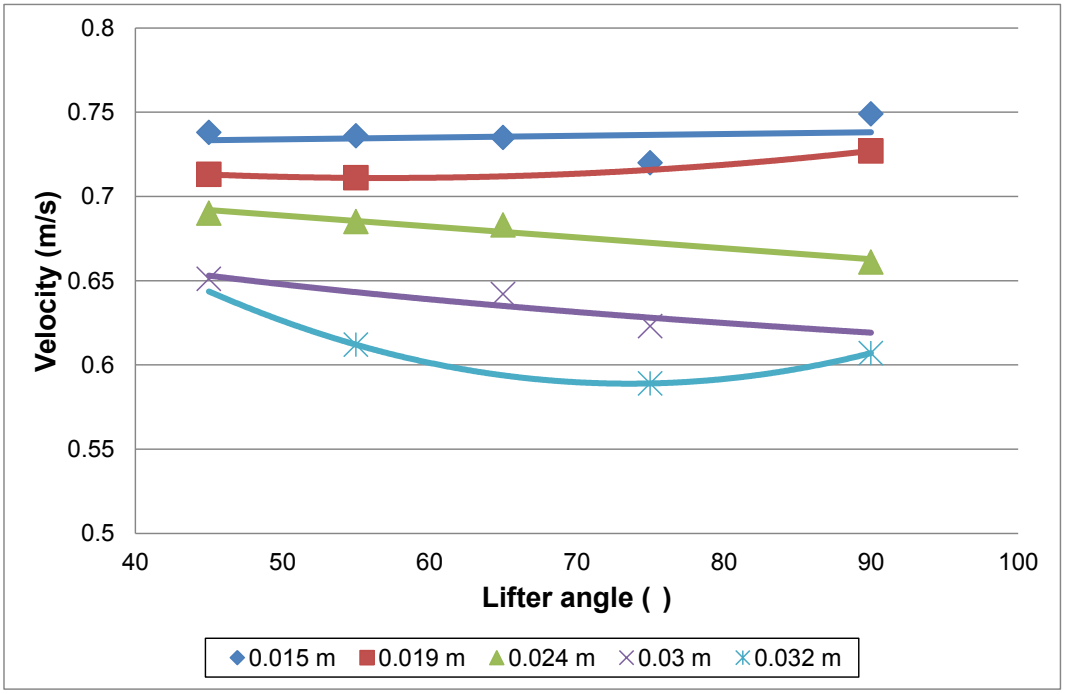

Figure 58: Effect of lifter face angle on the velocity profile at constant mill speed of 70% of critical and 40 % filling level.

4.4 Effect of lifter face angle on measured power draw

4.4.1 Measured power draw

Mill power is a function of a variety of operational and physical properties associated with the charge within the mill; namely loading, mill speed and lifter design (Dong and Moys, 2003). Govender and Powell (2006) showed how using the angular velocity and measured voltage, the power of a lab scale mill can be measured during PEPT experiments.

In section 3.5, the elaborate procedure of determining the calibration factor (K) can be found as this factor was used in subsequent measured power draw calculations. The resultant power calculations, which were done by multiplying the torque and rotational speed, are shown in this section. The power was calculated using the method used by Bbosa *et al*., (2011), where they compared three different methods to calculate power draw. This section will show results from two of these methods; namely the measured power and torque per bin approach.

4.4.2 Comparison of power calculated from PEPT and Torque sensor

The measured power was calculated using Equation 7, where K is the calibration factor, V_{ave} is the average voltage at steady state and ω is the angular velocity. The uncertainty associated with this power calculation is described by Equation 8. The parameter which has the greatest influence on the power uncertainty is the voltage and so the contribution made by the angular velocity has been ignored. ΔV represents the standard deviation of the measured voltage as stated by Bbosa *et al.,* (2011).

$$\boldsymbol{P_{Measured} = KV_{ave}\omega} \quad \text{Equation 7}$$

$$\boldsymbol{P_{Measured} = \left(\frac{\Delta V}{V_{ave}}\right)} \quad \text{Equation 8}$$

The power from PEPT experiments was calculated using the torque per bin approach as described by Equation 9. The uncertainty for this method was found in the x_i and this value was considered to remain constant throughout all the calculations. It was based on the width of each bin being 0.3 (diameter of the mill) for 100 bins.

$$\boldsymbol{P_{bin} = \frac{Mg}{T}\sum_{i=1}^{n} x_i t_i \alpha_i} \quad \text{Equation 9}$$

Where M is the mass, g is the acceleration due to gravity, T is the total time of the experiment, x_i is the x- coordinate, t_i is the time fraction and α_i is the angular velocity of the particle.

The results at the varying mill charge fillings are shown in Figures 59 to 61. The data shows that as the mill filling was increased, the power became noticeably different. At the 20 % filling, the power draw was within statistical agreement for the steeper face angles. This suggest that the torque per bin approach was a good way of approximating power as it took into account the residence time each particle spent in a particular voxel. The shallower face angles showed no agreement in the power draw for the two methods used. To further verify that all the components of the charge make a contribution to the power draw as suggested by Cleary (2001), showing that a lower charge filling should result in lower power values. Clermont and de Haas (2010) have shown in their work that there is no linear relationship between power draw and charge filling degree. They suggest that a slight change in power draw can be attributed to alterations made in filling degrees.

As the charge filling was increased, these differences in power draw became more pronounce for all lifter face angles. Data at the mill speeds has been placed in Appendices. The results at the different mill speeds showed that the power draw was within statistical agreement for the intermediate lifter face angles and more variation at the extremes.

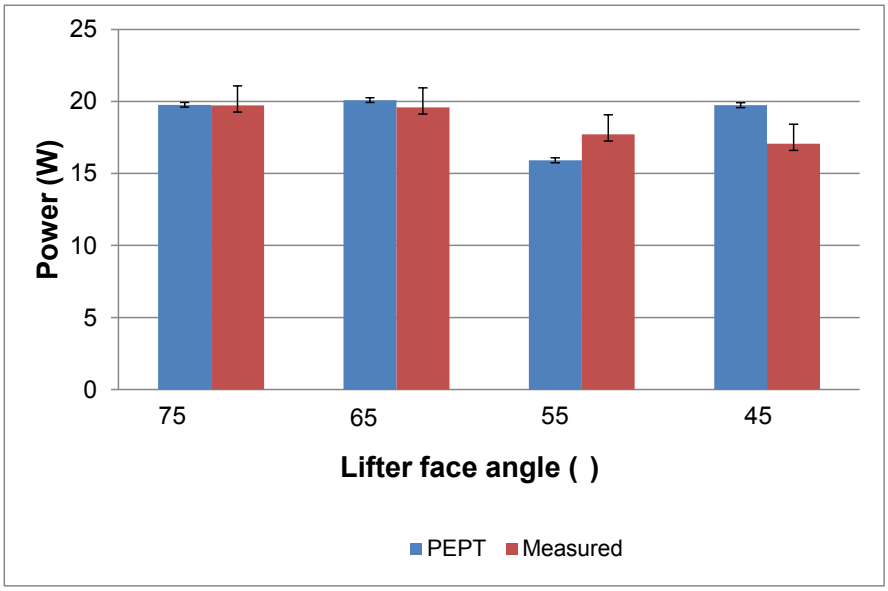

Figure 59: Comparison of PEPT and measured power at 20 % charge filling and 70 % critical speed for the different lifter face angles investigated.

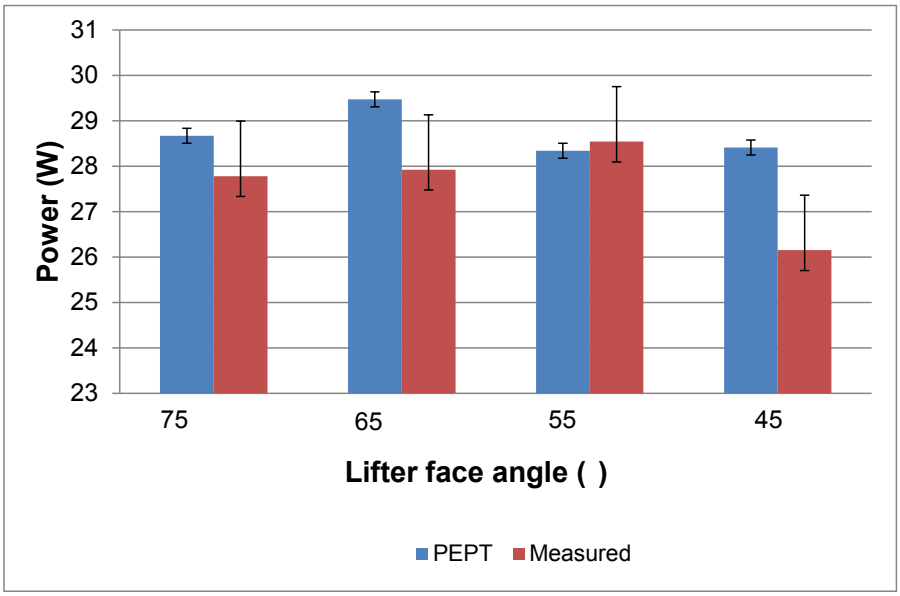

Figure 60: Comparison of PEPT and measured power at 30 % charge filling and 70 % critical speed for the different lifter face angles investigated.

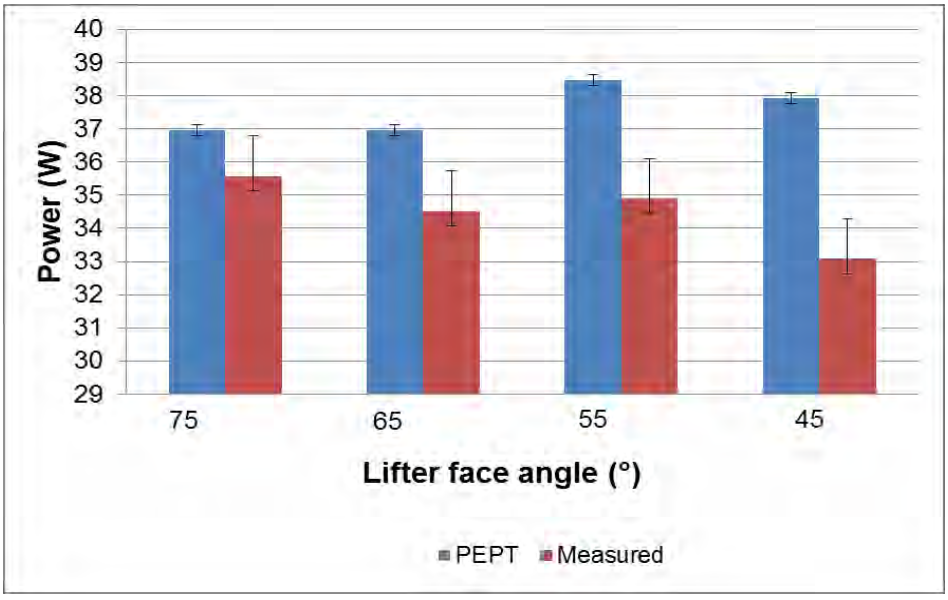

Figure 61: Comparison of PEPT and measured power at 40 % charge filling and 70 % critical speed for the different lifter face angles investigated..

.

4.5 Comparison of PEPT data with MillTraj for impact toe

In order to further investigate the validity of the results, the experimental specifications were used in MillTraj, which is a model based on the physics of motion of charge in order to determine the motion of the outermost grinding media in tumbling mills. These predictions are based predominantly on the influence of the liner and other operating conditions (www.milltraj.com/milltraj). Although this is not a direct comparison since the MillTraj results are given at 10 % charge filling, they are still a good proxy to show what is expected to happen to the outermost charge as the angle of the lifter is altered. Figure 62 to Figure 64 show the results at the different mill speeds with face angles from 90 to 45 °.

As seen already, the most aggressive angle will project the charge further to the right of the mill as the mill speed is increased from 55 to 85 % of the critical speed. Further, at each speed setting, the impact toe position moves from the right to the left of the mill with the 90 ° lifter being the furthest to the right, which is in good agreement with the data from PEPT.

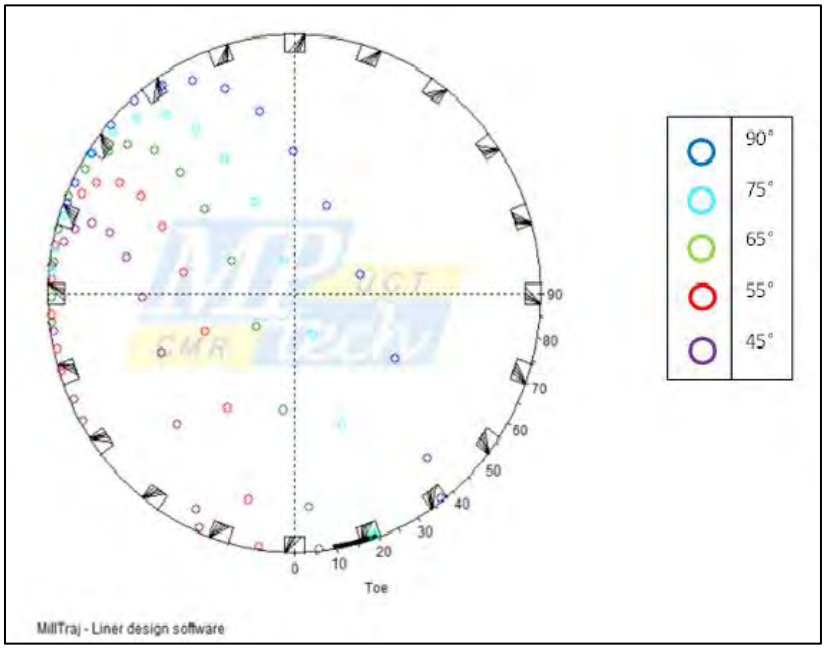

Figure 62: MillTraj result of the outermost charge at 55 % of the critical speed for all the angles.

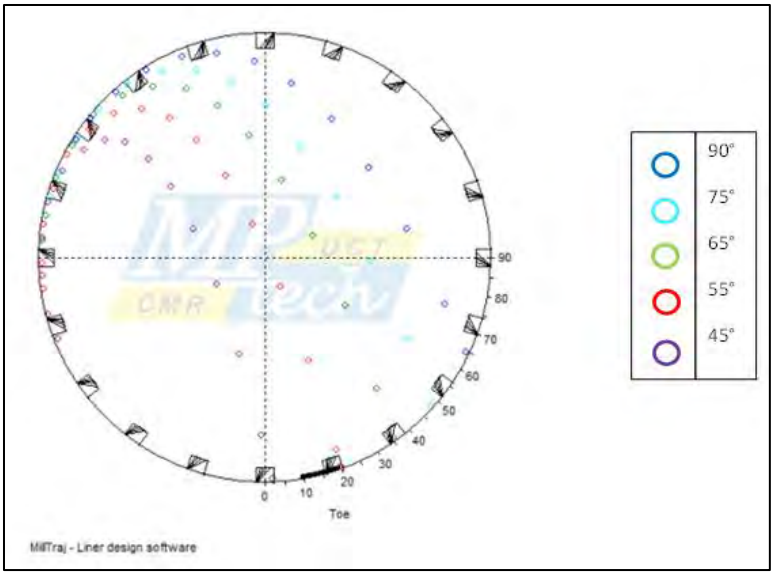

Figure 63: MillTraj result of the outermost charge at 70 % of the critical speed for all the angles

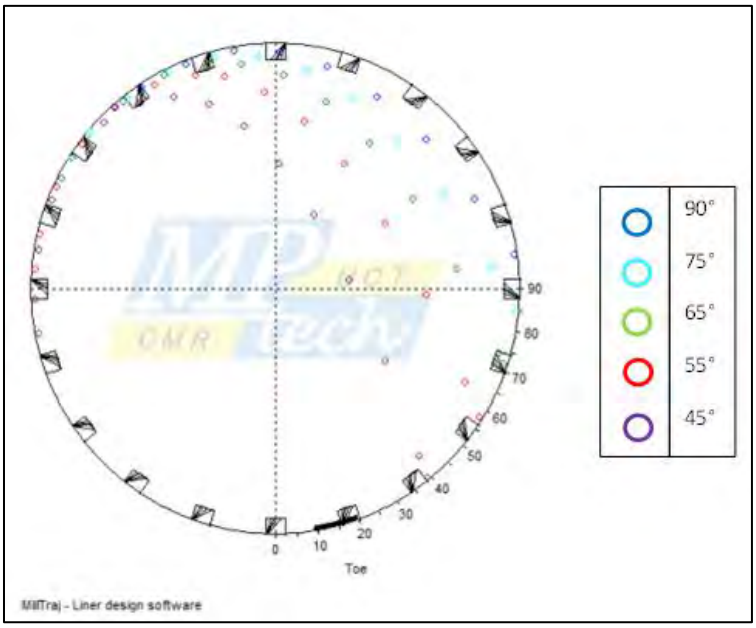

Figure 64: MillTraj result of the outermost charge at 85 % of the critical speed for all the angles

The results of the face angle have demonstrated the importance of designing liners and lifters with a good understanding of how they will affect the trajectory of the charge. Once again, it is important to note that the more aggressive lifters will encourage more cataracting motion than the shallower angles but coupled with optimum operational conditions damage to the liners can be curbed.

CHAPTER 5

5. CONCLUSIONS

This chapter focuses on the key observations from the test work. The main conclusions are presented and the recommendations for future work related to assessing the influence of lifters on the performance of tumbling mills are given. The work conducted has shown that the use of PEPT as a tool for investigating charge motion can be beneficial in adding to the body of work done on tumbling mills. Traditionally work done on lifter angles has been performed using x-ray filming and taking snapshots of lab scale tumbling mills with Perspex ends, which made it possible to view the inside of the mill. Authors who have employed this technique are Powell (1993), Govender and Powell (2006) and Rezaeizadeh *et al*., (2010). Discrete element modelling has also been used to explore the same work by Cleary (2001) and Makokha *et al*., (2007).

5.1 Main observations

5.1.1 Effect of lifter face angle on charge characteristics with varying mill speed

Centre of Circulation (CoC)

- There was no clear trend in the CoC positions with changes in the lifter face angle. The positions seemed to band in one region suggesting that the CoC is a weak function of mill speed. This discrepancy could be due to the data extraction. The CoC is located at approximate coordinates of (-0.0740, -0.0620).
- At the lowest mill speed setting (55 % of critical speed), the position of the CoC for all the angles were closest to the centre of the mill and moved towards the mill shell with an increase in mill speed. This shows that the closer the CoC is to the mill shell, cataracting and eventually centrifugation are more likely to occur. This is in agreement with what was observed by Powell and Nurick (1996), who showed that the radial position of CoC will move outward from the mill centre as the mill speed increases. This can be demonstrated by looking at the 65 ° lifter, which had coordinates of (-0.0643, -0.0660) at 55 % critical speed and shifted to (-0.0773, -0.0611) at 85 % critical speed.

Impact toe angle

- The toe angle increased from the 45 ° lifter angle up to 75 ° lifter and then decreases as the lifter is increased from 75 to 90 °.This is in line with what is expected since the steeper angles should cause the charge to be lifted higher, thus the charge is more likely to be thrown onto the mill shell.
- At the 55 and 70% of critical mill speed settings, the differences in impact angles were not as large as those seen for the 85 % mill speed. At 55 % critical speed the highest impact toe angle is noted to be approximately 49 °, and 80 ° at 85 % critical speed. This could be due to the fact that at higher mill speeds, the lift forces are changing with increase in speed.

Shoulder angle

- The shoulder angle increased from the shallower lifter face angles to the steeper angles as a result of the higher lifting action associated with steeper lifter face angles.
- The charge appeared to rise higher with an increase in mill speed for all lifter face angles but there wasn't a large difference observed in the shoulder angle values between 55 and 70 % of critical speed. The greatest differences were seen between 70 and 85 % of critical speed. This suggests that coupling high mill speed with steeper lifter angles will result in particles being lifted higher.

Velocity profile

- At the lowest mill speed setting of 55 % of critical speed, an increase in the velocity was noted from the 45 °up to 65 °lifter and then a decrease from 65 °to 90 °. This implies that for the current conditions, it is best to operate at the lifter face angle that exhibits the highest velocities (65 °). Caution should be taken to ensure that the charge impact in the bulk toe and not on the mill shell. A similar trend seems to exist for the higher speed settings (70 and 85 % of critical speed) as well, although not as obvious at these higher mill speeds.
- As the distance from the mil centre increased, the results showed lower velocity values. This can be attributed to the fact that the charge closest to the mill will take on the velocity of the mill, which would be higher than the charge in the bulk bed region closer to the mill centre.

5.1.2 Effect of lifter face angle on charge characteristics with varying mill filling degrees

Centre of Circulation (CoC)

- The CoC positions banded together in the same region and there was no clear trend in relation to the lifter face angle. This is a reflection of the dynamic nature of the charge in the bulk charge region.
- Unlike with speed, there are clear bands for each charge filling level, which moved towards the mill centre. This could be due to the fact that as the charge is increased, and a more pronounced shift in the CoC is visible. This suggests that the position of the CoC is more strongly a function of the volumetric charge filling. Taking the data for the 65 ° lifter, the coordinates were (-0.0983, -0.0684) at 20 % filling level and (-0.0618, -0.0589) at 40 % filling level.

Impact toe angle

- A general increase in impact toe angle was observed for lifters from 45 to 70 ° followed by a decrease from the 70 to 90 ° lifter. This maximum at approximately 70 ° lifter for all filling degrees investigated suggests that this is where the mill should operate for the current conditions.
- There was no sharp decrease in the impact toe angle at the lowest filling level of 20 %. There is just an increase in the impact toe angle as the lifter angle became steeper, which suggests that the charge was shifting to the left. This is counter intuitive since the expectation would be for the charge to be thrown more towards the mill shell and not inward toward the bed especially at the lower filling level.

Shoulder angle

- General trend observed was an increase in the shoulder angle as the lifter face angle became steeper from 45 to 90 °. An increase in volumetric filling was expected to increase the position of the shoulder as there is more charge in the mill.

Velocity profile

- At the lowest filling degree, the velocity decreased from 45 to 70° lifter and then increased from 70 to 90 °. The initial decrease could be due to the fact that the charge is sparsely packed and result in the shallower lifters failing to lift the charge high enough to cause high velocities. With an increase in the lifter angle, the charge was able to lift the charge higher and key in more charge between the lifters. At the higher filling degrees, there were minimal changes observed in the velocity for distances closest to the mill shell. For both 30 and 40 % charge filling degrees, the velocity remained constant at approximately 0.74 m/s. The perceivable changes were seen at radial distances above 0.024 m.
- The charge experienced higher velocities closer to the mill shell. This could be a result of the charge assuming the speed of the mill.

5.1.3 Effect of lifter face angle on measured power draw

The power draw calculated using the torque per bin method was compared to the measured power. At 20 % filling the two methods were in good statistical agreement for the steeper lifter angles. As the charge filling was increased, the results showed disparities between the two methods. The torque per bin method, which used PEPT data, was consistently higher than the measured power. This could be attributed to the fact that the PEPT data took into account the time spent by each particle in a voxel. The measured power underestimated this as the angular velocity of the mill was used, whereas PEPT determined the angular velocity of each particle. A

5.1.4 Comparison of PEPT and MillTraj impact toe results

The path followed by the outer layer of particles is the same in both PEPT and MillTraj. This shows the credibility of using PEPT for investigating motion in opaque systems such as tumbling mills.

5.2 Main conclusions

The main conclusions drawn from the study performed to assess the influence of lifter face angle using the positron emission tracking system are given prominence in this section. The study has shown that the Positron Emission Particle Tracking (PEPT) system can provide charge kinematic information that can be analysed to evaluate the influence of lifter face angle on charge trajectory. The key conclusions that address the hypotheses formulated for this thesis are:

5.2.1 Influence of lifter face angle on toe position charge expansion

The probability density maps have shown that increasing the lifter face angle leads to expansion of the charge. This was more pronounced for the experiments performed at 55 and 70 % critical mill speeds. At 80 % critical mill speed the charge expansion with increase in lifter face angle was not significant because the particles tended to be lifted higher because the mill was operated closer to centrifuge.

5.2.2 Influence of lifter face angle on toe position

The toe angle increased with lifter face angle for the lifter face angles ranging from 45 to 70 °. However, a decrease was observed when the lifter face angle increased from 70 to 90°. The reasons for this are still being investigated because the 90° lifter face angle experiments were performed by a different researcher using the same mill and the composition of the charge might have been different.

5.2.3 Influence of lifter face angle on toe position shoulder position

The shoulder angle increased with lifter face angle for the range of lifter face angles tested. This indicates that increasing the lifter face angle results in the charge being lifted higher before releasing it into the cascading and cataracting regions.

5.2.4 Influence of lifter face angle on velocity profiles

The velocity profiles were determined along a radial line from the mill to the CoC. The velocities of the particles were shown to be higher closer to the mill shell and decreased as they approached the equilibrium surface.

5.3 Recommendations for future work

- The work conducted in this thesis focused significantly on the bulk bed region, with only a qualitative analysis on the charge in free flight. Future work should attempt to investigate the behaviour of charge in the cataracting region as this will give more insight into the energies involved in impact breakage. This will create a more holistic view of motion in tumbling mills as it will demonstrate how much influence the free falling charge contributes to the total energy associated with breakage in these systems. This can be done using DEM which may allow more tests to be done and the PEPT results from this work can be used to validate the simulation outcomes.
- The influence of lifters on the charge kinematics is mainly due to height, face angle and spacing. It is recommended that to extend the work to lifter spacing but this should include a statistical design of experiments and the work should be

performed using DEM which can allow multiple experiments to be performed at a lower cost than PEPT. Investigating the effect of lifter spacing, face angle, and height on charge motion in DEM will allow for a complete assessment of the interactions between lifter height, face angle and spacing to be taken into account if a statistical design of experiments is used.

- For the PEPT experimental work only one glass bead was tracked. It would be beneficial to track several particles simultaneously in order to investigate the interaction between the particles. This would provide a more realistic view of the mill environment where contacts between particles are also captured and analysed, which is important when assessing the influence of lifers in industrial scale tumbling mills. Although the interactions happen in the PEPT system the information is not extracted because the focus of the analysis is based on time averaged velocity data of one particle.

REFERENCES

Agemura, C. K., Kauten, R. J. & McCarthy, K. L. (1995). Flow Fields in Straight and Tapered Screw Extruders Using Magnetic Resonance Imaging. *Journal of Food Engineering*. 25: 55-72.

Axelsson, B., Msaki, P. & Israelsson A. (1984). Subtraction of Compton-scattered photons in single photon emission computerized tomography. *Journal of Nuclear Medicine*. 25: 490-494.

Bailey, D. L. & Meikle, S. R. (1994). A convolution-subtraction scatter correction method for 3D PET. *Physics in Medicine and Biology.* 39: 411-424.

Bakalis, S., Cox, P. W., Russell, A. B., Parker, D. J. & Fryer, P. J. (2006). Development and use of positron emitting particle tracking (PEPT) for velocity measurements in viscous fluids in pilot scale equipment. *Chemical Engineering Science*. 61: 1864-1877.

Barigou, M. (2004). Particle Tracking in Opaque Mixing Systems: An Overview of the Capabilities of PET and PEPT. *Trans IChemE, Part A, Chemical Engineering Research and Design*. 82: 1258- 1267.

Bbosa, L. (2013). *Probability based models for the power draw and energy spectra of a tumbling mill.* A thesis submitted in fulfilment of the requirements of the degree of Doctor of Philosophy. Cape Town: University of Cape Town.

Bbosa, L., Govender, I., Mainza, A. N. & Powell, M. S. (2011). Power draw estimations in experimental tumbling mills using PEPT. *Minerals Engineering*. 24: 319-324.

Bergström M., Eriksson, L., Bohm, C., Blomqvist, G & Litton, J. (1983). Correction for scattered radiation in a ring detector positron camera by integral transformation of the projections. *Journal of Computer Assisted Tomography.* 7: 42-50.

Bertrand, F., Leclaire, L. A. & Levecque, G. (2005). DEM-based models for the mixing of granular materials. *Chemical Engineering Science*. 60: 2517-2531.

Bridgewater, J., Forrest, S. & Parker, D. J. (2004). PEPT for agglomeration*? Powder Technology*. 140: 187-193.

Brodner, H. (2013). *Assessing the influence of lifter profiles on the velocity profile and the charge toe and shoulder using data from the PEPT system*. A thesis submitted in

fulfilment of the requirements of the degree of Master of Science in Chemical Engineering. Cape Town: University of Cape Town.

Chiruvella, R. V., Jaluria, Y., Karwe, M. V. & Sernas, V. (1996). Transport in a twin-screw extruder for the processing of polymers. *Polymer Engineering Science*. 36: 1531-1540.

Clermont, B. & de Haas, B. (2010). Optimization of mill performance by using online ball and pulp measurements. *The Journal of The Southern African Institute of Mining and Metallurgy.* 110: 133-140.

Cleary, P. W. (1998). Predicting charge motion, power draw, segregation and wear in ball mills using discrete element methods. *Minerals Engineering*. 11 (11): 1061-1080.

Cleary, P. W. (2001). Charge behaviour and power consumption in ball mills: Sensitivity to mill operating conditions, liner geometry and charge composition. *International Journal of Mineral Processing*. 63: 79-114.

Cleary P. W., Morrison, R. & Morrell, S. (2003). Comparison of DEM and experiment for a scale model SAG mill. *International Journal of Mineral Processing.* 68: 129-165.

Cole, K. E., Buffler, A., van der Meulen, N. P., Cilliers, J. J., Franzidis, J-P., Govender, I., Liu, C. & van Heerdan, M. R. (2012). Positron emission particle tracking measurements with 50 micron tracers. *Chemical Engineering Science*. 75: 235-242.

Cooper, S. & Coronella, C. J. (2005). CFD simulations of particle mixing in a binary fluidized bed*. Powder Technology*. 151: 27-36

Dong, H. & Moys, M. H. (2003). Load behaviour and mill power. . *International Journal of Mineral Processing.* 69: 11-28.

Dong, H. & Moys, M. H. (2003). Measurement of impact behaviour between balls and walls in grinding mills. *Minerals Engineering*. 16: 543-550.

Edwards, I., Axon, S.A., Barigou, M. & Stitt, E. H. (2009). Combined Use of PEPT and ERT in the study of Aluminium Hydroxide Precipitation. *Industrial & Engineering Chemistry Research*. 48: 1019-1028.

Fan, X., Parker, D. J. & Smith M. D. (2006). Labelling a single particle for positron emission particle tracking using direct activation and ion-exchange techniques. *Nuclear Instruments and Methods in Physics Research A*. 562: 345-350.

Fortsch, D. S. (2006). Ball charge loading- impact on specific power consumption and capacity. *IEEE-IAS Cement Industry Committee*.

Govender, I. & Powell, M. (2006). An empirical power model derived from 3D particle tracking. *Minerals Engineering*. 19: 1005-1012.

HBM. (2012). T20WN Torque Transducer data sheet. *Hottinger Baldwin Messtechnik (HBM)*.

Hlungwani, O., Rikhotso, J., Dong, H., & Moys, M. H. (2003). Further validation of DEM modelling of milling: effects of liner profile and mill speed. *Minerals Engineering*. 16: 993-998

Hong, S. & Kim, B. (2002). Effects of lifter bars on the ball motion and aluminium foil in tumbler ball mill. *Materials Letters*. 57: 275-279

Kalala, J. T., Breetzke, M. & Moys, M. H. (2008). Study of the influence of liner wear on the load behaviour of an industrial dry tumbling mill using the Discrete Element Method (DEM). *International Journal of Mineral Processing*. 86: 33-39.

Kallon, D. V. V., Govender, I. & Mainza, A. N. (2011). Circulation rate modelling of mill charge using positron emission particle tracking. *Minerals Engineering*. 24: 282-289.

Khakhar, D. V., Orpe, A, V., Andresén, P. & Ottino, J. M. (2001). Surface flow of granular materials: model and experiments in heap formation. *Journal of Fluid Mechanics*. 441: 255-264.

Koral, K. F., Clinthorne, N. H. & Rogers, W. L. (1986). Improving emission-computed tomography quantification by Compton-scatter rejection throughout offset windows. *Nuclear Instruments and Methods in Physics Research A.* 242: 610-614.

Laforest, R., Cutler, P. D. & Daube-Witherspoon, M. E. (1999). Extra shielding for improved signal-to-noise in 3D whole-body PET. *Proceedings of the IEEE Medical Imaging Conference (Seattle, WA)*.

Makokha, A. B., Moys, M., Bwalya, M. M.& Kimera, K. (2007). A new approach to optimising the life and performance of worn liners in ball mills: Experimental study and DEM simulation. *International Journal of Mineral Processing*. 84: 221-227.

Maleki-Moghaddam, M., Yahyaei, M., Banisi,, S. (2012). Converting AG to SAG mills: The Gol-E-Gohar Iron Ore Company case. *Powder Technology.* 217: 100-106.

McIvor, R. E., (1983). Effects of Speed and Liner Configuration on Ball Mill Performance. *Mineral Engineering.* 618-621.

Morrell, S. (1993). *The prediction of power draw in wet tumbling mills*. A thesis submitted in fulfilment of the requirements of the degree of Doctor of Philosophy. Queensland: University of Queensland.

Morrell, S., Valery, W., Banini, G & Latchireddi, S. (2001). Developments in AG/SAG mill modelling. *Mining and Mineral Process Engineering*. 4: 71-84.

Moys, M. H., (1993). A model of mill power as affected by mill speed, load volume, and liner design. *Journal of The South African Institute of Mining and Metallurgy.* 93: 135-141.

National Instruments (2010). LabView SignalExpress 2010. *National Instruments, Copyright © 1999- 2010, v9. 3.0.*

Nillson, G., (1979). Lining design for grinding mills: Influence on economy and capacity. *CIM Bulletin.*

Parker, D. J., Broadbent, C. J., Fowles, P., Hawkesworth, M. R. & McNeil, P. (1993). Positron emission particle tracking- a technique for studying flow within engineering equipment. *Nuclear Instruments and Methods in Physics Research A.* 326: 592-607.

Parker, D. J., Allen, D. A., Benton, D. M, Fowles, P., McNeil, P. A., Tan, M. & Beynon, T.D. (1997). Developments in particle tracking using the Birmingham Positron Camera. *Nuclear Instruments and Methods in Physics Research A*. 392: 421-426.

Pérez-Alonso, C. & Delgadillo, J. A. (2012). Experimental validation of 2D DEM code by digital image analysis in tumbling mills. *Minerals Engineering*. 25: 20-27.

Powell, M. S. (1993). A study of charge motion in rotary mills, with particular reference to the grinding action. Thesis. Department of Mechanical Engineering, University of Cape Town.

Powell, M.S. & McBride, A. T. (2004). A three-dimensional analysis of media motion and grinding regions in mills. *Minerals Engineering*. 17: 1099-1109.

Powell, M. S., Morrell, S. & Latchireddi, S. (2001). Development in the understanding of South African style SAG mills. *Minerals Engineering*. 14: 1143-1153.

Powell, M. S. & Nurick, G. N. (1996). A study of charge motion in rotary mills. Part 1-extension of the theory. *Minerals Engineering*. 9: 259-268.

Powell, M.S., Smit, I., Radziszewski, P., Cleary, P., Rattray, B., Eriksson, K. & Schaeffer, L. (2006) The Selection and Design of Mill Liners. In: Kawatra, S. K. *Advances in Comminution.* Colorado, USA: Society for Mining, Metallurgy, and Exploration, Inc. (SME).

Powell, M. S., Weerasekara, N. S., Cole, S., LaRoche, R. D. & Favier, J. (2011). DEM modelling of liner evolution and its influence on grinding rate in ball mills. *Minerals Engineering*. 24: 341-351.

Rezaeizadeh, M., Fooladi, M., Powell, M. S. & Mansouri, S. H. (2010). Experimental observations of lifter parameters and mill operation on power draw and liner impact loading. *Minerals Engineering*. 23: 1182-1191.

Rogers, R. S. C., Shoji, K., Hukki, A. M. & Linn, R. J. (1982). The effect of liner design on the performance of a continuous wet ball mill. *XIV International Mineral Processing Congress*. Canada.

Shao, L. & Karp, J. S. (1991). Cross-Plane Scattering Correction- Point Source Deconvolution in PET. *IEEE Transactions on Medical Imaging*. 10: 234-239.

Sichalwe, K., Govender, I. & Mainza, A.N. (2011). Characterising porosity of multi-component mixtures in rotary mills. *Minerals Engineering*. 24: 276-281.

Spinks, T, J., Jones, T., Bloomfield, P. M., Bailey, D. L., Miller, M., Hogg, D., Jones, W. F., Vaigneur, K., Reed, J., Young, J., Newport, D., Moyers, C., Casey, M. E., & Nutt, R.

(2000). Physical characteristics of the ECAT EXACT3D positron tomograph. *Physics in Medicine and Biology.* 45: 2601-2618.

Taberlet N., Richard, P. & Hinch, E. J. (2006). S shape of a granular pile in a rotating drum. *Physical Review E* 73, 050301: 1-4.

Toor, P., Franke, J., Powell, M., Bird, M. & Waters, T. (2013). Designing liners for performance not life. *Minerals Engineering.* 43-44: 22-28.

Wills, B. A., & Napier-Munn, T. (2006). *Mineral Processing Technology.* 7th Ed., Elsevier Science & Technology Books, Oxford.

Yang, Z., Parker, D. J., Fryer, P. J., Bakalis, S. & Fan, X. (2006). Multiple-particle tracking-an improvement for positron particle tracking. *Nuclear Instruments and Methods in Physics Research A*. 564: 332-338.

Yang, Z., Fryer, P. J., Bakalis, S., Fan, X., Parker, D. J. & Seville, J. P. K. (2007). An algorithm for tracking multiple, freely moving particles in a Positron Emission Particle Tracking system. *Nuclear Instruments and Methods in Physics Research A*. 577: 585-594.

APPENDICES

Appendix A- Power draw

The truncated voltage data from the LABView Software is given in Table 7. The average of the voltage values in each column was calculated and their difference was used to calculate the torque. The product of the voltage with the calibration factor, K gave the resultant torque for this particular set of data. For this work, the calibration factor K was 2.10.

$$Torque\ (T) = \Delta\, Voltage \times K \qquad \text{Equation 1}$$

Table 7: LABView software output for the voltage readings

X Value	Voltage (V), max	Voltage (V), min
0	0.097932	-0.334477
0.001	0.101748	-0.330662
0.002	0.096661	-0.330662
0.003	0.092845	-0.32939
0.004	0.092845	-0.323031
0.005	0.087758	-0.319216
0.006	0.086486	-0.312857
0.007	0.085215	-0.316672
0.008	0.086486	-0.320488
0.009	0.087758	-0.310313
0.01	0.082671	-0.321759
0.011	0.087758	-0.316672
0.012	0.087758	-0.317944
0.013	0.091573	-0.325575
0.014	0.092845	-0.323031
0.015	0.092845	-0.325575
0.016	0.101748	-0.334477
0.017	0.100476	-0.325575
0.018	0.097932	-0.334477
0.019	0.10302	-0.333206
0.02	0.097932	-0.333206
0.021	0.100476	-0.330662
0.022	0.099204	-0.325575
0.023	0.092845	-0.324303
0.024	0.092845	-0.323031

0.025	0.087758	-0.317944
0.026	0.086486	-0.314129
0.027	0.086486	-0.314129
0.028	0.087758	-0.320488
0.029	0.083943	-0.311585
0.03	0.082671	-0.314129
0.031	0.087758	-0.314129
0.032	0.082671	-0.316672
0.033	0.092845	-0.324303
0.034	0.094117	-0.319216
0.035	0.095389	-0.324303
0.036	0.101748	-0.330662
0.037	0.096661	-0.324303
0.038	0.099204	-0.333206
0.039	0.10302	-0.331934
0.04	0.10302	-0.330662

Once the torque value had been calculated, it was used to determine the power draw as a result of torque lever arm. The power was the product of the torque with the mill rotational speed (55, 70 and 85 % of critical speed) converted to rad/s. This was done using Equation 2.

$$Speed\ \left(\frac{rad}{s}\right) = \frac{speed\ (rpm) \times 2\pi}{60s} \qquad \text{Equation 2}$$

Table 8: Speed conversions for the power draw calculations

Speed (% of critical speed)	Speed (rpm)	Speed (rad/s)
55	42.5	4.45
70	54.1	5.67
85	65.6	6.87

The charge power draw distribution of the PEPT data gave information on how it is influenced by lifter face angle.

The PEPT power and Measured power plots at 55, 70 and 85 % of critical is shown below.

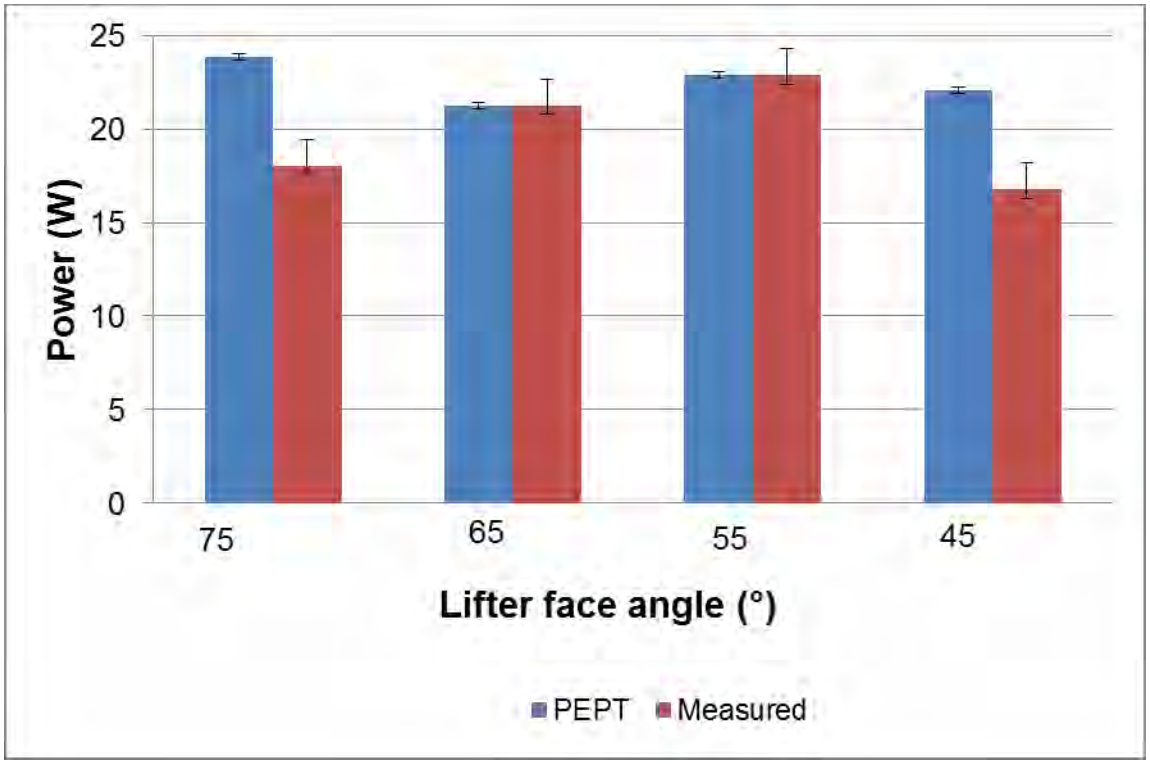

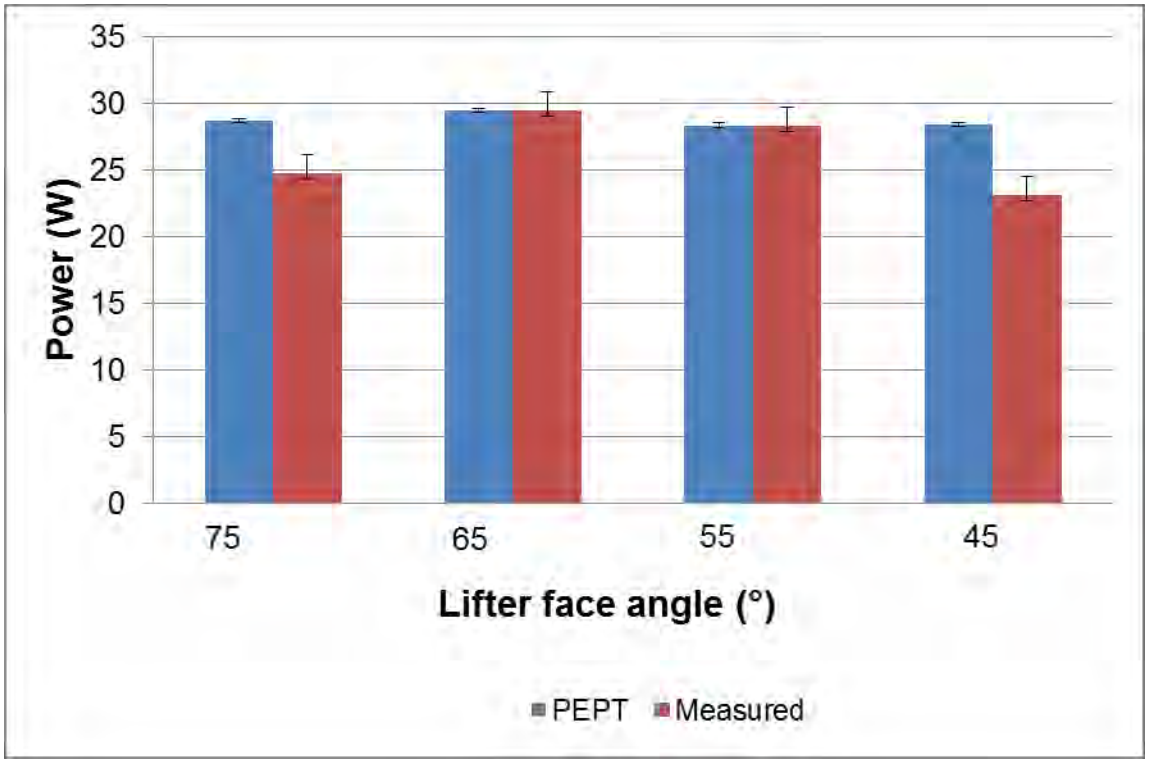

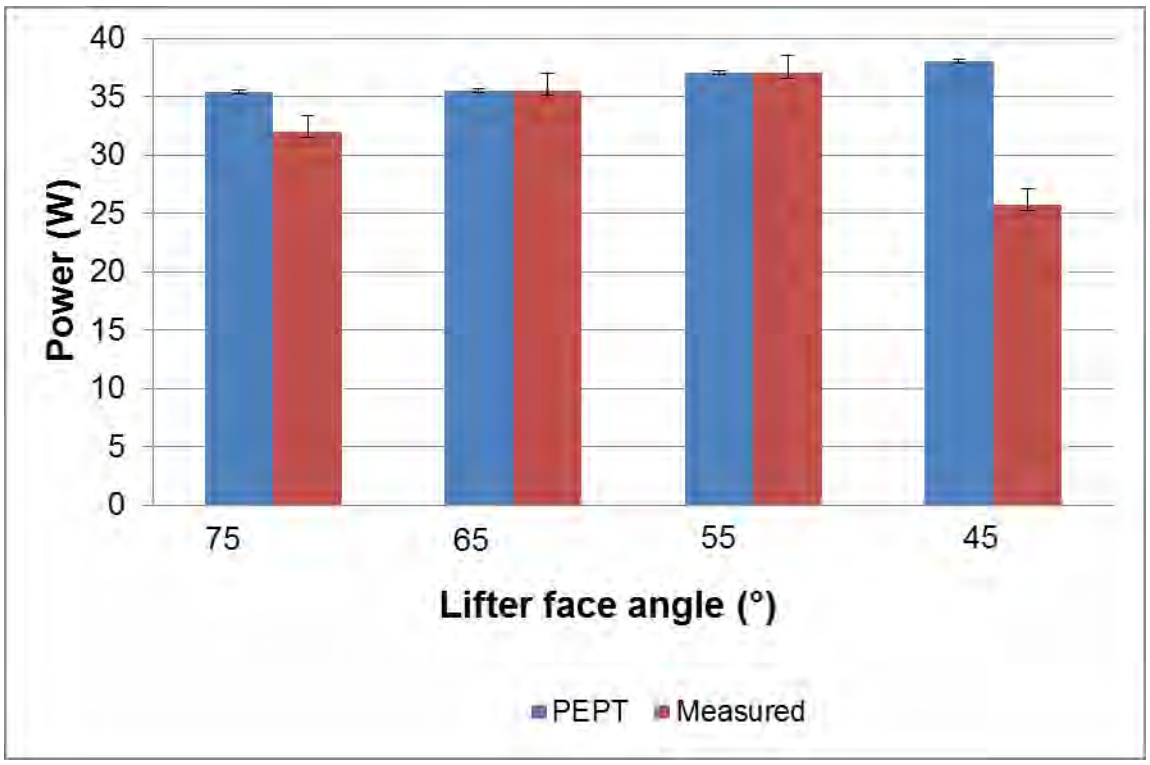
40
35
30
25
20
15
10
5
0
Power (W)
75
65
55
45
Lifter face angle (°)
PEPT
Measured

Appendix B- PEPT data

Raw data

A truncated version of the data obtained from PEPT is given in Table 9. This data is was the output received from the *cbatchtrack* program, which inputs the number of events (*N*), f_{opt} (% of lines used to work out the triangulation of the lines of response (LOR's) and the maximum allowable error (the % deviation from the centroid). The data here is shown for 200 events and a f_{opt} of 15 %.

Table 9: Raw data obtained from PEPT

t	x	y	z	error
87.3	-91	39.9	24	1.6
89.6	-87.2	40.3	24.1	1.5
92	-87.7	38	24	1.4
94.4	-87.9	38.9	24.5	1.2
96.8	-86.9	38	23.5	1.2
99.2	-85.8	37.4	23.7	1.5
101.5	-84.7	35.5	23.6	1.6
104.1	-84.6	35	24.5	1.4
106.5	-83.8	33.9	23	1.2
108.9	-83.2	33.5	22.9	1.3
111.7	-83.2	32.7	23.5	1.6
114.1	-81.6	31.9	23.4	1.3
116.4	-81	31.1	21.8	1.5
119.2	-80.7	28.6	23.8	1.1
121.7	-78.3	28.2	22.4	1.4
124.5	-78.6	27.8	23.7	1.4
126.9	-77.3	26.4	23.8	1.5
128.9	-75.7	25.4	22.9	1.6
131.8	-74.6	25	22.7	1.2
134.3	-74.5	23.7	22.7	1.3
136.9	-73.6	22.6	23.6	1.6
139.7	-71.7	21.3	24.5	1.3
142.3	-71.1	18.4	23.6	0.9
145.4	-70.5	17.9	24.3	1.5
147.6	-68.8	16.7	24.2	1.2
150	-67.1	15.1	24.7	1.5
152.4	-66.3	14.5	24	1.6
155.3	-64.3	12.3	24.6	1.3
158.1	-63.4	11.2	25.1	1.2
160.9	-62.4	8	25.6	1.8

Velocity profile data

The tangential velocity data was extracted from the radial line shown below. This radial line goes through the Centre of Circulation (CoC) and gives information of the velocity profile. This line is governed by Equation 11 below (Bbosa, 2013):

$$V\,(r,\theta) = a_1 \sin(b_1 r + c_1) + a_2 \sin(b_2 r + c_2) \qquad \text{Equation 11}$$

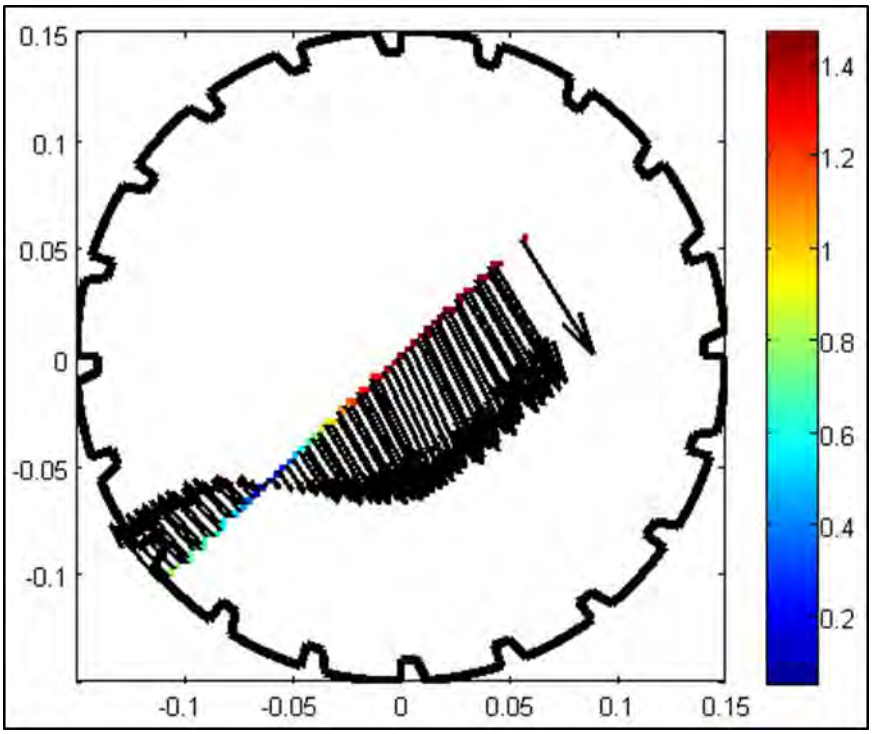

Appendix C- Velocity data

This is the data that was used to plot the velocity profiles at different distances along the radial line for the different mill speeds investigated. .

Lifter angle	Condition					
		0.015	0.017	0.022	0.028	0.032
90	90_30_55	0.535	0.547		0.458	0.435
75	75_30_55		0.582	0.557	0.514	0.475
65	65_30_55	0.6		0.564	0.524	0.491
55	55_30_55	0.579	0.566	0.536		
45	45_30_55	0.536	0.52	0.481	0.41	0.345

Lifter angle	Condition					
		0.015	0.019	0.024	0.03	0.038
90	90_30_70	0.752	0.709		0.562	0.36
75	75_30_70	0.741	0.706	0.663	0.577	0.414
65	65_30_70	0.743	0.711	0.671	0.59	0.431
55	55_30_70	0.739	0.706	0.663	0.581	0.4
45	45_30_70	0.738	0.705	0.661	0.579	0.401

Lifter angle	Condition					
		0.015	0.024	0.026	0.035	0.039
90	90_30_85	0.925	0.789	0.75	0.548	0.328
75	75_30_85		0.775		0.525	0.375
65	65_30_85	0.91	0.815	0.78	0.59	0.447
55	55_30_85	0.917	0.835	0.806	0.64	0.505
45	45_30_85	0.883	0.774	0.732	0.496	0.341

The results for the velocity profiles along the radial lines for 30 and 40 % filling degrees are given below.

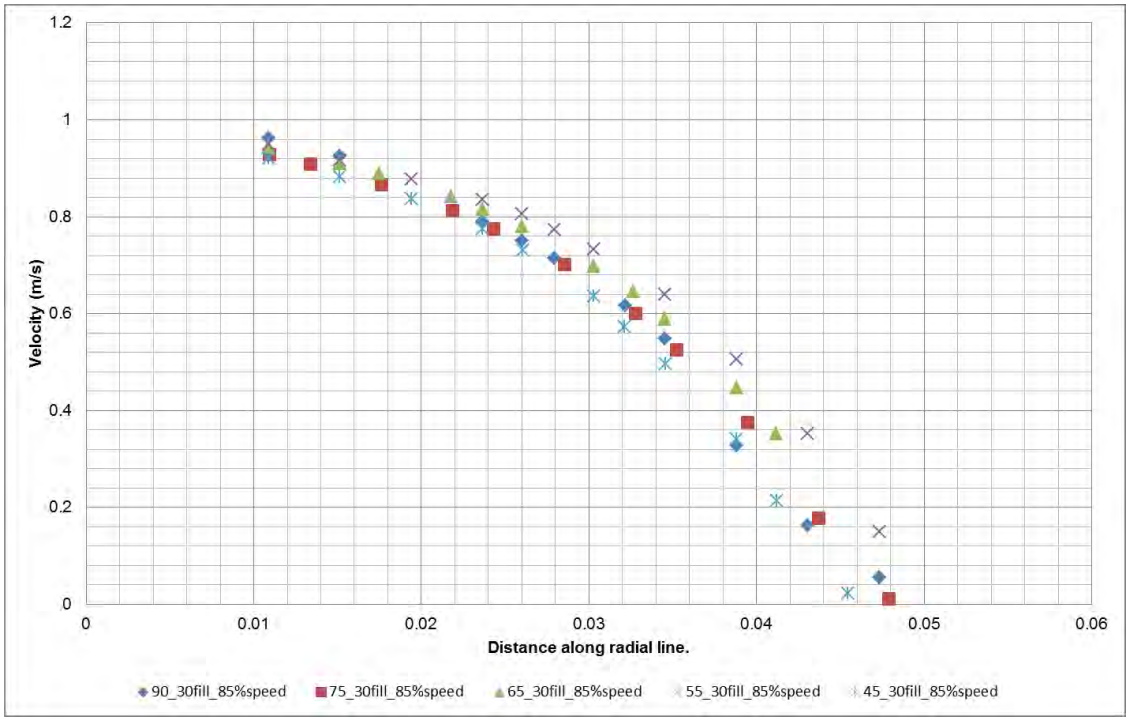
1.2
1
0.8
0.6
0.4
0.2
0
Velocity (m/s)
0
0.01
0.02
0.03
0.04
0.05
0.06
Distance along radial line.
90_30fill_85%speed
75_30fill_85%speed
65_30fill_85%speed
55_30fill_85%speed
45_30fill_85%speed

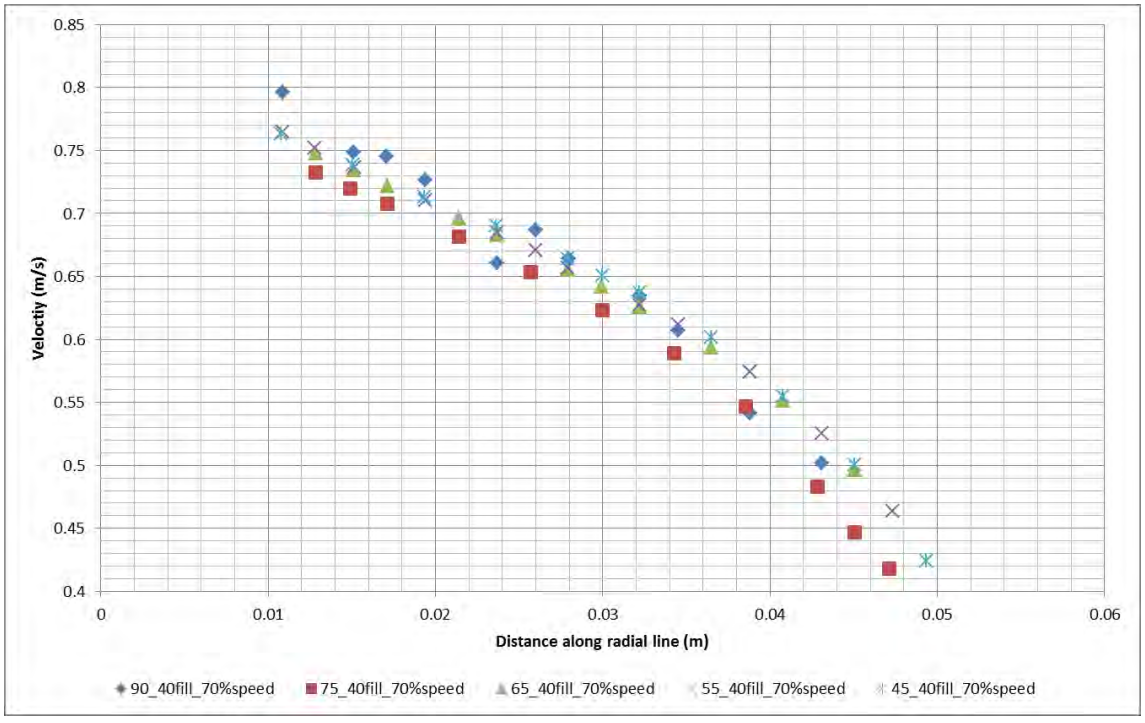
0.85
0.8
0.75
0.7
0.65
0.6
0.55
0.5
0.45
0.4
Velocity (m/s)
0
0.01
0.02
0.03
0.04
0.05
0.06
Distance along radial line (m)
90_40fill_70%speed
75_40fill_70%speed
65_40fill_70%speed
55_40fill_70%speed
45_40fill_70%speed